UNIVERSITY OF CALIFORNIA, MERCED

REDOX AND OXYGEN CONTROL ON WATER QUALITY AND MERCURY CYCYLING IN THE PROFUNDAL ZONE OF CALIFORNIA RESERVOIRS

A dissertation submitted in partial satisfaction of the requirements

for the degree of Doctor of Philosophy

by

Byran Fuhrmann

Dissertation Committee:

Professor Marc Beutel, Chair

Professor Peggy O'Day

Professor Marie-Odile Fortier

Professor Priya Ganguli

Spring 2020

The Dissertation of Byran Fuhrmann is approved, and it is acceptable in quality and form for publication on microfilm and electronically:

_____

Professor Peggy O'Day

_____

Professor Marie-Odile Fortier

_____

Professor Priya Ganguli

_____

Professor Marc Beutel, Chair

University of California, Merced

2020

Table of Contents

Acknowledgements

I would first and foremost like to thank my parents, without whom this would not be possible. My father, for serving as a role model of unwavering determination and stoicism, while exposing me to the challenges in life so that I could grow to become resilient. Although this quote is attributed to a different Bruce, I think it best describes the fortitude you instilled in me - “Do not pray for an easy life, pray for the strength to endure a difficult one”. My mother, the most caring person I know. You always supported my ambitions, expressed belief in my ability and encouraged me to pursue higher objectives in life. There were times in life when I doubted myself and I can honestly say that having your unwavering support made all the difference in my path forward. I am truly one of the most fortunate people alive to have parents that encouraged me to pursuit my dreams and provided just enough support to allow me to achieve them while maintaining the ability to enjoy the satisfaction of self-reliance. To Grandma Conway and all my uncles and aunts, especially Whit, Goggle, Tony, Nancy, and Susie for your unconditional love, support, and laughter. Much love to my 50+ cousins, I have enjoyed every moment we’ve spent together and I wish we lived closer.

There have also been many people in my life who have shown me unconditional love and support, as if I was part of their own family. To Danette and Dennis, your seemingly endless faith in my ability to progress, your support, and your unconditional love for me as a person has provided me with the blessing of a second family. To my brothers Duggan, Opie, Keith, Evan, and Diro we’ve been through so much together, you have provided so much encouragement for me throughout my endeavors, and I will always consider you to be part of my family. To my lab family Liying and Christian, I could not have made it through all of the lab work without seeing your friendly faces and continually receiving your support. Liying you have been a second mother for me and Christian you were the little brother I always wanted. To Mark and Melissa, who brought genuine positivity with them when they entered the lab family. To Louis, my African brother who has been a beacon of good-will, laughter, loyalty, positivity, and the source of deep wisdom. To Daniel and Melissa, my Summer Ct family and my mentors who provided me with the insight into grad school at UC Merced and inspired me with their own successful dissertation defenses. To Coty, Crystal, and Prosper, my SNRI family who cared so deeply for me. To Andrew, Sarah, and Jeff, my City of San Diego family who provided me true friendship, endless insight and engaged in philosophic conversations while out on a boat collecting green water. To my CALMS family who took me in with open arms and fostered my undying love for lakes and reservoirs, ultimately altering my career trajectory and fueling my passion for lake management.

To my friends Kyle, Keith, DJ, Conde, Angel, Dese, Ahmed, Gilbert, Uba, Jono, Brock, Preston, Dereck, Jorge, Hubb, and the many others who have been there for me during the good times and the difficult times. You have all had an integral part in my success and pursuit of continual improvement. Many of you have been there for me during

difficult times. Many of you inspired and challenged me to use my energy to make a positive impact on the world and I will never forget that or stop trying to do so. To Terry, Bob, Bradley, and Jerry, my North Coast Labs mentors. To the environmental engineering undergrads that I have has the pleasure of working with at UC Merced. You have such a positive outlook on life and a hunger for knowledge that I am very confident of your imminent success and your ability to improve the planet. Last, but certainly not least, to Marc, Peggy, Marie-Odile, Priya, Mark Marvin-DiPasquale, and Imad, my mentors and role models who helped me navigate the uncertain transition as a young professional and provided me with ample opportunities to excel. I have learned so much from you and you have done so much to help prepare me for the transition into the next phase of my life and career. I was truly blessed to have such great role models and such deep sources of knowledge. I can honestly say that every single person listed has played some part in fueling my drive to progress and my personal growth. I therefore promise you all that this is only the beginning of my journey and that I will use all of the motivation that you have provided me with to continue my quest to harness my ikigai and make the world a better place.

Byran Fuhrmann

Ph.D. Candidate, Environmental Systems
University of California, Merced
5200 North Lake Road, Merced, CA 95340
Email: bfuhrmann@ucmerced.edu

Education

2016 – Present	Doctoral Candidate, Environmental System. University of California, Merced.
2015 – 2016	Master of Science, Environmental Engineering Sciences, Water Resources Management. University of Florida.
2015 – 2016	Engineering Entrepreneurship Graduate Certificate. University of
2014 – 2015	Florida.
	Master of Business Administration, Strategic Sustainability.
2014	Humboldt State University.
	Bachelor of Science, Chemistry. Humboldt State University.

Honors and Awards

2019	Southern California Edison Fellowship Recipient	$10,000
	Professional Development Fellowship	$1,000
2018	National Environmental Monitoring Conference Speaker Scholarship	$1,000
	UC Water Graduate Student Video Competition	$1,000
	Environmental Systems Bobcat Fellowship	$3,240
	Professional Development Fellowship	$1,000
	Graduate Fellowship Incentive Program	$200
2017	Environmental Systems Bobcat Fellowship	$6,000
	UC Merced Professional Development Scholarship	$1,500
2015	Grad Slam! UC Merced Campus Champion	$5,000
2014	Business Development Internship	$5,000
2005	Humboldt State University MBA Scholarship	$3,000
2004	Eagle Scout, Boy Scouts of America	
	Black Belt, World Taekwondo Federation	

Leadership Roles

2017 – Present	Northern California Director, California Lake Management Society.
2019	Environmental Systems Seminar Series Graduate Student Leader.
	UC Merced Representative. California Council on Science &
2018 – 2019	Technology: Science Translators Showcase.
2018	Session Chair, Reservoir Quality. American Ecological Engineering Society.

Professional Experience

2014 – 2016 **Quality Assurance Manager.** Responsible for all aspects of the Quality Assurance program for both the environmental and GLP portions of the lab and ensured regulatory compliance. Main duties including training employees in quality assurance and GLP procedures, annual ELAP certification and proficiency testing, leading EPA compliance audits for GLP laboratory studies, LIMS and data management, SOP and method compliance documentation, reporting data to clients and regulators.

2014 **Quality Assurance Assistant.** Assisted with the QA program, proficiency testing, method and SOP documentation. Ensured data integrity by verifying GC-MS, HPLC, and ICP-MS chromatograms were accurate. Performed thermometer, pipette, and balance verification/calibration.

Research Experience

2016-2019 Lead graduate researcher for Hodges Reservoir water quality monitoring and treatability program. Findings presented in conferences, technical reports and publications. Program focus including chemical cycling and the impact on water treatability, mercury cycling at the sediment-water interface and impact on bioaccumulation, and hypolimnetic oxygenation.

2018 Developed new protocol for nitrate column regeneration used in colorimetric flow injection nitrate analysis at UC Merced Environmental Analytical Laboratory

Developed methodology for sediment methylmercury analysis.

2016 – 2017 Measured sediment nutrient, metal and mercury release in sediment chamber incubation projects to assess impact of oxic and anoxic conditions for Soulajule Reservoir, CA, San Pablo Reservoir, CA, and Rivanna Reservoir, VA.

Teaching

Fall 2019 – Spring 2020 **Field Methods of Environmental Chemistry (Instructor).** The course focuses on principles of chemical cycling in lakes/reservoirs and study the impact of water quality on treatability and the production of potable water. Includes methods of sample collection, preservation, lab analyses, jar testing and data analysis. Students also develop research projects for engineering solutions to address eutrophication.

Spring 2019 **Environmental Chemistry (Lab Instructor).**
Responsible for instruction and supervision of lab section. Lab involved principles of chemical analyses of environmental samples, including ICP-OES, TOC analysis, Ion Chromatography, spectrophotometry, and Hg/MeHg analysis by CVAFS.

Spring 2017, Spring 2018 **Water and Wastewater Treatment (Teaching Assistant).**
Topics include reactor kinetics, mass balances, microbial energetics, activated sludge treatment, nitrification, denitrification, and anaerobic digestion. Included field trips to Gallo Winery treatment facility, Merced treatment plant, and EBMUD treatment facility.

Publications

Beutel, M.W., Fuhrmann, B., Herbon, G., Chow, A., Brower, S., Pasek, J., 2020. Cycling of methylmercury and other redox-sensitive compounds in the profundal zone of a hypereutrophic water supply reservoir. Hydrobiologia.

Duvil, R., Beutel, M.W., Fuhrmann, B., Seelos, M., 2018. Effect of oxygen, nitrate and aluminum addition on methylmercury efflux from mine-impacted reservoir sediment. Water Research, 144, 740-751.

Beutel, M., Garcia-Gallardo, T., Falcon-Rojas, A., Fuhrmann, B., Hansen, A., 2018. Use of oxygenation to repress release of redox-sensitive compounds from profundal sediment in the valle de bravo reservoir, Mexico. International Journal of Environmental Pollution, 34(6), 17-20.

Publications in Prep

Fuhrmann, B., Beutel, M., O'Day, P.A., Tran, C., Funk, A., Brower, S., Pasek, J., Seelos, M., (in prep). Effects of mercury, organic carbon, and microbial inhibitor addition on methylmercury cycling at the profundal sediment-water interface of a sulfate-rich hypereutrophic reservoir. Water Research.

Fuhrmann, B., Beutel, M., Ganguli, P., Zhao, L., Brower, S., Funk, A., Pasek, J., (in prep). Profundal zone dynamics of methylmercury production, transport and degradation during thermal stratification in a hyper-eutrophic reservoir. Total Science of the Environment.

Fuhrmann, B., Fortier, M-O., Beutel, M., (in prep). Economic analysis and life cycle assessment of hypolimnetic oxygenation of Upper San Leandro reservoir. Environmental Science and Technology.

Newsletter Articles

Beutel, M., Fuhrmann, B., Brower, S., Pasek, J., O'Day, P., 2018. Seasonal and Redox-Mediated Patterns of Methylmercury Release from Profundal Sediment in Hodges Reservoir, California. Calm Waters, 13-14.

Conference Presentations

Fuhrmann, B., Beutel, M., Pasek, J., Marvin, M., Brower, S., Funk, A., O'Day, P., 2019. Consequences of Inorganic Hg, Organic Carbon, and Microbial Inhibitors on Hg Methylation. California Lake Management Society. San Diego, CA. (Oral)

Fuhrmann, B., Beutel, M., Pasek, J., Marvin, M., Brower, S., Funk, A., O'Day, P., 2019. Consequences of Inorganic Hg, Organic Carbon, and Microbial Inhibitors on Hg Methylation. Delta Tributaries Mercury Council. Sacramento, CA. (Oral)

Beutel, M., Fuhrmann, B., Pasek, J., Marvin, M., Brower, S., Funk, A., O'Day, P., 2019. Mercury Cycling in a Eutrophic Reservoir. American Ecological Engineering Society. Asheville, NC. (Oral)

Beutel, M., Rimondi, V., Lattanzi, P., Costagliola, P., Fuhrmann, B., 2019. Biomonitoring Mercury Contamination of the Landscape: Concentrations and Speciation in Tree Bark Near the Abbadia San Salvatore Mining District, Italy. American Ecological Engineering Society. Asheville, NC. (Oral)

Conn, M., Beutel, B., Fuhrmann, B., Brower, S., Funk, A., 2019. Seasonal Zooplankton Community Structure and Mercury Bioaccumulation in a Hypereutrophic Reservoir. American Ecological Engineering Society. Asheville, NC. (Oral)

Fuhrmann, B., Beutel, M., Pasek, J., Marvin, M., Brower, S., Funk, A., 2018. Effects of Lake Oxygenation on Mercury Cycling in Hodges Reservoir. California Lake Management Society. North Lake Tahoe, CA. (Oral)

Fuhrmann, B., Beutel, M., Pasek, J., Marvin, M., Brower, S., Funk, A., O'Day, P., 2018. Mercury Cycling in California Reservoirs: Takeaways and Management Strategies to Repress Bioaccumulation. American Ecological Engineering Society. Houston, TX. (Oral)

Beutel, M., Garcia-Gallardo, T., Falcon-Rojas, A., Fuhrmann, B., Hansen, A., 2018. The Use of Oxygenation to Repress the Release of Redox Sensitive Compounds from Profundal Sediment in the

Valle de Bravo Reservoir, Mexico. International Symposium on Sediment Management. San Cristobal, Mexico. (Oral)

Beutel, M., Fuhrmann, B., Brower, S., Pasek, J., 2018. Experimental Assessment of Oxygenation to Repress Methylmercury Release at the Profundal Sediment-water Interface in Hodges Reservoir, California, USA. Restoration of Eutrophic Lakes. Lahti, Finland. (Oral)

Fuhrmann, B., Beutel, M. Marvin-Dipasquale, M., Pasek, J., Brower., S., O'Day, P. 2018. Sediment Incubations to Assess MeHg Dynamics in a Hyper-Eutrophic Reservoir. Society of Environmental Toxicology and Chemistry. Sacramento, CA. (Poster)

Brower, S., Pasek, J. Fuhrmann, B., Beutel, M., 2018. Baseline Mercury Control Studies of Lake Hodges, San Diego. Statewide Reservoirs Mercury Control Program Technical Presentations. Sacramento, CA. (Oral)

Seelos, M., Beutel, M., Fuhrmann, B., 2018. Mitigating Mercury Methylation in a Mine-impacted Reservoir using Hypolimnetic Oxygenation, Guadalupe River Watershed, San Jose. Statewide Reservoirs Mercury Control Program Technical Presentations. Sacramento, CA. (Oral)

Fuhrmann, B., 2017. The Role of Oxygen in the Fight for Clean Water. University Friends Circle. Turlock, CA. (Oral)

Brower, S., Fuhrmann, B., Pasek, J., Beutel, M., 2018. Managing for Methylmercury: A Hodges Case Study. California Lake Management Society. Big Bear, CA. (Oral)

Fuhrmann, B., Beutel, M., Pasek, J., 2017. Patterns of Mercury Release from Profundal Sediment of California Reservoirs under Oxic and Anoxic Conditions. International Conference for Mercury as a Global Pollutant. Providence, RI. (Poster)

Fuhrmann, B., 2017. The Role of Oxygen in the Fight for Clean Water. Atwater Rotary Club. Atwater, CA. (Oral)

Fuhrmann, B., Beutel, M., Pasek, J., 2017. Hypolimnetic Oxygenation to Restore Ecosystem Function. American Ecological Engineering Society. Athens, GA. (Oral)

Fuhrmann, B., 2017. The Role of Oxygen in the Fight for Clean Water. UC Office of the President. San Francisco, CA. (Oral)

Fuhrmann, B., Harris S., 2015. Regression Analysis of the Humboldt Housing Market. Humboldt Association of Realtors. Eureka, CA. (Oral)

Fuhrmann, B., Anderson, C., Busher, C., 2015. Telonicher Marine Science Laboratory Business Analysis. Telonicher Marine Science Laboratory. Trinidad, CA. (Oral)

List of Tables

Chapter 1

Chapter 2

Chapter 3

List of Figures

Chapter 1

Chapter 2

Chapter 3

Abstract

Redox and oxygen control on water quality and mercury cycling in the profundal zone of California reservoirs

by

Byran Fuhrmann
Doctor of Philosophy in Environmental Systems
University of California, Merced

California reservoirs are vital resources that serve as a source of raw water for drinking water production, as well as providing other beneficial uses such as flood control, recreation, and wildlife habitat. These benefits can be limited by the excessive growth of algae and poor water quality associated with nutrients enrichment and eutrophication. In eutrophic reservoirs, nutrients can be released from profundal sediment when oxygen is depleted in the bottom water. These nutrients can exacerbate eutrophication if mixed into surface waters. Hypolimnetic anoxia is associated with a variety of additional water quality issues including reduced water treatment efficiency and the release of toxins.

The first objective of this dissertation was to investigate the economic implications and greenhouse gas emissions associated with hypolimnetic oxygenation, a system designed to prevent anaerobic conditions in bottom waters to improve water quality and treatability. This study performed an economic analysis and a life cycle assessment (LCA) of a hypolimnetic oxygenation system (HOS) installed in Upper San Leandro (USL), a drinking water reservoir in Oakland, California. The assessment compared water treatment and reservoir management operations under two scenarios, past conditions without a HOS and current conditions where a HOS is operated to improve water treatability. The largest economic benefit and reduction in greenhouse gas emissions (GHG) for the HOS scenario relative to previous operations was obtained from the reduction in ozone use for disinfection in the water treatment process. Construction costs had a more substantial impact than the cost of oxygen use in the net present value (NPV) of the HOS over its lifetime. In contrast, the LCA revealed that HOS oxygen use contributed the larger proportion of GHG emissions. Overall, results indicate that the implementation of HOS in USL was profitable and will lead to reduced GHG emissions over the assumed 60-year life of the system.

The second objective of this research was to investigate mercury cycling in Hodges Reservoir, a hypereutrophic sulfate-rich reservoir in San Diego, California. Anaerobic conditions at the sediment-water interface are associated with the buildup of methylmercury (MeHg), an organic form of mercury produced by anaerobic bacteria, in profundal sediment and water. MeHg poses a threat to ecosystem and human health due to its ability to bioaccumulate in aquatic food webs. The overarching goal of this work was to gain deeper insight into MeHg biogeochemical cycling during anaerobic conditions in the profundal zone to inform reservoir management about key mechanisms involved in mercury production, with the aim of lowering mercury bioaccumulation and protecting human and wildlife health.

The first study in this effort tracked MeHg production, degradation, and release into hypolimnetic water while anaerobic conditions were prevalent at the sediment-water interface. This involved tracking MeHg in the sediment, porewater, and water column, as well as associated parameters of interest such as redox acceptors and organic matter. Sediment-associated MeHg was greatest at the onset of anaerobic conditions, suggesting MeHg production in profundal sediment may be greatest during the oxic-anoxic transition, due to the abundance of redox acceptors to fuel anaerobic respiration. The depletion of bioavailable iron-oxide occurred simultaneously with the liberation of MeHg from the sediment, suggesting iron-oxide dissolution led to the release of organic-matter-associated MeHg to overlay water. The activity of sulfate-reducing bacteria (SRB) in the late spring and early summer was associated with the build-up of MeHg in profundal sediment. The depletion of sulfate in the porewater during mid-summer appears to have led to methanogenesis and high levels of biodemethylation.

A second study used microcosm incubations of profundal sediment and bottom water to assess seasonal patterns of MeHg cycling under various chemical treatments. Treatments included addition of air, organic carbon, and microbial inhibitors. Both aeration and sodium molybdate, a SRB inhibitor, generally caused a decrease in MeHg concentration, likely by inhibiting SRB activity. A methanogenic inhibitor resulted in a significant increase in MeHg concentration, indicating a suppressive effect by methanogens on net MeHg production, potentially due to enhanced microbial demethylation. Pyruvate resulted in a significant increase in MeHg concentration in the spring when the sediment-water interface was moderately reduced, but caused a significant decrease in the fall under highly reduced conditions. Acetate resulted in a significant increase in MeHg concentration, likely due to the stimulation of acetogenic SRB.

Collective results highlight the complex temporal dynamics of MeHg cycling at the sediment-water interface, which is regulated by organic matter composition, redox acceptor availability, and sediment microbial community structure and activity. MeHg production and release at the sediment-water interface was elevated under moderately reduced conditions, which may be the primary period of MeHg entry into the water column and aquatic food web entry. This indicates that management strategies to repress mercury bioaccumulation should focus on the key window of moderately reducing conditions during the onset of anaerobic conditions. Hypolimnetic oxygenation, if it is designed and operated to maintain an oxygenated sediment-water interface, could be a viable approach to repress the MeHg release observed with iron-oxide dissolution and MeHg production in the surficial sediment by SRB. The study also showed that that the sediment-water interface transitioned to be a net sink for MeHg during highly reduced conditions in the fall, likely due to enhanced demethylation by methanogens. Thus, highly reduced conditions appear to be a sink for MeHg in the profundal zone. This indicates that care must be taken to ensure the sediment-water interface is fully oxygenated to prevent mildly reducing conditions associated with MeHg production and release. Together, the results of this comprehensive research suggest that hypolimnetic oxygenation can be an economically viable and environmentally sound solution to enhancing source water treatability while potentially reducing MeHg bioaccumulation.

Chapter 1

Economic analysis and life cycle assessment of hypolimnetic oxygenation of Upper San Leandro reservoir

Abstract

A hypolimnetic oxygenation system (HOS) is a novel approach used to inject pure oxygen into the bottom water of eutrophic lakes and reservoirs to improve water quality by suppressing release of contaminants from the sediment, reducing associated summer algal blooms and improving source water treatability. HOS require a significant capital investment for the initial construction, as well as ongoing operating costs to purchase oxygen and perform system maintenance. However, this cost can be offset and exceeded by the savings incurred in water treatment operations due to enhanced treatability of the source water. There is currently a lack of information regarding the impact of HOS implementation in eutrophic drinking water reservoirs on the carbon footprint and financial benefit of the associated water treatment operations. This study performed an economic analysis and a life cycle assessment (LCA) of the HOS that was installed in a drinking water reservoir, Upper San Leandro (USL), in Oakland, CA in 2001. Both analyses determined that a reduction in ozone use in the disinfection treatment process resulted in the largest benefit overall. The economic analysis revealed that construction costs resulted in a larger net present value (NPV) reduction than the cost of oxygen used in the HOS over its lifetime. The LCA revealed that HOS oxygen use contributed a much larger proportion of greenhouse gas (GHG) emissions and the emissions related to HOS construction were negligible relative to other processes. The results suggest that the implementation of HOS in the USL reservoir will be moderately profitable and lead to reduced GHG emissions over the assumed 60-year life of the system.

1. Introduction

Manmade reservoirs are important assets which are used to store source water for potable water production. This importance is highlighted in areas such as California, which is the most populated state in the United States with the highest total water demand. In the state, approximately 75% of municipal water supply comes from surface waters such as rivers, lakes and reservoirs (Dieter et al., 2018). This need for water storage is further accentuated during drought conditions, such as the recent California drought from 2011 to 2017, which was one of the most devastating in the state's history (Kam et al., 2019). A variety of studies have also indicated that increasing temperatures and precipitation fluctuations due to climate change are likely to enhance the frequency of droughts in the future in California (Aghakouchak et al., 2014; Diffenbaugh et al., 2015; Mann and Gleick, 2015). California also experiences a Mediterranean climate in which very little precipitation occurs during the spring through fall season. This further enhances the need for water storage during this period and reservoirs are generally the main source of drinking water supply in Mediterranean regions (Marcé and Armengol, 2009).

Many California lakes and reservoirs experience eutrophication, or large-scale algae blooms due to the input of nutrients such as nitrate, phosphate, and ammonia, which stimulate algal production (Horne and Goldman, 1994). This loading of nutrients can be due to external sources, internal sources, or as is commonly the case, a combination of both. External sources include stormwater runoff in populated areas and agricultural runoff in rural areas. A key internal nutrient source in thermally stratified reservoirs is release from the sediment, which occurs at high rates when the sediment-water interface becomes anaerobic (Beutel and Horne, 1999). Anaerobic conditions develop at the sediment-water interface of productive reservoirs during thermal stratification, when the reservoir separates into distinct layers. Thermal stratification occurs as the surface water, or epilimnion becomes warmer and less dense while reduced wind speeds at the surface reduce the potential for mixing with the bottom water or hypolimnion. This physical separation isolates the hypolimnion from the atmosphere and prevents it from replenishing the oxygen that is depleted during bacterial respiration, leaving the hypolimnion devoid of oxygen in reservoirs with high rates of microbial respiration.

The input of nutrients from the anaerobic sediment also creates a positive feedback on eutrophication as it diffuses upwards and stimulates algal growth in surface waters. The algae have short lifespans and sink back down to the sediment after dying, further enhancing the rates of hypolimnetic microbial respiration and returning the nutrients which they had uptaken. Anaerobic conditions at the sediment water interface can also lead to the release of large quantities of dissolved manganese (Mn), produced during the microbially mediated reduction of manganese and iron oxides (Horne and Goldberg, 1994). Eutrophication in drinking water reservoirs often leads to increased treatment costs and chemical usage due to water quality issues such as cyanotoxins and taste and odor compounds (T&Os) produced by algae and cyanobacteria present in the source water (Smith et al., 2002). Additionally, dissolved Mn creates must be removed during the treatment process, which requires the use of oxidants such as chlorine, leading

to enhanced costs and potentially forming disinfection biproducts (DPBs) when organic matter from algal biomass in the source water reacts with chlorine.

Hypolimnetic oxygenation is a relatively new technique which has been successfully utilized to improve water quality in lakes and reservoirs (Beutel and Horne, 1999; Horne and Beutel, 2019; Preece et al., 2019). In 2002, a hypolimnetic oxygenation system (HOS) was installed in USL reservoir, the focus of this study, for the purpose of reducing internal nutrient loading and improving water treatability. This study provides an economic evaluation of HOS implementation at USL utilizing historical treatment data, construction costs, and ongoing operational costs such as the purchase of oxygen and maintenance of the HOS to determine if implementation of the HOS is financially justified. In addition to the economic feasibility of reservoir oxygenation, environmental impacts should also be considered, especially contributions to climate change, as HOS requires a large quantity of raw materials and pure liquid oxygen, which can both be transported great distances. This study also evaluates and compares the life cycle greenhouse gas (LC-GHG) emissions directly related to potable water production from the USL Reservoir in a life cycle analysis (LCA) comparing the current scenario where a HOS system is operated to improve water treatability against an alternative scenario in which standard operations continued and the HOS was never installed. Previous LCAs have been performed on water treatment practices to compare the carbon emissions of individual treatment processes (Bonton et al., 2012; Igos et al., 2014; Vince et al., 2008). However, to our knowledge there is no published LCA that investigates greenhouse gas (GHG) emissions related impact of oxygenation of a drinking water reservoir to enhance water treatability.

2. Methods

2.1 Study site

Upper San Leandro reservoir (USL) is a drinking water reservoir located in Oakland, CA, a highly populated and urbanized area. USL has a surface area of 620 acres, a storage capacity of 41,000 acre-ft and typically stores 29,500 acre-ft (Mark Mobley, personal communications). The reservoir water is treated by the Upper San Leandro Water Treatment Plant (USLWTP), which is in close proximity. The reservoir receives approximately 75% of its input from local stormwater runoff and 25% from imported sources. Because of the high nutrient loading from local runoff, the reservoir has experienced a variety of water quality issues due to algal blooms and eutrophication (Horne et al., 2003; Mobley, 2003). This has led to the accumulation of a large amount of organic matter in the surficial sediment in the profundal zone. Summer stratification, and the anaerobic conditions that follow, lead to internal nutrient loading and manganese release from surficial sediment in the hypolimnion, further degrading water quality. Internal nutrient and metals loading has led to a variety of water quality issues which made source water treatability more difficult, including multiple times where the threshold for T&Os in the source water exceeded the national standards by more than 100 times (Horne at al., 2003).

In 2001, the utility implemented a HOS to reduce internal nutrient and metal releases, thereby lowering algal blooms, T&Os, and treatment costs, while enhancing treatment capacity. HOS consist of an on-shore oxygen storage tank or facility with a flow control to adjust the delivery rate and an underwater diffuser which is positioned just above the sediment-water interface in the profundal zone of the reservoir. Although on-site pure oxygen production can be accomplished with pressure swing adsorption technology, this method has higher capital costs, maintenance requirements, and cannot meet higher oxygen demands that may be required by unforeseen circumstances and therefore truck deliveries generally supply the oxygen storage tank with liquid oxygen. USL reservoir's oxygen storage tank is 6,000 gallons and the HOS diffuser was initially 9,600 ft long (Mobley et al., 2019). Approximately 500,000 kg of oxygen over the course of 173 days was delivered during initial operations in 2002 to successfully prevent anaerobic conditions and many of the associated water quality issues (Table 1.1). The delivery of oxygen began at around 6,350 kg per day due to a high sediment oxygen-demand caused by the buildup of organic matter from prior eutrophication but dropped and eventually stabilized at around 1,450 kg per day (Jung, 2003). The HOS installation and operation led to a large reduction in ozone use for disinfection, the elimination of the hydrogen peroxide pre-treatment system, and a moderate decline in chlorine use. In 2012, the HOS diffuser system was extended by 4,000 ft to cover a larger distance. The HOS is still being successfully employed at the time of this publication. The HOS at USL has an expected lifetime of between 50-100 years with an average expectation of 60 years (Mark Mobley, personal communications).

2.2 Economic Analysis

The economic feasibility of the HOS system was calculated for a baseline scenario, a minimum benefit scenario, and a maximum benefit scenario. The baseline scenario utilized construction, installation, and estimated maintenance costs obtained from the lead project engineer (Mark Mobley, personal communications). Data regarding the baseline treatment operations and chemical savings was based on the average values for the three years prior to and one year following the HOS installation and operation, as well as the HOS oxygen requirement from the first year of HOS operation (Horne et al., 2003; Jung, 2003; Mobley, 2003). The baseline scenario assumes an average HOS operational lifetime of 60 years. The minimum benefit scenario assumes the most frequent maintenance schedule, minimum daily potable water production, a minimum annual HOS operational period, a minimal HOS lifetime, minimum chemical cost savings, and a maximum HOS oxygen requirement. The maximum benefit scenario assumes the least frequent maintenance schedule, maximum daily potable water production, a maximum annual HOS operational period, a maximum HOS lifetime, maximum chemical cost savings, and a minimum HOS oxygen requirement. Financial parameters, such as maintenance requirements, potable production rates, chemical treatment savings, and HOS oxygen usage, were assumed for each scenario (Table 1.2). Detailed information regarding assumptions and parameters used in the economic analysis is described in Appendix 1.

The economic feasibility of the HOS system installation and operation at USL reservoir was evaluated for the baseline, minimum benefit, and maximum benefit scenarios using four standard metrics of profitability for capital project investments. These metrics were calculated by compiling a cash flow analysis using the financial parameter assumptions. The first financial metric that was employed to evaluate the HOS profitability was the net present value (NPV) which determines the current value of all future cash inflows and outflows based on the time value of money and an assumed discount rate, or the desired interest rate of return for the investment. The discount rate can be determined by evaluating the rate of return expected by alternative capital investment opportunities, such as lending the project capital to investors or investing in the stock market. The NPV was also determined for the baseline, minimum, and maximum values for the following individual processes: construction of the HOS, maintenance of the HOS, HOS oxygen use, ozone required for treatment, hydrogen peroxide required for treatment, and chlorine required for treatment.

The expected return on investment from alternative investment opportunities can be compared to the internal rate of return (IRR), the second metric utilized, which calculates the interest rate return on investment for the project while considering the present value of future financial processes. The calculated IRR of a potential project is directly comparable to the discount rate and a significantly higher IRR indicates a sound investment, while a lower IRR implies the project is not financially viable. The historical average stock market return is 10%, meaning that project with an IRR of greater than 10% appear to be financially sound investments, while projects at or below 10% IRR are considered inferior investments (Vaga, 1990). Therefore, a 10% discount rate was be assumed in the NPV calculation and it also served as the benchmark for comparison in the IRR calculation.

The third standard metric used in this economic evaluation is the benefit-cost-ratio (BCR). The BCR is the present value of all cash inflows or financial benefits derived from the project divided by the present value of all cash outflows or costs associated with the project. A project with a calculated BCR greater than one is considered financially profitable, while a BCR less than one indicates the project is likely a poor investment. The fourth standard metric used to evaluate HOS implementation at USL is the payback period. The payback period is a metric which determines the precise amount of time that is required for the initial project costs to be recovered through cost savings or cash inflows associated with the project.

2.3 Comparative LCA

The LCA methodology utilized adheres to the ISO Life Cycle Assessment framework, containing four main steps: the goal and scope, inventory analysis, impact assessment, and interpretation of the results (Finkbeiner et al., 2006). The main goal of the LCA portion of this study is to compare the LC-GHG emissions related to potable water treatment of source water from USL reservoir under two scenarios: the first real world scenario in which a HOS was installed and operated to enhance treatment efficiency at the USLWTP (HOS scenario) and the second hypothetical scenario where a HOS was not installed and standard USLWTP processes continued as usual pre-2002

(standard scenario). Each scenario was evaluated for an equal time period, which was set to the expected lifetime of the HOS. There are three specific goals for this analysis. The first is to determine what impact the installation and operation of the HOS will likely have on the total LC-GHG emissions related to reservoir operations and raw water treatment over the useful lifetime of the system compared to the standard scenario where the HOS was not installed. The second specific goal is to determine which factors and processes utilized in the LCA are the most important drivers of LC-GHG emissions overall. The final goal is to determine how changing important drivers of the LCA model influences LC-GHG emissions by performing sensitivity and Monte Carlo analyses. The life cycle impact assessment method used was the Environmental Protection Agency's Tool for the Reduction and Assessment of Chemical and Other Environmental Impacts 2.1(EPA TRACI 2.1) (Bare, 2012). The functional unit in this analysis was one million gallons (MG) of potable water that is produced from source water from the USL reservoir by the USLWTP and that meets or exceeds EPA standards. This study focuses on the global warming impact category with indicator units of kg CO2, scaled to the functional unit of 1 MG produced. This LCA will only consider emissions due to the construction, installation, and maintenance of the HOS, comparable treatment processes that were observed to change due to HOS operation and quantifiable (ozone, hydrogen peroxide, and chlorine use), and reservoir management activities (reservoir gas emissions in the standard scenario and oxygen use in the HOS scenario).

The system diagrams show individual processes related to treatment operations and reservoir management for each scenario and the system boundary (Figure 1.1). The data regarding the treatment operations, chemical usage, annual operational period, and HOS oxygen use paralleled that of the economic analysis which was limited to data from three years prior to and one year following HOS installation and operation. Methane emissions for the standard scenario were assumed based on a diffusive flux equation derived from the study of 53 seasonally anoxic lakes and reservoirs (Bastviken et al., 2004). The treatment and reservoir management parameters utilized in each LCA scenario, such as potable production rates, chemical treatment requirements, electricity requirements, transportation distances, reservoir methane emissions, and HOS oxygen usage were assumed based on available data (Table 1.3). Detailed information regarding assumptions and parameters used in the economic analysis is described in Appendix 1. The system diagram shows individual processes related to the HOS construction for the HOS scenario and the system boundary (Figure 1.2). Detailed information regarding the raw materials used in the construction of the HOS and the maintenance schedule was obtained from the lead project engineer (Mark Mobley, personal communications). The locations of material production, transportation of raw materials, use of electricity and resources required for the installation were assumed based on available data sources. Parameters related to the construction, installation, and maintenance of the HOS, such as raw material use and transportation distances were assumed based on available data (Table 1.4). Detailed information regarding assumptions and parameters used in the LCA are also described in Appendix 1.

2.4 Sensitivity and uncertainty analyses

Sensitivity analyses were performed on both the economic forecast utilizing the NPV calculation and the LCA model, which included both the HOS scenario and the standard scenario. Sensitivity analyses were performed by varying one input parameter to its minimum or maximum value while maintaining all other parameters at baseline values. Monte Carlo analyses were also performed for the economic NPV calculation and the LCA model total LC-GHG emissions for each scenario. Monte Carlo analyses were performed using 10,000 simulations in Python(x,y) code using the individual probability distributions of the input parameters in order to determine the probability distribution of the NPV for the economic forecast and the LC-GHG emissions for each of the two modeled LCA scenarios. Due to insufficient data to inform the probability distributions for individual input parameters, Monte Carlo analyses were performed using triangular, normal, and uniform distributions with endpoints between the minimum and maximum parameter values to compare the effect of distribution types on Monte Carlo results. The three probability distribution Monte Carlo simulations were analyzed for a difference in the mean of the HOS and standard scenarios using a one-way ANOVA statistical test in SPSS and the conventional value of $p < 0.05$ was used to signify a statistically significant difference.

3. Results

3.1 Economic model results

The baseline economic model resulted in a NPV of $185k and an IRR of 13.7%, with the minimum benefit scenario exhibiting a -$522k NPV and -0.907% IRR, while the maximum benefit scenario displayed a $1.48M NPV and a 40.0% IRR (Table 1.5, Figure 1.3). The baseline model calculated a BCR of 2.41, with the minimum benefit scenario finding a BCR of 0.529 and the maximum benefit scenario obtaining a BCR of 3.90. The payback period was found to be 11.6 years for the baseline scenario, with a range of 67.2 years for the minimum benefit scenario and 4.83 years for the maximum benefit scenario. The NPV calculation of individual parameters for minimum, baseline, and maximum values shows that construction resulted in the largest cost overall which was fixed at -$694k NPV and the baseline HOS oxygen cost was less than one-half of this value at -$304k, ranging from a minimum NPV of -$402k to a maximum NPV of -$163k (Figure 1.4). Ozone savings were the most profitable component at $595k for the baseline value NPV ($316k to $1.13M), followed by hydrogen peroxide savings at a baseline value of $476k NPV ($271k to $843k). Chlorine savings were substantially lower at a baseline value of $119k NPV ($0 to $372k). Maintenance costs were relatively minor for all assumed values.

The economic sensitivity analysis indicates that ozone and hydrogen peroxide savings were the most sensitive parameters (Figure 1.5). Altering the ozone requirement parameter resulted in a total HOS NPV ranging from -$91k for the minimum benefit parameter value to $722k for the maximum benefit parameter value, while the hydrogen

peroxide requirement resulted in a total HOS NPV of -$18k for the minimum benefit parameter value and $549k for the maximum benefit parameter value. Daily potable water production (total HOS NPV ranging from $152k to $674k), and the chlorine requirement (total HOS NPV ranging from $66k to $473k), were also moderately sensitive parameters. HOS daily oxygen requirement, (total HOS NPV ranging from $122k to $312k), and annual days of operation (total HOS NPV ranging from $77k to $294k), displayed a modest impact on the overall NPV. The HOS lifetime and the total maintenance costs for the HOS were found to have little impact on the total HOS NPV.

The Monte Carlo analyses average NPV ranged from $356k for the normal probability distribution to $480k for the uniform probability distribution (Figure 1.6). In addition, 48.3% of the uniform, 29.5% of the normal, and 30.5% of the triangular probability distribution simulations resulted in a NPV greater than $500k, while 6.8% of the uniform, 10.1% of the normal, and 4.5% of the triangular probability distribution simulations resulted in a negative NPV. There was a substantial amount of variation between simulation results in each model and the standard deviations were moderately large, relative to the means of the results, ranging from $226k for the triangular probability distribution to $316k for the uniform probability distribution. The overall range of simulation values was extensive overall, with the uniform distribution displaying the lowest overall range and the normal distribution displaying the largest range.

3.2 LCA model results

The baseline LCA model showed a moderate decrease in LC-GHG emissions for the installation and operation of the HOS at USL, with the HOS scenario exhibiting emissions of 296 kg CO2eq/MG treated water compared with 394 kg CO2eq/MG for the standard scenario (Figure 1.7). The ozone treatment production process was the most significant source of GHG emissions in each model, contributing 143 kg CO2eq/MG to the HOS scenario (ranging from 107 to 179 kg CO2eq/MG in the sensitivity analysis) and 259 kg CO2eq/MG (ranging from 185 to 326 kg CO2eq/MG). The chlorine requirement in the treatment process was also a major contributor to the total LC-GHG emissions in each scenario, but there was not as substantial of a difference between the two scenarios, with the HOS scenario exhibiting an emissions of 84 kg CO2eq/MG (ranging from 59 to 117 kg CO2eq/MG in the sensitivity analysis) compared with 103 kg CO2eq/MG (ranging from 72 to 142 kg CO2eq/MG) for the standard scenario. Reservoir methane emissions produced 24.6 kg CO2eq/MG (ranging from 15.3 to 40.9 kg CO2eq/MG) for the standard scenario, while HOS oxygen use resulted in emissions of 69.4 kg CO2eq/MG (ranging from 26.6 to 100 kg CO2eq/MG). Emissions related to hydrogen peroxide treatment and HOS construction were relatively insignificant overall relative to the magnitude of impacts from other processes.

The results of the LCA were most sensitive to the ozone requirement for both scenarios, with the HOS scenario LC-GHG emissions ranging from 261 to 332 kg CO2eq/MG and the standard scenario emissions ranging from 320 to 460 kg CO2eq/MG as the ozone requirement was varied from its minimum to its maximum value (Figure 1.8). HOS oxygen requirement was also a sensitive parameter for the HOS scenario, as changing its value from its minimum to its maximum resulted in a range of LC-GHG

emissions from 262 kg CO2eq/MG to 313 kg CO2eq/MG. The chlorine requirement in the treatment process was a moderately sensitive parameter, leading to LC-GHG emissions from 276 kg CO2eq/MG to 318 kg CO2eq/MG for the HOS scenario and 369 kg CO2eq/MG to 420 kg CO2eq/MG for the standard scenario as its value was varied within its range. Other processes with somewhat sensitive parameters include electricity for chlorine production (410 to 441 kg CO2eq/MG for the HOS scenario, 561 to 600 kg CO2eq/MG for the standard scenario), daily potable water production (405 to 432 kg CO2eq/MG for the HOS scenario, 573 to 577 kg CO2eq/MG for the standard scenario), and reservoir area for the standard scenario (392 to 398 kg CO2eq/MG). The annual operational period in both scenarios, and hydrogen peroxide requirement in the standard scenario, were relatively stable processes, demonstrating no substantial difference in emissions as their values were varied from their minimum to their maximum for either scenario.

The LCA Monte Carlo simulations resulted in average simulation emissions that were comparable to the baseline model for all three probability distribution functions, with the HOS scenario means ranging from 286 to 295 kg CO2eq/MG and the standard scenario means ranging from 393 to 398 kg CO2eq/MG (Figure 1.9). The HOS scenario mean was significantly greater than the standard scenario mean for all three probabilities ($P < 0.001$, n=10,000). The HOS scenario demonstrated lower variation for all three distribution simulations, with a range in the standard deviation of 15.3 kg CO2eq/MG in the normal distribution to 29.0 kg CO2eq/MG in the uniform distribution, compared to the standard scenario, which demonstrated a standard deviation range of 30.8 kg CO2eq/MG in the triangular distribution to 43.6 kg CO2eq/MG in the uniform distribution. Overall, the uniform probability distribution analysis resulted in the largest uncertainty in the results of each scenario and the largest overlap of ranges between the scenarios, while the normal and triangular probability distributions resulted in lower variation and less overlap between the scenarios.

4. Discussion

4.1 Economic feasibility of oxygenation at USL

The positive results of the baseline economic analysis and all three probability distribution Monte Carlo simulations suggest that HOS implementation in USL is economically justified and financially lucrative over the life of the system. Economic analysis metrics (Figure 1.3) show that HOS implementation would be moderately profitable under the baseline parameter assumptions, highly profitable under the maximum benefit assumptions, but not financially justified under the minimum benefit assumptions with an assumed discount rate of 10%. The 11.6-year payback period determined by the baseline economic analysis is reasonably fast for an investment with a 60-year expected lifetime and the 13.7% IRR indicates a satisfactory return on investment when compared with a 10% discount rate (Figure 1.3). Additionally, the BCR > 1.0 (2.41) and the $185k NPV of the baseline model are positive indicators that the HOS is a profitable venture under the assumptions provided. The economic Monte Carlo simulations suggest that the baseline economic model result of $185,000 underestimates

the expected NPV and the overall profitability of the HOS at USL, with all three probability distribution models demonstrating an average NPV of at least $350k (Figure 1.6). Additionally, the cumulative probability of an NPV lower than $0, an indicator of financial loss, was much smaller than the cumulative probability of an NPV greater than $500k, indicating that the HOS is more likely to be highly profitable than to be economically infeasible. The results of our economic analysis of the HOS in USL demonstrate that it was a sound investment with a high probability of being financially profitable over the lifetime of the system.

NPV results (Figure 1.4) and the economic sensitivity analysis (Figure 1.5) show that the reduction in ozone and hydrogen peroxide use had the largest impact on the model predictions, demonstrating that the economic feasibility of the HOS in USL is driven by the reduction in treatment costs due to improved source water quality. The required dose of these disinfectants is primarily based on the concentration of T&Os that are produced by cyanobacteria in the source water (Jung, 2003). Research suggests that both urbanization and climate change will enhance the intensity and frequency of future eutrophication events, along with the cyanobacteria that frequently accompany eutrophic conditions (Marcé and Armengol, 2009; Savage et al., 2010; Paerl, 2009). This indicates that the USLWTP may experience an enhanced source water treatability benefit in the future, as non-oxygenated reservoir water quality would be expected to be further degraded. Multiple long-term studies have shown that reservoir oxygenation can be effective in reducing water column concertation of nutrients such as ammonia and phosphate that can lead to phytoplankton blooms (Beutel and Horne, 1999; Horne and Beutel, 2019; Preece et al., 2019). The large impact of the reduction in disinfectant use on the economic viability of the HOS and the prediction of enhanced future reservoir eutrophication, which can be alleviated by oxygenation, indicates that the HOS may be even more profitable than the baseline economic model suggests.

The daily potable water production and the annual days of HOS operation were also important parameters in the economic model, indicating that the total volume of treated water produced during the system lifetime is a vital factor that regulates the economic viability of the HOS at USL. The daily potable water production is likely most heavily influenced by the supply and demand of the service region, while the annual days of operation will be primarily determined by the period of thermal stratification, which is controlled by the duration of warm weather in the area. However, the economic sensitivity analysis shows that the HOS lifetime is insignificant on the overall NPV, demonstrating the significance of the time value of money and showing that initial savings due to enhanced treatability control the overall economic viability of the project. Therefore, potable water production and HOS operations in the first 20 to 30 years of operations likely dominate the overall economic feasibility of the HOS. The length of thermal stratification is unlikely to significantly change during that time frame, but the supply and demand of drinking water has been shown to be temporally dynamic (Dieter et al., 2018). Although this study only obtained data for potable water production for the first year after installation in 2002, we can speculate on how the supply and demand of drinking water may have changed during the past 18 years based on population growth and water resources of the region. USL is located in between Alameda and Contra Costa County and receives runoff from both areas (Horne et al., 2003; Mobley, 2003). The total

population of the combined area increased moderately from about 2.4 million to 2.8 million from the period between 2000 and 2018 (U.S. Census Bureau, 2020). This area was also impacted by the 2011-2017 California drought (Kam et al., 2019). This likely led to increased reliance on source water treatment for drinking water production. These factors indicate it is possible that the total treatability benefit of the HOS was underestimated under the assumption that the daily potable water production at USLWTP was consistent with the baseline expectations from the first year following operations in 2002. These results further support the contention that the baseline economic analysis may have underestimated the profitability of the HOS and the system may be highly profitable over the total lifetime of the system.

4.2 Oxygenation and GHG emissions at USL

The LCA model results, demonstrating 25% lower emissions for the baseline model and significantly lower average Monte Carlo simulations for all three parameter probability distributions, indicates that HOS implementation in USL to improve source water treatability is likely to reduce overall LC-GHG emissions. The baseline LCA results revealed that a moderate reduction in LC-GHG emissions could be expected from the installation and operation of the HOS at USL with a much tighter range of potential LC-GHG emissions overall compared with the economic analysis, indicating higher model confidence (Figure 1.7). As previously mentioned, multiple studies have shown oxygenation to have a sustained long-term benefit in improving water quality and other studies have shown future predictions of further degraded water quality in eutrophic reservoirs, indicating that the treatability benefit observed by USLWTP in the first year of operations will continue and may be enhanced. The Monte Carlo simulations resulted in very similar distributions regardless of the probability distribution, except for the fact that both scenarios had a much high variance and range of potential outcomes under the uniform probability distribution simulation (Figure 1.9). The triangular and normal probability distributions found a very high likelihood of the HOS scenario leading to decreased emissions with a highly significant difference ($p < 0.001$) between the means of the two scenarios and only 4.4% overlap for the normal distributions and 5.2% overlap between the scenarios for the triangular distribution. Even with the larger variance, there was still a highly significant difference ($p < 0.001$) between the means of the uniform probability distribution scenarios and only 14.2% overlap between the scenarios. Overall, the results of the LCA reveal a high probability that the HOS implementation at USL will lead to a reduction of GHG emissions over the lifetime of the system.

The sensitivity analysis results (Figure 1.8) indicate that ozone requirement in the treatment process is the most critical parameter. Chlorine requirement was also found to be an important parameter, demonstrating that the HOS impact on LC-GHG emissions will be primarily based on the observed improvement of water quality in USL reservoir over the lifetime of the HOS. As ozonation was found to be a highly significant parameter in the economic analysis, its prominence in the LCA model is not surprising. The reliance of the LCA model on the ozonation parameter provides further evidence to support the potential of the HOS to reduce LC-GHG emissions due to the previously mentioned potential for enhanced future eutrophication of non-oxygenated reservoirs.

The reduction in chlorine requirement can be primarily attributed to the reduction in dissolved manganese in the reservoir source water, as chlorine was used to control the levels of dissolved manganese through oxidative precipitation (Jung, 2003). The previously mentioned reviews of hypolimnetic oxygenation in reservoirs also noted a substantial and sustained decrease in manganese release in oxygenated reservoirs, so this benefit could be expected to continue into the future (Beutel and Horne, 1999; Preece et al., 2019; Gantzer et al., 2009). Together, the ozone and chlorine requirement in the source water treatment process comprises more than 75% of the total emissions in the HOS scenario, signifying the importance of water treatment operations on the LC-GHG emissions and demonstrating the requirement of the HOS to improve treatability in order to reduce overall emissions.

HOS construction accounted for less than 1% of the total LC-GHG emissions for the HOS Scenario and HOS oxygen use accounted for more than 20% of the HOS scenario emissions, indicating that HOS oxygen demand plays a much larger role in determining overall system LC-GHG emissions compared to raw material use and transportation. The LCA sensitivity analysis also demonstrates the important of oxygen transfer efficiency. HOS oxygen use was found to be a highly sensitive parameter, while none of the parameter assumptions regarding the raw material sourcing or transportation had any noticeable impact on the total LC-GHG emissions (Figure 1.8). Oxygen transfer efficiency has been shown to vary widely among HOS systems and based on reservoir characteristics such as depth, hypolimnion temperature, and oxygen demand (Beutel and Horne, 1999; Singleton and Little, 2006; McGinnis and Little, 1998). Research on long-term oxygenation at two separate reservoirs revealed that hypolimnetic oxygen demand decreases by approximately 50% over the period of five years, likely due to the mineralization of legacy organic matter (Gantzer et al., 2009). If this result is observed at USL reservoir, HOS oxygen use will decrease substantially and the overall HOS scenario LC-GHG emissions could decrease by up to 14% (Figure 1.8). This study found that HOS oxygen use is a much larger contributor to the total system LC-GHG emissions, indicating that HOS efficiency of oxygen transfer and changes in system oxygen demand appears to be the most important factors when considering the HOS system design on the LC-GHG emissions.

4.3 Limitations of this study and future work

Our results are primarily limited by the availability of data regarding the impact of oxygenation on the reduction in chemical usage in treatment processes. This includes the lack of observational data, which was limited to 3 years of treatment data prior to HOS implementation and one year of data post-HOS implementation (Jung, 2003; Mark Mobley, personal communications). Future conditions are also highly unpredictable and may vary widely from the observed impacts of the HOS on treatability, which were utilized in the baseline economic and LCA models but are likely captured the Monte Carlo analyses through analyzing the combined impacts of the possible ranges in input parameter values. Although this study found a positive economic impact and reduction in LC-GHG emissions, primarily due to the reduction in the use of treatment chemicals,

oxygenation may have provided additional benefits that were not encapsulated in this analysis. Coagulant polymer dosage was found to be reduced significantly after the implementation of the HOS, but this was not included in the LCA or economic analysis due to the lack of quantitative data for USLWTP coagulant polymer use. A recent study found that hypolimnetic oxygenation in a drinking water reservoir led to a substantial reduction in chemical treatment costs, of which more than 17% could be attributed to reduced coagulant and polymer use (Mobley et al., 2019). Additionally, two separate LCAs on conventional water treatment of surface water sources found that coagulant use accounted for more than 20% of the total LC-GHG emissions (Barrios et al., 2008; Vince et al., 2008). Overall, the data limitation in this LCA and economic analysis suggests that oxygenation at USL may have led to additional and potentially substantial economic benefits and reductions in LC-GHG emissions that were not captured in this study's analyses.

4.4 Implications for sustainable reservoir management and drinking water treatment

The contrasting results of the greater importance of construction costs in the economic analysis compared with the substantially larger emissions related to HOS oxygen use in the LCA indicates that oxygen transfer efficiency is a more significant driver of LC-GHG emissions, while construction costs appear to be more important in the overall financially profitability of HOS implementation. As previously mentioned, hypolimnetic oxygen transfer efficiency plays an important role in the overall emissions of HOS and can range from around 30% to more than 95% depending on the system design and reservoir characteristics (Beutel and Horne, 1999; Gantzer et al., 2009; McGinnis and Little, 1998). The HOS at USL utilizes a linear bubble plume system which is moderately inexpensive, simple, and has generally shown high transfer efficiencies in deep (>20 m) reservoirs with high oxygen demands when low oxygen input rates are used (Beutel and Horne, 1999; Gantzer, 2009). Singleton et al. (2007) created and validated a model to predict the oxygen transfer rate and efficiency of linear bubble plume systems which includes the gas flow rate, diffuser length, width, and placement depth, as well as water temperature, conductivity and oxygen concentration. This model was used by Gantzer et al. (2009) which found a very high efficiency of around 95% in a 62 m deep reservoir with a feed rate of 1,000 kg O2/day and around 80% oxygen transfer efficiency in a 21 m deep reservoir with a feed rate of 2,100 kg O2/day. The higher feed rate in the shallower reservoir was required to supply enough oxygen to meet a larger oxygen demand. This demonstrates how a linear bubble plume diffuser system can be extremely efficient in deeper reservoirs with lower oxygen demands, but also shows how reduced efficiencies could be expected in shallower reservoirs with higher oxygen demands. A Speece Cone is a more complex system that consists of an inverted steel cone where oxygen gas and hypolimnetic water, moved with a large submerged electrical pump, are injected into the top of the cone to maximize contact time and oxygen transfer efficiency (Speece, 1994). These systems have been predicted to maintain high oxygen transfer efficiencies of around 95% in depths of less than 10 m while still delivering large quantities of oxygen (> 2,000 kg O2/day)

(McGinnis and Little, 1998). However, these complex systems require electricity for operation and are much more expensive to implement, with an installation and constructions costs ranging between $1.8 to $2.9 million in two San Diego reservoirs (Little, n.d.; Orlowski, 2014). These systems also have the benefit of discharging oxygenated horizontally over the sediment, which may better maintain oxygenated conditions at the sediment-water interface, the site of biogeochemical recycling of nutrients and metals, relative to line diffuser systems which discharge oxygen upwards (Beutel et al., 2020; Beutel et al., 2014). The USL reservoir has a moderate maximum hypolimnion depth of approximately 35 m, a moderately high hypolimnetic oxygen demand, and the optimized feed rate during initial operations was 1,450 kg O2/day, suggesting that it would likely have a moderately high transfer efficiency rate of around 80% (Horne et al., 2003; Jung, 2003). These results suggest that predictive models of oxygen transfer efficiency can be of great use to reservoir managers who are considering hypolimnetic oxygenation to improve water quality in a drinking water reservoir.

The potential for increased future eutrophication and harmful algal blooms could result in enhanced treatability benefits of future drinking water reservoir oxygenation, leading to increased economic feasibility and environmental sustainability of HOS implementation. Evidence suggests that urbanization and climate change will enhance the severity of eutrophication and algal blooms, due in part to enhanced urban runoff and agricultural runoff as well as increased nitrogen deposition (Carey et al., 2012; O'Neil et al., 2012; Savage et al., 2010; Paerl, 2009). The IPCC also predicts increased ambient air temperatures and a longer period of warm weather in the future (Marcé and Armengol, 2009). This could potentially lead to longer period of favorable conditions for algal growth, an increased period of thermal stratification, and enhanced hypolimnetic oxygen depletion due to higher rates of microbial respiration caused by warmer water (Horne and Goldman, 1994; O'Neil et al., 2012). With the expectation that urbanization and climate change will likely magnify the overall occurrence and impacts of eutrophication, hypolimnetic oxygenation of drinking water reservoirs may be a valuable tool to reduce future accelerating burdens of increased treatability challenges, resulting in financial gains and reductions in GHG emissions into the future.

5. Conclusions

This analysis of oxygenation at USL reservoir is intended to inform reservoir managers about the potential economic impact and potential drop in net GHG emissions related to HOS to enhance treatability of raw water from eutrophic drinking reservoirs. This study also highlights the most critical components and how they can be optimized to reduce emissions and increase overall profitability. The results of the economic analysis suggest that initial construction costs are the largest economic burden and must be offset with enhanced treatability, which is dependent on the reduction in chemical usage and the total volume of drinking water produced, while the HOS oxygen requirement is less important overall. The LCA results suggest that enhanced treatability is also important, but that construction is insignificant to the total LC-GHG emissions. Instead the HOS oxygen requirement contributes a substantial amount to overall emissions. The insight into the overall impact on carbon emissions will be relevant to other eutrophic reservoirs

that experience degraded water quality and require advanced treatment measures due to anaerobic conditions, but the impact on emissions will vary greatly based on site specific water quality and the treatment processes. Overall, this LCA can be utilized in conjunction with the economic analysis to enlighten reservoir owners and operators as to the overall impact of oxygenation so that they can make informed decisions based on the current water quality and treatment efficiency of the source water in the reservoirs which they manage.

6. References

Aghakouchak, A., Cheng, L., Mazdiyasni, O., Farahmand, A., 2014. Global warming and changes in risk of concurrent climate extremes: Insights from the 2014 California drought. Geophysical Research Letters, 41(24), 8847–8852.

Bare, J., 2012. Tool for the Reduction and Assessment of Chemical and Other Environmental Impacts (TRACI) TRACI version 2.1 User's Guide. US EPA Office of Research and Development, Washington, DC, EPA/600/R-12/554, 2014

Beutel, M.W., Fuhrmann, B., Herbon, G., Chow, A., Brower, S., Pasek, J., 2020. Cycling of methylmercury and other redox-sensitive compounds in the profundal zone of a hypereutrophic water supply reservoir. Hydrobiologia, in press.

Beutel, M., Dent, S., Reed, B., Marshall, P., Gebremariam, S., Moore, B., Shallenberger, E., 2014. Effects of hypolimnetic oxygen addition on mercury bioaccumulation in Twin Lakes, Washington, USA. Science of The Total Environment, 496, 688-700.

Beutel, M.W., 2003. Hypolimnetic Anoxia and Sediment Oxygen Demand in California Drinking Water Reservoirs. Lake and Reservoir Management, 19(3), 208–221.

Beutel, M.W., Horne, A.J., 1999. A Review of the Effects of Hypolimnetic Oxygenation on Lake and Reservoir Water Quality. Lake and Reservoir Management, 15(4), 285–297.

Barrios, R., Siebel, M., Helm, A.V.D., Bosklopper, K., Gijzen, H., 2008. Environmental and financial life cycle impact assessment of drinking water production at Waternet. Journal of Cleaner Production, 16(4), 471–476.

Bastviken, D., Cole., J., Pace, M., Tranvik, L., 2004. Methane emissions from lakes: Dependence of lake characteristics, two regional assessments, and a global estimate, Global Biogeochm. Cycles, 18, GB4009.

Bonton, A., Bouchard, C., Barbeau, B., Jedrzejak, S., 2012. Comparative life cycle assessment of water treatment plants. *Desalination*, *284*, 42–54.

Britton, L.J., Ferreira, R.F., Averett, R.C., 1974. Limnological Data from Selected Lakes in the San Francisco Bay Region (pp. 24–25). Menlo Park, CA: United States Geological Survey, Water Resources Division.

Carey, C. C., Ibelings, B. W., Hoffmann, E. P., Hamilton, D. P., Brookes, J. D., 2012. Eco-physiological adaptations that favour freshwater cyanobacteria in a changing climate. Water Research, 46(5), 1394–1407.

Clarke, K. C., Hoppen, S., Gaydos, L., 1997. A self-modifying cellular automaton model of historical urbanization in the San Francisco Bay area. Environment and Planning B: Planning and Design, 24(2), 247–261.

Dolman, A.M., Rücker, J., Pick, F.R., Fastner, J., Rohrlack, T., Mischke, U., Wiedner, C., 2012. Cyanobacteria and Cyanotoxins: The Influence of Nitrogen versus Phosphorus. PLoS ONE, 7(6).

Dieter, C.A., Maupin, M.A., Caldwell, R.R., Harris, M.A., Ivahnenko, T.I., Lovelace, J.K., Barber, N.L., Linsey, K.S., 2018. Estimated use of Water in the United States in 2015. U.S. Geological Survey Circular 1441, Reston, VA, p. 65.

Diffenbaugh, N. S., Swain, D. L., Touma, D., 2015. Anthropogenic warming has increased drought risk in California. Proceedings of the National Academy of Sciences, 112(13), 3931–3936.

Finkbeiner M., Inaba A., Tan R.B.H, Christiansen K., Klüppel H-J., 2006. The new international standards for Life Cycle Assessment: ISO 14040 and ISO 14044. Int J Life Cycle Assess 11:80– 85

Gantzer, P.A., Bryant, L.D., Little, J.C., 2009. Controlling soluble iron and manganese in a water-supply reservoir using hypolimnetic oxygenation. Water Research, 43(5), 1285–1294.

Gantzer, P.A., Bryant, L.D., Little, J.C., 2009. Effect of hypolimnetic oxygenation on oxygen depletion rates in two water-supply reservoirs. Water Research, 43(6), 1700–1710.

Godskesen, B., Meron, N., Rygaard, M., 2018. LCA of Drinking Water Supply In Hauschild, M., Rosenbaum, R.K., Olsen, S.I., 2018. Life cycle assessment: theory and practice (pp. 840-842). Cham, Switzerland: Springer.

Goel, N., Salveson, A., 2012. City of Palo Alto Long Range Facilities Plan for the Rwqcp, Appendix P - Ozone Sizing and Cost Estimate for TOrC Removal (pp. 2–11). Palo Alto, CA: City of Palo Alto.

Hanley, R., Joyce, M., Hall, T., Monaghan, S., Wall, B., Page, D., 2011. Water Treatment Manual: Disinfection. Wexford, Ireland: Office of Environmental Enforcement.

Horne, A. J., Beutel, M., 2019. Hypolimnetic oxygenation 3: an engineered switch from eutrophic to a meso-/oligotrophic state in a California reservoir. Lake and Reservoir Management, 35(3), 338–353.

Horne, A. J., Rowan, R., Toms, C., 2003. The 2002 Oxygen Bubble Plume Hypolimnetic Oxygenation System in Upper San Leandro Reservoir: Effectiveness for Internal Nutrient Load Reduction, Effect on Benthic Blue-Green Algae and Potential to Reduce Taste and Odor Causing Blue Green Algae. Report to East Bay Municipal District. University of California, Berkeley.

Horne, A. J., Goldman, C. R., 1994. Limnology. New York: McGraw-Hill.

Houghton, J.T, Ding, Y., Griggs, D.J., Noguer, M., van der Linden, P.J., Dai, X., Maskell, K., Johnson, C.A., 2001. Climate Change 2001: The Scientific Basis, Third Assessment Report of the Intergovernmental Panel on Climate Change. Cambridge, United Kingdom: The Press Syndicate of the University of Cambridge.

Igos, E., Dalle, A., Tiruta-Barna, L., Benetto, E., Baudin, I., Mery, Y., 2014. Life Cycle Assessment of water treatment: what is the contribution of infrastructure and operation at unit process level? Journal of Cleaner Production, 65, 424–431.

Johnson, T., Schreifels, J., Dorn, J., Hoer, M., Cooley, D., Siegel, K., 2020. The Emissions & Generation Resource Integrated Database Technical Support Document for eGRID with Year 2018 Data. Rockville, MD: U.S. EPA Office of Atmospheric Programs Clean Air Markets Division.

Jung, R., 2003. Upper San Leandro Hypolimnetic Oxygenation System Preliminary Evaluation Report. Process Engineering Section, East Bay Municipal Utility District.

Kam, J., Stowers, K., Kim, S., 2019. Monitoring of Drought Awareness from Google Trends: A Case Study of the 2011–17 California Drought. Weather, Climate, and Society, 11(2), 419–429.

Little, J. (n.d.). Introduction to Oxygenation and Aeration Systems. Blacksburg, VA: Civil and Environmental Engineering, Virginia Tech.

Mann, M.E., Gleick, P.H., 2015. Climate change and California drought in the 21st century. Proceedings of the National Academy of Sciences, 112(13), 3858–3859.

Marcé, R., Armengol, J., 2009. Water Quality in Reservoirs Under a Changing Climate. The Handbook of Environmental Chemistry Water Scarcity in the Mediterranean, 73–94.

McGinnis, D. F., Little, J.C., 1998. Bubble dynamics and oxygen transfer in a speece cone. Water Science and Technology, 37(2).

Mercer, L. J., Morgan, W. D., 1985. Conservation Using a Rate of Return Decision Rule: Some Examples from California Municipal Water Departments. Water Resources Research, 21(7), 927–933.

Mobley, M., Vice President and Principal Engineer, Mobley Engineering, personal communication, September 10, 2019.

Mobley, M., 2012. Upper San Leandro CA, 2012. Retrieved from http://www.mobleyengineering.com/usl2.html#

Mobley, M., Gantzer, P., Benskin, P., Hannoun, I., Mcmahon, S., Austin, D., Scharf, R., 2019. Hypolimnetic oxygenation of water supply reservoirs using bubble plume diffusers. Lake and Reservoir Management, 35(3), 247–265.

Mobley, M., Jung, R., Lai, H., 2003. Upper San Leandro Hypolimnetic Oxygenation System. North American Lake Management Society. Foxwoods Resort, Connecticut.

Mobley, M. Ruane, J., Harshbarger, D., 2000. And then it sank… The development of an oxygen diffuser for hydropower. Hydrovision. Charlotte, North Carolina.

Moore, B., Mobley, M., Little, J., Kortmann, B., Gantzer, P., 2015. Aeration and Oxygenation Methods for Stratified Lakes and Reservoirs (pp. 21-28). NALMS: Lakeline.

Novak, K., Loughlin, A., Mann, M., 2011. Bulk or on-site generation: what's your hypochlorite solution. Paper presented at the Ohio Water Environment Association, Sandusky, OH.

O'Neil, J., Davis, T., Burford, M., Gobler, C., 2012. The rise of harmful cyanobacteria blooms: The potential roles of eutrophication and climate change. Harmful Algae, 14, 313–334.

Orlowski, L., 2014. Lake Hodges Reservoir Water Quality Assessment Study Final Conceptual Planning Report. San Diego, CA: Brown and Caldwell.

Paerl, H.W., 2009. Controlling Eutrophication along the Freshwater–Marine Continuum: Dual Nutrient (N and P) Reductions are Essential. Estuaries and Coasts, 32(4), 593–601.

Perkins, R., Slavin, E., Andrade, T., Blenkinsopp, C., Pearson, P., Froggatt, T., Godwin, G., Parslow, J., Hurley, S., Luckwell, R., Wain, D. 2019. Managing taste and odour metabolite production in drinking water reservoirs: The importance of ammonium as a key nutrient trigger. Journal of Environmental Management, 244, 276–284.

Preece, E.P., Moore, B.C., Skinner, M.M., Child, A., Dent, S., 2019. A review of the biological and chemical effects of hypolimnetic oxygenation. Lake and Reservoir Management, 35(3), 229–246.

Savage, C., Leavitt, P.R., Elmgren, R., 2010. Effects of land use, urbanization, and climate variability on coastal eutrophication in the Baltic Sea. Limnology and Oceanography, 55(3), 1033–1046.

Schindler, D.W., 2006. Recent advances in the understanding and management of eutrophication. Limnology and Oceanography, 51(1, pt. 2), 356–363.

Singleton, V.L., Gantzer, P., Little, J.C., 2007. Linear bubble plume model for hypolimnetic oxygenation: Full-scale validation and sensitivity analysis. Water Resources Research, 43(2).

Singleton, V.L., Little, J.C., 2006. Designing Hypolimnetic Aeration and Oxygenation Systems − A Review. Environmental Science & Technology, 40(24), 7512–7520.

Smith, V.H., Sieber-Denlinger, J., Denoyelles, F., Campbell, S., Pan, S., Randtke, S.J., Strasser, V.A., 2002. Managing Taste and Odor Problems in a Eutrophic Drinking Water Reservoir. Lake and Reservoir Management, 18(4), 319–323.

Speece, R.E., 1994. Lateral thinking solves stratification problems. Wat. Qual. Int. 3:12-15.

Sproul, E., Barlow, J., Quinn, J.C., 2019. Time Value of Greenhouse Gas Emissions in Life Cycle Assessment and Techno-Economic Analysis. Environmental Science & Technology, 53(10), 6073–6080.

Teefy, S., Manager of Water Quality, East Bay Municipality District, personal communication, September 3, 2019.

U.S. Census Bureau, 2020. Contra Costa County, California; Alameda County, California. Retrieved from ttps://www.census.gov/quickfacts/fact/table/contracostacountycalifornia,alamedacountycalifornia/PST045219

Vaga, T., 1990. The Coherent Market Hypothesis, Financial Analysts Journal, 46:6, 36-49.

Vince, F., Aoustin, E., Bréant, P., Marechal, F., 2008. LCA tool for the environmental evaluation of potable water production. Desalination, 220(1-3), 37–56.

Table 1.1 Pre and Post-HOS water quality and treatment associated parameters

Hypolimnetic water quality parameters	Pre-HOS	Post-HOS
Dissolved Oxygen (mg/L)	0 to 2	5 to 15
Phosphate (ug-P/L)	225	147
Ammonia (ug-N/L)	270	8
Nitrate (ug-N/L)	180	420
TOC (mg/L)	~ 5	~ 5
Manganese		↓↓
Treatment associated parameters	**Pre-HOS**	**Post-HOS**
Geosmin (ng/L)	~ 200	< 5
BGA population at outlet (filaments/cm^2)	~68,000	~15,000
THMs (ug/L)	41	18
Bromides (mg/L)	0.04	0.045
Total chemical cost ($/MG)	~$80	~$50
Cl_2 dose		-18%
Ozone dose		-45%
H_2O_2 dose		Eliminated
Alum Dose		↑
Coagulant polymer dose		↓↓

TOC – Total Organic Carbon
BGA – Blue-Green Algae
THM – trihalomethane
MG – Million Gallons
Cl_2 – Chlorine
H_2O_2 – Hydrogen peroxide

Table 1.2 Financial parameter assumptions

Parameter	Units	Baseline Value	Minimum Benefit	Maximum Benefit	Source for Baseline Value	Source for Range
HOS initial construction (2002)	$	$512,000			e	
HOS expansion (2012)	$	$520,000			e	
Maintenance cost	$/event	$39,000	$62,200	$27,400	a	N/A
Maintenance schedule	Frequency	Every 12 yrs	Every 10 yrs	Every 15 yrs	e	e
Potable water production	MG/day	23.0	19.9	30.0	d	N/A
Operational period	day/yr	173	153	193	d,f	N/A
HOS lifetime	yr	60	50	100	e	e
Ozone reduction	mg/L	2.25	1.57	2.94	d	N/A
H_2O_2 reduction	gal/MG	1.55	1.16	1.88	a	N/A
Chlorine reduction	mg/L	2.50	0	5.35	d	N/A
HOS oxygen use	ton/day	1.60	2.00	0.80	a	c
Ozone cost savings	$/MG	$15.00	$10.50	$19.60	d,f	N/A
H_2O_2 cost savings	$/MG	$12.00	$8.98	$14.60	d,f	N/A
Chlorine cost savings	$/MG	$3.00	$0	$6.42	d,f	N/A
HOS oxygen cost	$/day	$162	$202	$80.80	d	c

[a] Based on average material pricing
[b] Based on requirement and treatment volume
[c] (Beutel, 2003; Gantzer et al., 2009)
[d] (Jung, 2003)
[e] (Mark Mobley, personal communications)
[f] (Mobley, 2003)

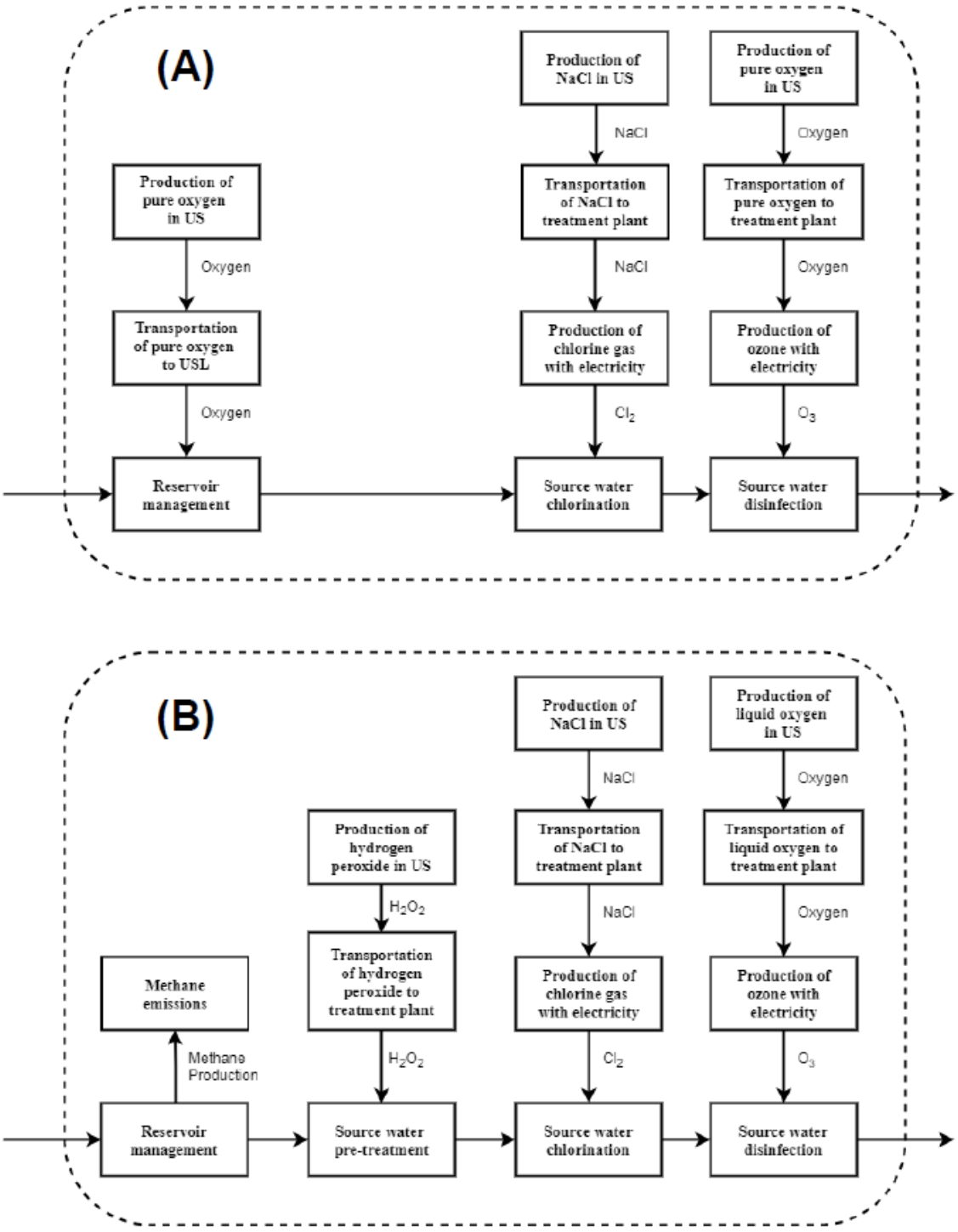

Figure 1.1 System Diagram for each modeled LCA scenario showing treatment process and reservoir gas emission system boundary. **(A)** HOS scenario and **(B)** Standard Scenario.

Table 1.3 Treatment and reservoir management parameters modeled in comparative LCAs

		Standard Operations			HOS Operations		
Parameter	Units	Base Value	Min Value	Max Value	Base Value	Min Value	Max Value
USLWTP Treatment							
Scenario lifetime	yr	60	50	100	60	50	100
Annual operation period	d	173	153	193	173	153	193
Potable water production	MG/d	19.9	19.9	25.9	23.0	19.9	30.0
Ozone Treatment							
Ozone requirement	mg/L	5.00	3.57	6.25	2.75	2.06	3.43
Oxygen use for O_3 production	kg/MG	189	135	237	104	78	130
Distance to oxygen supplier	km	32.3	28.3	48.3	32.3	28.3	48.3
Electricity to produce O_3	kWh/kg	11.3			11.3		
Hydrogen Peroxide Treatment							
50% H_2O_2 requirement	gal/MG	1.55	1.16	1.88			
50% H_2O_2 usage	kg/MG	7.02	5.26	8.52			
Chlorine treatment							
Chlorine requirement	mg/L	13.9	10.4	17.4	11.4	8.55	13.9
NaCl use	kg/MG	157.8	118.2	197.7	129	97.2	162
Distance to NaCl supplier	km	37	32	40	37	32	40
Electricity to produce Cl_2	kWh/kg	4.8	4.4	5.5	4.8	4.4	5.5
Reservoir Management Activities							
Methane emissions	kg/yr	1,470	1,120	1,800			
Daily oxygen use	kg/d				1,450	726	1,810

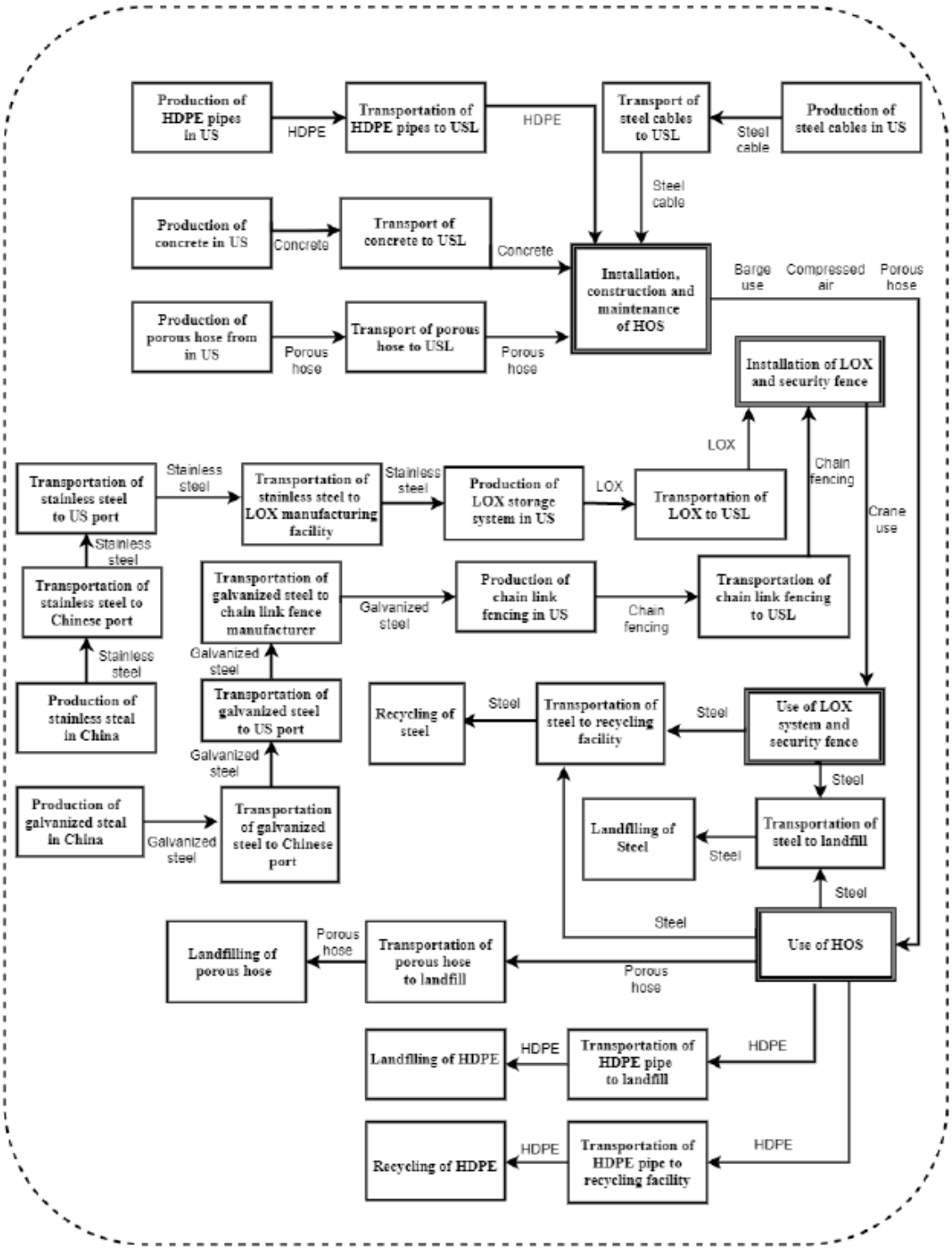

Figure 1.2 HOS construction, installation, and maintenance system boundary.

Table 1.4 HOS and oxygen use parameters modeled in the HOS scenario LCA

Parameter	Units	Min Value	Base Value	Max Value	Base Source	Range Source
HOS construction and maintenance						
HDPE use	kg		23,900		c	
Fraction recycled HDPE used	-	0	0.5	1.0	N/A	N/A
Distance to HDPE source	km	31.2	36.6	41.8	a	b
Porous hose use	kg		2,100		c	
Porous hose lifetime	yr	10	12	15	c	c
Distance to hose source	km	21.8	29.8	40.3		b
Steel cable use	kg	4,880	9,750	19,500	c	
Distance to cable source	km	50.2	58.9	68.9	a	b
Concrete use	kg		61,000		c	
Distance to concrete source	km	30.1	38.1	39.9	a	b
HOS installation time	hr	25	100	200	N/A	N/A
Barge transport distance	km	231	242	248	N/A	N/A
Barge reservoir use	km	28.4	42.6	85.2	N/A	N/A
Barge weight	kg	122,000	244,000	488,000	N/A	N/A
Oxygen storage (LOX) construction						
Stainless steel (S. steel) use	kg	4,880	9,750	19,500	N/A	N/A
S. steel source to port distance	km	1,700	1,800	2,000	a	b
S. steel ocean transport distance	km	9,000	9,500	10,000	a	b
S. steel distance to LOX producer	km	48.3	51.5	60.0	a	b
Galvanized steel (G. steel) use	kg	62.3	111	171	c	N/A
G. steel distance to port	km	1,700	1,800	2,000	a	b
G. steel ocean transport distance	km	9,000	9,500	10,000	a	b
Chain link fence source distance	km	59.4	68.1	76.4	a	b
LOX construction time	hr	5	10	40	N/A	N/A
LOX install time	hr	0.5	2.0	4.0	N/A	N/A
LOX delivery distance	km	45.9	55.1	61.6	c	b
Recycling and Landfilling						
Distance to recycling center	km	31.7	36.6	39.5	a	b
Distance to landfill	km	25.1	27.5	47.4	a	b
Fraction of steel recycled	-	0.25	0.75	1.0	N/A	N/A
Fraction of HDPE recycled	-	0	0.5	1.0	N/A	N/A

[a] Largest supplier in regional area
[b] Alternative routes by google maps
[c] (Mark Mobley, personal communications)

Table 1.5 Economic analysis results

Parameter	Units	Baseline Value	Min Benefit	Max Benefit
Ozone reduction	$/yr	$59,700	$31,900	$113,500
H_2O_2 elimination	$/yr	$47,700	$27,300	$84,300
Chlorine reduction	$/yr	$11,900	$0	$37,200
HOS oxygen use	$/yr	-$28,000	-$39,000	-$12,400
Total annual HOS operation	$/yr	$91,300	$20,200	$222,600
Net present value (NPV)*	$	$185,000	-$522,000	$1,480,000
Internal rate of return (IRR)	%	13.7%	-0.907%	40.0%
Benefit-to-cost ratio (BCR)*	-	2.41	0.529	3.90
Payback period	years	11.6	67.2**	4.83

*Assuming a 10% Discount Rate

**Greater than the operational period assumed

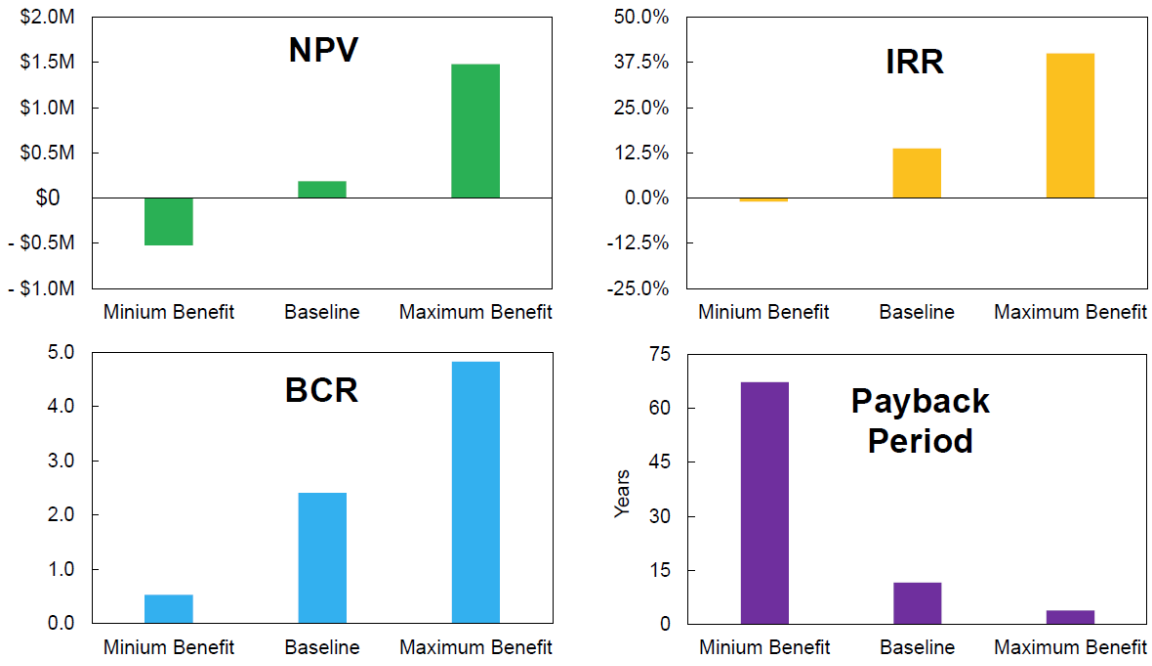

Figure 1.3 Net Present Value (NPV), Internal Rate of Return (IRR), Benefit-cost Ratio (BCR) and Payback Period of USL HOS under the minimum benefit, baseline, and maximum benefit scenarios.

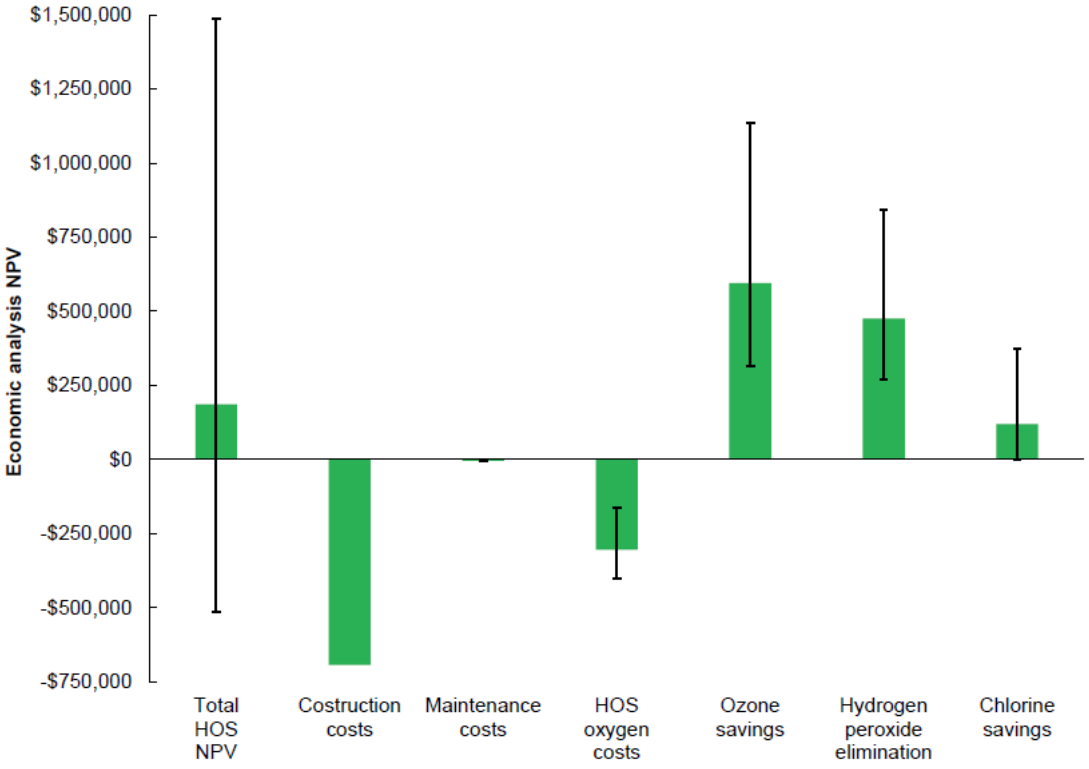

Figure 1.4 Net Present Value (NPV) of the HOS project and of individual parameters. The bars represent the baseline NPV calculated for each individual aspect of the HOS economic impact and the total combined HOS NPV. The error bars represent the range for the maximum benefit and minimum benefit scenarios.

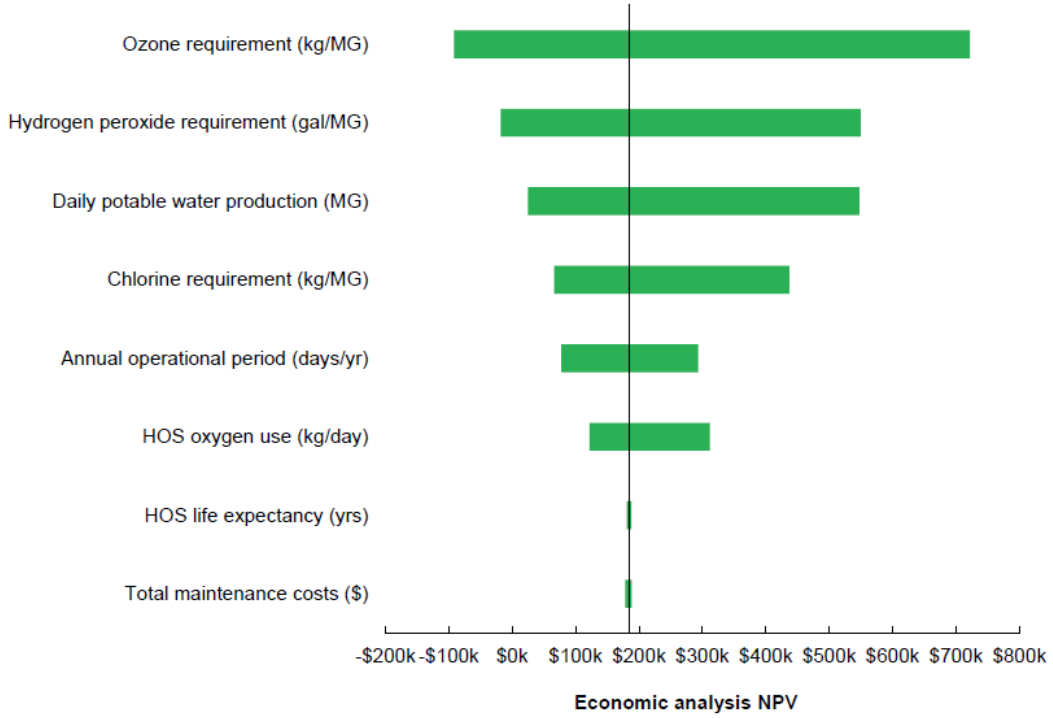

Figure 1.5 Sensitivity NPV analysis for the modeled parameters of the economic analysis. The black line at $185,000 represents the NPV when the baseline parameter values are used. The green bar spans the range of NPVs for each parameter when a parameter is changed from its minimum value to its maximum value. Parameters were excluded from this graph if the total difference between the minimum and maximum parameter values resulted in less than a $5,000 NPV difference.

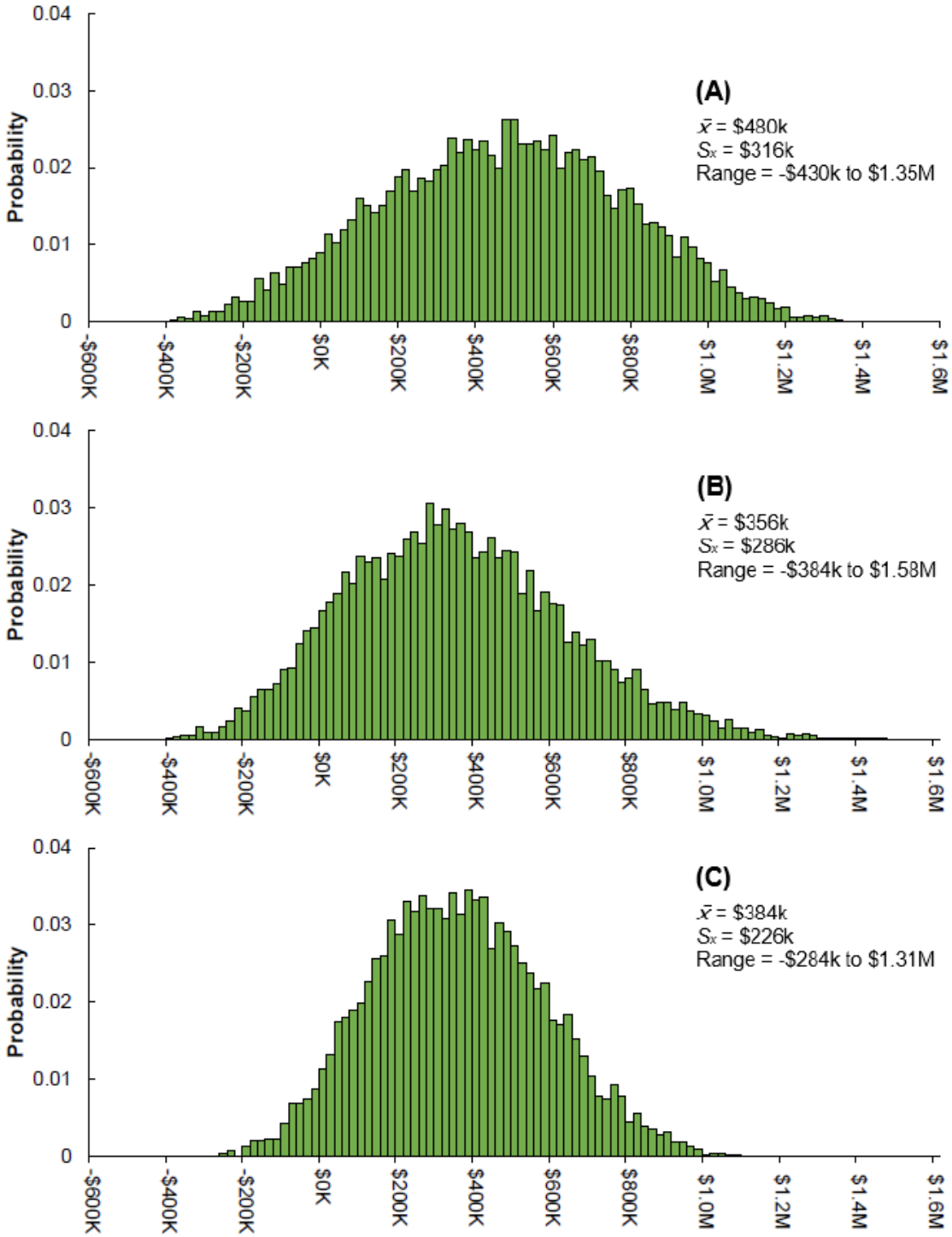

Figure 1.6 Monte Carlo results of probabilistic NPV calculations for USL HOS economic analysis. **(A)** Uniform data distribution, **(B)** Normal data distribution, **(C)** Triangular data distribution.

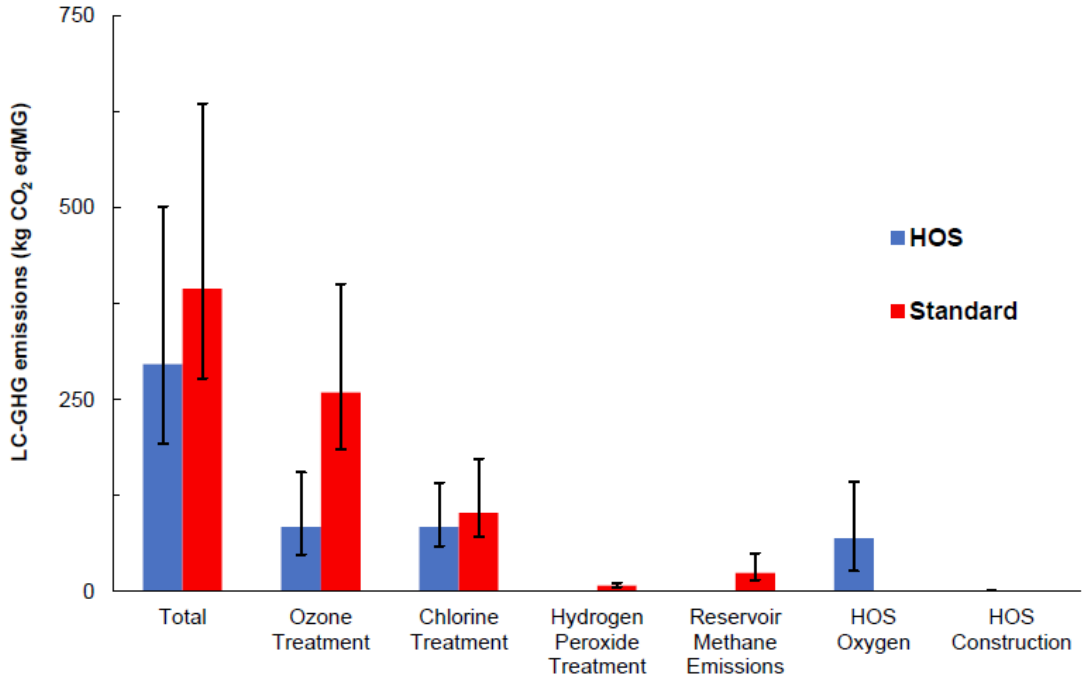

Figure 1.7 Results of the baseline LCA comparison between the reservoir with an operating HOS and a hypothetical normal reservoir. The error bars represent the range for the maximum emissions and minimum emissions results.

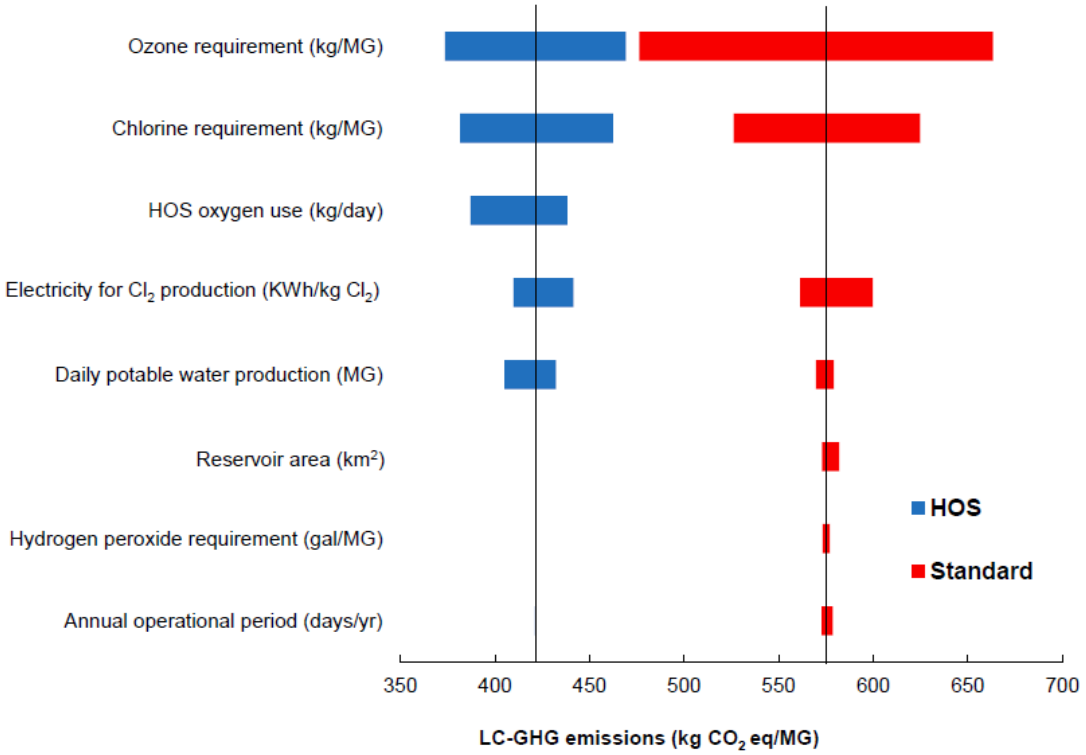

Figure 1.8 Sensitivity analysis for the modeled parameters of the HOS and normal scenario. The black line at 421 kgCO2 eq/MG represents the emissions for HOS scenario and the black line at 575 kgCO2 eq/MG represents the emissions for normal scenario when baseline parameter values are used. The red bar spans the range of LC-GHG emissions for each parameter for the normal scenario when a parameter is changed from its minimum value to its maximum value. The blue bar spans the range of LC-GHG emissions for each parameter for the HOS scenario when a parameter is changed from its minimum value to its maximum value. Parameters were excluded from this graph if the total difference between the minimum and maximum parameter values resulted in less than a 2 kgCO2 eq/MG difference.

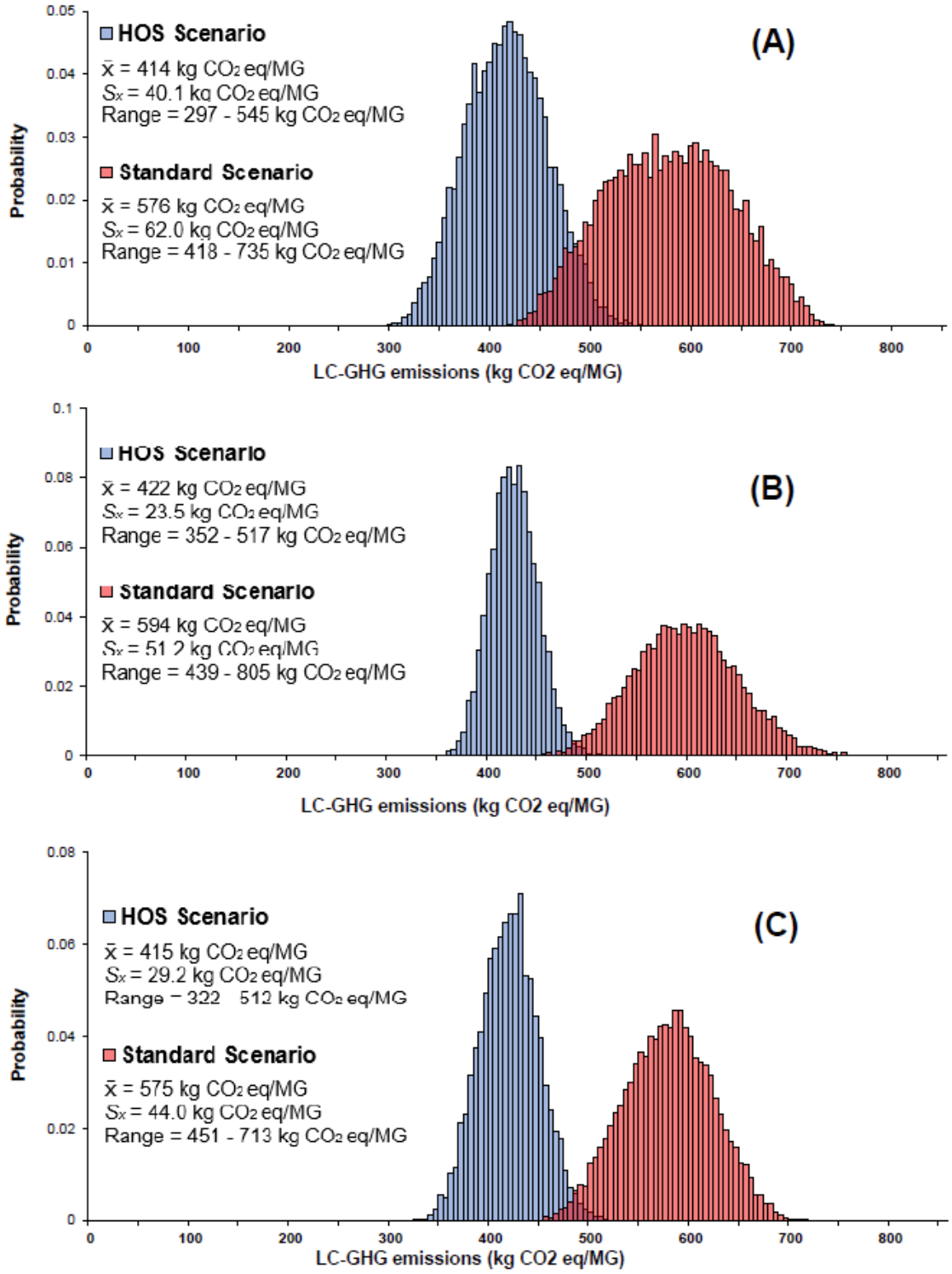

Figure 1.9 Monte Carlo results of probabilistic distribution of HOS and standard LCA scenarios. **(A)** Uniform data distribution, **(B)** Normal data distribution, **(C)** Triangular data distribution.

Chapter 2

Profundal zone dynamics of methylmercury production, transport and degradation during thermal stratification in a hyper-eutrophic reservoir

Abstract

Methylmercury (MeHg), an organic form of mercury that readily bioaccumulates, builds up in anaerobic profundal sediment of productive lakes and reservoirs, which can lead to MeHg release into the hypolimnion where it can enter in aquatic food webs. This study tracked MeHg production, degradation, and release into hypolimnetic water approximately monthly during the period of thermal stratification in the profundal zone of hypereutrophic Hodges Reservoir, San Diego. Associated parameters of interest such as redox acceptors and dissolved organic carbon (DOC) were also measured, with the aim of relating temporal patterns of MeHg production, degradation, and release to biogeochemical parameters at the sediment-water interface. Results demonstrated that large quantities of sediment-associated MeHg were present at the onset of thermal stratification and anaerobic conditions, suggesting MeHg production in profundal sediment may be greatest during moderately reduced redox conditions of the oxic-anoxic transition, due to the abundance and constant replenishment of electron acceptors to fuel anaerobic respiration. MeHg release from the profundal sediment into the hypolimnetic water column and the highest seasonal total water column MeHg concentration was observed while highly bioavailable iron-oxide depletion was rapidly occurring, suggesting iron-oxide dissolution led to the release of OM-associated MeHg. Sulfate-reducing bacteria (SRB) activity in the late spring and early summer, as demonstrated by a reduction in porewater sulfate and enhancement of porewater sulfide, was associated with the build-up of MeHg in profundal sediment. The depletion of sulfate in the porewater during mid-summer appears to have led to methanogenesis and high levels of demethylation, as sediment associated MeHg was dramatically reduced and there was no enhancement of water column MeHg. Results highlight complex temporal dynamics of MeHg production, degradation, and transport into the water column mediated by various microbial groups during different stages of thermal stratification as redox acceptors are depleted and conditions become more reduced. Our study suggests that an early window of reduced conditions may be the primary period of MeHg entry into the water column where it is most susceptible to food web entry. In addition, results demonstrate that the sediment-water interface may become a net sink for MeHg during highly reduced conditions.

1. Introduction

Mercury is a toxic heavy metal with no known biotic function. Human exposure to elevated levels of mercury can cause a variety of serious health problems such as neurological disorders, kidney failure, paralysis, and even death. In the US, mercury contamination is prevalent in approximately 50% of EPA superfund sites (Bigham et al., 2016) and the World Health Organization currently considers mercury to be one of the top ten chemicals of major public health concern (Bose-O'Reilly et al., 2010). Mercury is typically found in trace concentrations in natural ecosystems. However, anthropogenic activity has dramatically increased the prevalence of mercury in the environment. Approximately 2 billion pounds of mercury has been extracted from naturally occurring ores like cinnabar. This extracted mercury is most frequently used in artisanal gold mining and released into the environment after being used (Hylander and Meili, 2003). Other anthropogenic sources of mercury pollution to the environment include coal burning, mining, and oil refinement which produce both volatile and water-soluble mercury (Futsaeter and Wilson, 2013). Water-soluble, inorganic mercury (iHg) species can directly contaminate nearby ecosystems as they are easily transported in water. Volatile mercury enters the atmosphere in the elemental gaseous form (Hg^0) where it reacts to form iHg. This form of mercury can be transported over large distances and returns to the earth with precipitation, accumulating in top soil and water bodies (Bigham et al., 2016).

In the process of mercury methylation, iHg is transformed into organic methylmercury (MeHg) by anaerobic bacteria (Bigham et al., 2016). The anaerobic bacteria specifically implicated in the production of MeHg include sulfate reducing bacteria (SRB), iron(III)-reducing bacteria (IRB), methanogens, and a small number of fermenters (Podar et al., 2015). Although not all anaerobic bacteria are capable of mercury methylation, no known aerobic bacteria have been identified, and MeHg typically accumulates in surface waters under anaerobic conditions (Podar et al., 2015). MeHg can be converted back into either iHg or Hg^0 by a process known as demethylation. MeHg demethylation can occur due to abiotic of biotic processes (Bigham et al., 2016). Abiotic demethylation primarily occurs in the surface water of lakes and reservoirs when MeHg is exposed to UV light (Paranjape, 2017). Biotic demethylation has been demonstrated by a variety of microorganisms and multiple pathways have been identified (Ullrich et al., 2001). Although aerobic organisms are have generally been found to express a greater ability to demethylate MeHg, there is a growing body of evidence that has found anaerobic organisms such as SRB and methanogens are prominent demethylators in freshwater sediments (Beutel et al., 2020; Korthals et al., 1987; Kronberg et al; 2018; Pak et al, 1998; Ullrich et al., 2001). It is important to consider that both iHg methylation and MeHg demethylation play important roles in regulating the net pool of MeHg in aquatic environments.

In productive lakes and reservoirs, such as Hodges Reservoir, the focus of this research, anaerobic conditions develop due to the depletion of oxygen in bottom water during thermal stratification. Thermal stratification is the process of a lake separating into three distinct layers due to temperature differences. The warm surface water is referred to as the epilimnion, the cold, dense bottom water is referred to as the hypolimnion and

encompasses the profundal zone, and the small transition zone between surface and bottom water is referred to as the metalimnion (Horne and Goldman, 1994). During thermal stratification, the hypolimnion is physically separated from the atmosphere and does not significantly interact with the epilimnion due to the metalimnion barrier. High levels of nutrients and organic matter can stimulate microbial activity, causing the depletion of oxygen and the physical separation prevents oxygen from being replenished, resulting in anaerobic conditions in the hypolimnetic profundal zone.

Although iHg and MeHg are both toxic, MeHg is known to bioaccumulate more efficiently in aquatic food webs, resulting in larger concentrations at higher trophic levels such as piscivorous fish, birds of prey, and humans (Futsaeter and Wilson, 2013). Therefore, reducing the conversion of iHg into MeHg is of utmost importance to reservoir managers of mercury-impaired lakes and reservoirs. Management strategies to reduce the impact of mercury contamination has classically involved dredging, which is extremely expensive, invasive, and has failed to resolve the issue in a variety of case studies (e.g., Bigham et al., 2016; Ullrich et al., 2001). Recent research has shown that enhancing the redox potential of anaerobic environments can suppress the accumulation of MeHg in the water column, potentially decreasing its entry into the food web (Duvil et al., 2018; Beutel et al. 2014; Beutel et al., 2016; Beutel et al., 2017; Vlassopoulos et al., 2018).

Tracking changes in MeHg concentration in the water column and sediment, as well as other fundamental parameters related to MeHg production, such as electron acceptors like sulfate and iron-oxide, allows for the qualitative descriptive understanding of the biogeochemical processes associated with trends in MeHg production and transport. This study involved monthly sampling of the water column and profundal sediment at two sites in Hodges Reservoir in Southern California, USA. The first objective of this study was to characterize temporal changes in MeHg concentration in the profundal sediment during thermal stratification and identify potential biogeochemical factors that influence this process. The second objective was to track the transport of MeHg into the water column and determine which environmental process may be involved in this transport. The overarching goal of this study was to synthesize the results of these two objectives to understand temporal anaerobic processes that impact the transport of MeHg into the water column where it can readily biomagnify in the aquatic food web. With a more comprehensive understanding of MeHg cycling at the profundal sediment-water interface and processes that influence the transport of MeHg into the water column, reservoir managers will be better able to develop effective management strategies aimed at repressing MeHg bioaccumulation in lakes and reservoirs and protecting human and wildlife health.

2. Methods

2.1 Study site

This research focuses on Hodges Reservoir, a hypereutrophic reservoir in San Diego, California located within the 64,000 hectare San Dieguito watershed, which

receives substantial inputs of urban and agricultural runoff. The high historical input of runoff has led to degraded water and sediment quality due to the introduction of large quantities of organic matter and nitrogen. When Hodges Reservoir becomes thermally stratified, aerobic microbial respiration in the hypolimnion leads to a depletion of dissolved oxygen (DO) and the onset of anoxic conditions. This anoxia results in the release of ammonia and phosphate from the profundal sediment, which stimulates algal growth if transported into the photic zone (Beutel et al., 2020). Chlorophyll a concentrations can exceed 100 µg/L during the summer at Hodges Reservoir. The water column contains a high concentration of sulfate (>150 mg/L) and sulfate reduction is a prominent process during the summer, with up to 30 mg/L sulfide observed in the hypolimnion during reduced conditions (Beutel et al., 2020). 2017 field monitoring revealed that MeHg accumulated in the profundal water column beginning in April, with concentrations peaking in June and July before decreasing between August to October (Beutel et al., 2020). In a 2018 laboratory incubation study, the increase of MeHg was speculated to be primarily the result of methylation by SRB, while the decrease in MeHg concentration was attributed to a transition into methanogenic conditions and enhanced rates of demethylation (Fuhrmann et al., in review).

2.2 Collection of sediment, porewater and water

In 2018, water column and sediment samples were collected approximately monthly from April to November at Hodges Reservoir. Reservoir water was collected every 3 m at a location in the reservoir that is approximately 19 m deep and in close proximity to the dam. For each sampling event, water was collected at each depth using a 2.2 L acrylic Van Dorn water sampler to fill a 200 mL HDPE bottle which was pre-preserved with 0.5 mL of 2 N Zinc Acetate for sulfide analysis (0.25% v/v) and a 1 L HPDE bottle for total suspended solids (TSS), dissolved organic carbon (DOC), total iron (Fe_T), and sulfate analysis. Additional water at the same depths was collected using a 1 L Teflon Kemmerer water sampler to fill trace metal grade certified, 125 mL FPE bottles for MeHg.

Profundal sediment from this location was also collected with an Ekman dredge, which was brought to the surface while maintaining at least 4-6 cm of hypolimnetic water overlaying the sediment. Sediment from approximately 0-3 cm below the surface was quickly transferred into an acid washed, 250 mL wide-mouth glass canning jar which was overfilled with hypolimnetic water to exclude air. Sediment and water samples were kept in the dark and placed on ice after procurement and during transport back to the laboratory. Samples were stored overnight at 4 °C and processed within 24 hours of collection. During processing in the lab, sediment was transferred to an anaerobic glovebox and homogenized. Porewater was extracted using four 50 mL centrifuge containers which were filled with sediment in an anaerobic glovebox, capped to exclude oxygen, and transferred to a Sorvall Super T21 refrigerated benchtop centrifuge. Porewater was extracted from the sediment by centrifuging at 4,000 RPM for 20 minutes at 4 °C according to Gobeil and Cossa (1993).

2.3 Water, porewater, and sediment chemical analysis

After each sampling event, approximately 250 mL of reservoir water was extracted from each 1 L HPDE bottle from each depth and filtered using Whatman GF/C 1.2 µm glass fiber filters. The filters were placed in an oven at 105 ^{o}C for 1 hour and the mass of TSS in each sample was determined by difference according to Standard Methods (Baird et al., 2005). Approximately 40 mL of water from each 1-L HPDE bottle was filtered with Whatman 0.45 µm nylon membrane filters and the filters were stored frozen in a 50 mL HPDE container for sulfate and DOC analysis. Approximately 10 mL of water from each 1 L HPDE bottle was decanted into 15 mL HPDE containers and preserved with 0.5% v/v nitric acid for Fe_T analysis. One 125 mL FPE bottle from each depth remained unfiltered. From July through November, an additional water sample in a 125 mL FPE bottle from each depth was also collected and filtered with acid washed Whatman GF/F 0.7 µm glass fiber filters using a fluoropolymer apparatus. Both the filtered and the unfiltered samples were preserved with 0.5% v/v trace metal grade hydrochloric acid and stored at 4 °C and in the dark before analysis for MeHg.

After porewater extraction, one 50 mL centrifuge tube was placed back into the anaerobic glovebox and the porewater was immediately analyzed for oxidation-reduction potential and DO using a calibrated Hatch HQ30D multiparameter portable meter. The measured ORP value was then standardized to the hydrogen electrode (Eh) based on the electrode and the storage solution, according to Baird et al. (2005). While still in the anaerobic glovebox, the porewater was decanted into a 250 mL HPDE bottle containing 1 mL of 2 N zinc acetate (0.4% v/v). This preserved porewater and the 250 mL water column samples that were field-preserved with zinc acetate were analyzed for sulfide by iodometric titration (0.1 mg/L method detection limit) according to Standard Methods (Baird et al., 2005). The porewater from another 50 mL centrifuge tube was filtered with a Whatman 0.45 µm nylon membrane filter and stored frozen in a 50 mL HPDE container. These filtered porewater samples and the filtered water column samples were analyzed for sulfate by ion chromatography (0.5 mg/L method detection limit), as well as DOC using a Shimitzu TOC analyzer (0.3 mg/L method detection limit) (Baird et al., 2005; USEPA, 1993). Approximately 10 mL of porewater from the third centrifuge tube was decanted into a 15 mL HPDE container, preserved with 0.5% v/v nitric acid, and analyzed for FeT using an ICP-OES (0.1 mg/L method detection limit) (Baird et al., 2005).

Water from the final 50 mL centrifuge tube was filtered with an acid washed Whatman GF/F 0.7 µm glass fiber filter using a fluoropolymer apparatus. The filtered porewater was placed in a trace metal clean amber glass vial, preserved with 0.5% v/v trace metal grade hydrochloric acid and stored at 4 °C and in the dark. Approximately 25 mL of these porewater samples ($MeHg_{pore}$), as well as the filtered or dissolved MeHg ($MeHg_D$) and unfiltered water column MeHg ($MeHg_T$) samples, were distilled at 125 ^{o}C under nitrogen gas flow. For sediment samples ($MeHg_{sed}$), approximately 1.0 gram of sediment was directly distilled at 140 ^{o}C under nitrogen gas flow according to Horvat et al. (1993).

The pH of the distillates was then adjusted to approximately 5.0 and the samples were treated with the ethylating agent sodium tetraethyl borate, converting MeHg to

volatile ethyl-MeHg. Samples were bubbled with nitrogen gas and ethyl-MeHg was trapped on a graphitic carbon trap. With argon gas flowing through the trap, the trap was heated and the desorbed ethyl-MeHg was passed through a gas chromatography column to separate ethyl-MeHg from other Hg species. The gas stream then passed through a pyrolytic chamber to convert the ethyl-MeHg to Hg(0), which was analyzed on a MERX automated modular Hg system (Brooks Rand Labs, Seattle WA, US) using cold vapor atomic fluorescence spectroscopy (CVAFS) based on USEPA method 1630 (USEPA, 2001). The method detection limit was 0.02 ng/L for MeHg in water and porewater and 1 ng/kg for sediment. Strict quality control procedures were followed including calibration blanks (< 50 pg per 25 ml sample), method blanks (< 1 pg per 25 ml sample), matrix spikes and matrix spike duplicates (acceptable recovery range 71-125%), and ongoing precision recovery samples (acceptable recovery range 77-123%), all of which were within the acceptable ranges.

Sediment was placed in an oven at 105 ^{o}C for 1 hour and the percent dry weight was determined by difference according to Standard Methods (Baird et al., 2005). Afterwards, sediment was transported to a furnace and heated at 550 ^{o}C for 1 hour and percent organic matter (% OM) was determined by difference (Dean, 1974). Sediment was also analyzed for amorphous ferric iron [Fe(III)a] (10 mg/kg method detection limit) following methods outlined in Marvin-DiPasquale et al. (2008). According to Wahid and Kamalam (1993), Fe(III)a is highly bioavailable for microbial reduction, while crystalline iron oxide is not.

2.4 Calculations and data analysis

Dry weight $MeHg_{sed}$ (ng/kg) was determined by dividing the wet weight $MeHg_{sed}$ by the percent dry weight of the sediment. The volume of porewater per kg of sediment was determined by the percent wet weight of the sediment. Sediment-pore water MeHg distribution coefficients (K_d, L/g) were calculated as the ratio of the dry weight $MeHg_{sed}$ (ng/kg) to the $MeHg_{pore}$ (pg/L). Based on water column $MeHg_T$ profiles and the reservoir's hypsographic curve, a volume-weighted concentration, estimated as the sum of concentration times associated water slab volume divided by total volume, was estimated for the entire water column ($MeHg_{vw}$). Porewater, sediment, water column, and partitioning data were tested for normality by assessing skewness and kurtosis. Non-normally distributed data was transformed using natural logarithms. Afterwards, this data set was analyzed by Pearson correlation analysis for linear relationships. Apparent correlations between water column parameters observed between $MeHg_T$ and Fe_T were assessed using linear regression analysis. Apparent correlations observed for $MeHg_D$ with sulfate and DOC were assessed using linear regression analysis and multiple regression analysis. Temporal water quality heat maps were produced using MatLab software and linearly interpolating data between the samples collected from the surface to the bottom water at 3m increments.

3. Results

3.1 Temporal sediment and water quality results

The oxidation-reduction potential (Eh) of the porewater indicated that the sediment-water interface was reduced throughout the period of thermal stratification from April through October (≤ 14 mV) and slightly reduced even after mixing in November (79 mV) (Figure 2.1). Porewater sulfate concentration was highest at the start of the study in mid-April (26 mg/L), was substantially depleted to a minimum value in mid-July (3.8 mg/L), rose considerably until late September, was subsequently depleted again during October, and rose again after mixing in November. A statistically significant positive relationship was observed between porewater Eh and porewater sulfate concentration ($p = 0.022$, $n = 8$) (Table 2.1). Fe(III)a was only elevated in the sediment at the start of the study (191 mg/kg), after which it was substantially depleted until it was no longer detectable in mid-July until late September and remained low afterwards (< 30 mg/kg).

Porewater sulfide concentration was moderate at the start of the study (25 mg/L), rose to a maximum value in mid-July (32 mg/L), slowly declined during August and September, before rising slightly in October, and then declined to a minimum value after mixing in November (15 mg/L) (Figure 2.1). During April, sulfide was not detected in bottom water, defined as the water sampled at a depth of 19 m near (~0.5 m above) the sediment-water interface, but bottom water sulfide concentration consistently rose until it reached a peak in late September before declining until it was not detected after mixing in early December. A statistically significant negative correlation was observed between sediment Fe(III)a concentration and bottom water sulfide concentration ($p = 0.034$, $n = 8$) (Table 2.1). DOC concentration was relatively high throughout the course of the study and experienced large fluctuations, with minimum values in April and July (~20 mg/L) and maximums in June and October (~60 mg/L). The sediment % OM was moderate at the start of the study, elevated in mid-July (23%), declined significantly to a study minimum in mid-August to late September (11%), and rose to a study maximum during mid-October through early December (~24%).

The concentration of Fe_T in the water column was greatest (120-160 ug/L) in the surface water at the start of the study and at a depth of 12-18 m in late May (Figure 2.2). Fe_T was moderate (40-60 ug/L) in the bottom water during July through August and largely absent in the water column after September. TSS concentration was generally low (≤ 10 mg/L) below a depth of 9 m, although it was slightly elevated at 15 m in late September and at 9-12 m in mid-October (~12 mg/L). The surface water TSS concentration was low (> 7 mg/L) at the start of the study in mid-April, moderate (7-12 mg/L) from May through June, greatest (> 15 m/L) in July and August, moderate in September, low during October, and moderate in November. The sulfate concentration in the water column was notably elevated (> 180 mg/L) throughout most of the study, except for the hypolimnetic bottom water from July through mid-October, which was generally between 120-180 mg/L. A study minimum was observed below 18 m in late September (~120 mg/L) (Figure 2.3). DOC concentration in the water column was generally below 10 mg/L except for high concentrations (~12 mg/L) in early July at 6 m

depth, mid-July at 18 m, late September at 18 m, October at 12 m, and the surface 3 m from July through September.

3.2 Methylmercury sediment and water quality results

$MeHg_{pore}$ was elevated in mid-April and late May (< 155 pg/L) with notably lower concentrations observed later in the study (< 50 pg/L) (Figure 2.1). A statistically significant positive relationship was observed between $MeHg_{pore}$ concentration and sediment Fe(III)a concentration ($p = 0.002$, $n = 8$) (Table 2.1). The $MeHg_{sed}$ concentration was dynamic throughout the study with highest concentrations in mid-April and mid-July (122 and 113 ng/kg) and lowest concentrations in mid-August and late September (36 and 48 ng/kg).

Water column $MeHg_{vw}$ was low in mid-April (104 ng/m^3), rose to a study maximum by late May (264 ng/m^3) and declined afterwards, reaching a minimum in early December (67 ng/m^3) (Figure 2.1). A statistically significant positive relationship was observed between porewater sulfide concentration and water column $MeHg_{vw}$ concentration ($p = 0.003$, $n = 8$) (Table 2.1). The MeHg K_d was low in mid-April through late May (< 0.7 L/g), elevated in early and mid-July (> 2.1 L/g) and moderate (1.2-1.9 L/g) afterwards. A statistically significant negative correlation was observed between MeHg K_d and sediment Fe(III)a concentration ($p = 0.037$, $n = 8$) (Table 2.1). A statistically significant negative relationship was also observed between MeHg K_d and the porewater MeHg concentration ($p = 0.018$, $n = 8$) (Table 2.1).

$MeHg_T$ concentrations in the water column were low (< 0.2 ng/L) in the upper 6 m of the water column throughout the study and after late October in the entire water column, while concentrations reached maximum values at depths of 15 m in May and 9 m in June (0.5- 0.6 ng/L) (Figure 2.2). An apparent correlation between $MeHg_T$ and Fe_T in the bottom water during the spring and early summer was observed (Figure 2.2). Linear regression analysis revealed a statistically significant positive correlation between $MeHg_T$ and Fe_T in the lower water column below 12 m for the period between mid-April to early July ($p = 0.035$, $R^2 = 0.373$, $n = 12$).

$MeHg_D$ was largely absent (< 0.06 ng/L) in the upper 9 m of the water column from mid-July to mid-October and in the entire water column afterwards, while a maximum $MeHg_D$ concentration (~0.2 ng/L) was observed in September from 15-18 m (Figure 2.3). An apparent correlation between $MeHg_D$ and both sulfate and DOC in the bottom water was observed during the fall (Figure 2.3). Linear regression analysis revealed a statistically significant negative correlation between $MeHg_D$ and sulfate in the water column from mid-July to November ($p < 0.001$, $R^2 = 0.378$, $n = 40$). A multiple regression revealed a statistically significant correlation between $MeHg_D$ and the DOC and sulfate concentrations in the water column below 15 m from August to October [$p = 0.044$, $R^2 = 0.645$, $n = 9$, $MeHg_D = -0.218 + (0.034 \times DOC) - (0.00015 \times sulfate)$].

4. Discussion

4.1 Sediment stored MeHg release during iron reduction

The initially high concentration of $MeHg_{sed}$ and $MeHg_{pore}$ in April, during a period of moderately high redox, suggests that high levels of MeHg production preceded the onset of thermal stratification and anaerobic conditions. In mid-April, both $MeHg_{sed}$ and $MeHg_{pore}$ were at maximum concentrations at the start of the study (122 ng/kg and 181 pg/L, Figure 2.1) while redox was elevated (14 mV, Figure 2.1) and small amounts of DO were present in the porewater (0.9 mg/L, data not shown). During this period, maximum concentrations of the electron acceptors Fe(III)a and sulfate were present in the surficial sediment, as well as a moderate concentration of sulfide (Figure 2.1). Hollweg et al. (2009) found the highest methylation rates in coastal sediments where there was some oxygen penetration into surficial sediment, which allowed for enhanced sulfate-sulfide cycling. Additionally, research on pelagic MeHg production has revealed that the oxic-anoxic boundary often contains the highest levels of MeHg, suggesting a methylation hotspot (Paranjape and Hall, 2017; Ullrich et al., 2001; Eckley and Hintelmann, 2006). Based on our observations, it appears that relatively elevated redox conditions in surficial sediment enhanced the accumulation of MeHg in profundal sediment and pore water by oxidizing biproducts of microbial respiration of known methylators, such as sulfide or iron(II), allowing for the continuous replenishment of electron acceptors in anaerobic microzones where SRB and/or IRB methylators may reside.

MeHg observed in sediment in mid-April appears to have been released into the bottom water column in mid-April to late May during the mineralization of organic matter, likely driven by iron reduction in surficial sediment. High rates of iron reduction were demonstrated by a rapid decline in sediment Fe(III)a between mid-April and late May (191 to 52 mg/kg, Figure 2.1), which was concurrent with the accumulation of Fe_T in the hypolimnion in late May (Figure 2.2). This period of iron reduction coincided with a reduction of $MeHg_{sed}$ (122 to 65 ng/kg, Figure 2.1), and a substantial release of MeHg into the hypolimnion as demonstrated by the large increase in $MeHg_{vw}$ (104 to 264 ng/m^3, Figure 2.1) and hypolimnetic $MeHg_T$ (Figure 2.2). The significant correlation between hypolimnetic $MeHg_T$ and Fe_T during this period demonstrates the connection between iron reduction and hypolimnetic MeHg accumulation. Previous studies have shown that MeHg has a high affinity for sediment OM and that iron reduction can result in the dissolution of iron-oxide bound OM (Adhikari and Yang, 2015; Feyte et al., 2010; Hintelmann and Harris, 2004; Lalonde et al., 2012), indicating that iron reduction can lead to the release of sediment-bound MeHg into the water column.

In our study, MeHg appears to be most soluble during periods of anoxia when highly bioavailable iron-oxide is present and iron reduction is likely taking place. This is demonstrated by the low MeHg K_d value in mid-April and late-May (< 0.70 L/g, Figure 2.1), a significant negative correlation between sediment Fe(III)a and the MeHg K_d, and a significant positive correlation between sediment Fe(III)a and $MeHg_{pore}$ (Table 2.1). Although IRB have been shown to be prominent methylators in some systems (Bravo et al., 2018; Fleming et al., 2006), our results suggest that rather than enhancing the production of MeHg, iron reduction led to the dissolution of MeHg-rich, sediment bound

OM which resulted in the bottom water column MeHg accumulation observed in early stratification.

4.2 MeHg accumulation in the sediment during sulfate reduction

SRB activity, as demonstrated by a reduction in porewater sulfate, appears to coincide with a buildup of MeHg in the profundal sediment. The consistently low Eh of the porewater, which was positively correlated with porewater sulfate concentration (Figure 2.1 and Table 2.1), as well as the presence of sulfide in the porewater throughout the study, shows that sulfate reduction was a prominent metabolic process in the profundal sediment during stratification at Hodges Reservoir. Sulfate reduction appeared to precede at the highest rate from late May to mid-July when porewater sulfate was reduced from 18.4 mg/L to a study minimum of 3.8 mg/L, and from late September to mid-October when porewater sulfate declined from 23 mg/L to 7.4 mg/L (Fig 2.1). These episodes of sulfate depletions coincided with increases in $MeHg_{sed}$, 65 to 113 ng/kg from late May to mid-July, and 48 to 86 ng/kg from late September to mid-October. Mercury methylation by SRB in profundal sediments has been observed by several previous studies (Duvil et al., 2018; Fuhrmann et al., in review; Gilmour et al., 1998; Paranjape and Hall, 2017). The observed pattern of porewater sulfate depletion and the enhancement of $MeHg_{sed}$ suggests that SRB mercury methylation was likely occurring and led to the accumulation of MeHg in the profundal sediment.

The buildup of porewater sulfide that occurs during SRB methylation appears to have led to a decreased solubility of the newly produced MeHg, reducing entry into the water column. Enhanced sediment MeHg binding, following the depletion of bioavailable sediment Fe(III)a and the increase in SRB activity in July, was demonstrated by a study maximum MeHg K_d (> 2 g/L, Fig 2.1). In addition, a significant negative correlation between sediment Fe(III)a and MeHg K_d (Table 2.1) suggests that MeHg solubility substantially declined after the depletion of bioavailable iron-oxide, as sulfate reduction became a more thermodynamically favorable redox process. There was also a notable increase in the MeHg K_d during other periods of high SRB activity; for example, MeHg K_d increased from 1.38 g/L in late September to 1.86 g/L in mid-October when porewater sulfide declined substantially (23 mg/L to 7.4 mg/L) and porewater sulfide increased from 21 to 24 mg/L, indicating enhanced SRB activity in the profundal sediment. Both porewater sulfide and sediment % OM rose considerable during each period when porewater sulfate was depleted and the MeHg K_d was enhanced, indicating either factor or the combination of the two may have played a role in the reduced solubility of MeHg. Previous studies have noted that MeHg sediment binding tends to be higher (higher K_d) under sulfidic conditions, likely due to adsorption of MeHg to metal sulfides and MeHg binding to thiols in sediments rich in organic matter (Skyllberg et al., 2008; Zhu et al., 2018). Our results indicate that sediment MeHg solubility is greater during the early stages of anaerobic conditions before the buildup of sulfide and organic matter at the sediment-water interface enhances MeHg binding.

4.3 Demethylation of MeHg in the sediment during methanogenesis

Sulfate reduction in mid-summer, as indicated by the reduction in porewater sulfate, appears to have exhausted porewater DOC and sulfate, leading to a reduction in SRB activity and the prevalence of methanogenic conditions and enhanced rates of demethylation in surficial sediment. In mid-July, porewater sulfate and DOC were both depleted to study minimum concentrations (3.8 mg/L and 18 mg/L), while sediment % OM increased to 23% (Figure 2.1). Directly following the enhancement of sediment % OM and the depletion of porewater sulfate and DOC, $MeHg_{sed}$ declined from 113 ng/kg to a study minimum of 36 ng/kg (Figure 2.1). This decline in $MeHg_{sed}$ was not accompanied by a significant increase in $MeHg_{pore}$ or accumulation of $MeHg_T$ in the bottom water, indicating that the reduction was likely due to degradation. SRB metabolism is primarily dependent on the availability of sulfate and labile carbon sources, as SRB do not demonstrate the ability to hydrolyze ploymers (Colleran et al., 1995). Methanogens and fermenters have been shown to participate symbiotically in the breakdown of more refractory polymeric organic matter (Flores, 2014), and this process can be the primary driver in sediment particulate organic matter mineralization during stratification in another hyper-eutrophic reservoir (Molongoski et al., 1980). Thus, low concentrations of porewater sulfate and labile organic carbon, combined with elevated particulate organic matter, may have provided a competitive advantage for methanogens over SRB at the sediment-water interface. Previous research on Hodges Reservoir found that inhibition of methanogenesis led to a dramatic enhancement of MeHg accumulation in experimental sediment-water microcosms (Fuhrmann et al., in review). The researchers found that this effect was generally more pronounced in the fall and concluded that methanogens were prominent demethylators in the surficial sediment under highly reducing conditions.

The prevalence of methanogenic conditions in the surficial sediment, and the accompanying demethylation of sediment associated MeHg, appears to have also led to a decline in MeHg accumulation in the hypolimnion. From mid-July to mid-August, a large reduction in water column $MeHg_{vw}$, from 237 ng/m^3 to 152 ng/m^3, was observed (Figure 2.1). Part of the decline in the $MeHg_{vw}$ can be attributed to the dilution of MeHg into the epilimnion which is much larger in total volume, as demonstrated by the disappearance of $MeHg_T$ between 6-9 m (Figure 2.2). However, this decline in water column $MeHg_{vw}$ was also concurrent with a substantial decline in the concentration of $MeHg_T$ in the hypolimnion, which fell from roughly 0.25 ng/L to 0.05 ng/L in the bottom 3 m during the same period (Figure 2.2). This decline in hypolimnetic MeHg is also notable because the MeHg K_d declined to a moderate value during this period, likely due to a reduction in porewater sulfide relating to lower SRB activity, which would reduce the pool of sulfide ligands that bind MeHg and enhance the solubility of MeHg at the sediment-water interface. Therefore, even with enhanced MeHg solubility, MeHg release into the bottom water column was dramatically reduced during the prevalence of methanogenic conditions. A previous study on Hodges Reservoir by Beutel et al. (2020) demonstrated that MeHg in the water column was also much lower under more highly reduced conditions in the fall of 2017. The study also reported lower efflux of MeHg from sediment under highly reduced versus moderately reduced conditions at the sediment-

water interface. Overall, these results suggest that the depletion of sulfate in the surficial sediment led to methanogenic conditions, demethylation of sediment associated MeHg, and suppressed MeHg accumulation in the hypolimnion during the fall.

4.4 Sulfate reduction and dissolved MeHg production in the water column

The low levels of sulfate and DOC in the porewater during the mid-summer appears to have produced an unsuitable habitat for SRB in the profundal sediment and led to enhanced SRB activity in the hypolimnetic water column, which was rich in sulfate. Sulfate was severely limited in the porewater during mid-July (3.8 mg/L, Figure 2.1), yet abundant in the in the hypolimnion (~180 mg/L, Figure 2.3), demonstrating the more favorable habitat for SRB. Enhanced water column activity by SRB is supported by the depletion of sulfate in the hypolimnion, which begins in July and becomes very substantial later in the fall (Figure 2.3). SRB activity in an anoxic and sulfidic hypolimnion during highly reduced conditions in the fall was also demonstrated by Diao et al. (2017), who noted a corresponding reduction in the sulfate concentration in the hypolimnion. Our results suggest that after sulfate and DOC was depleted in the sediment and methanogenic conditions prevailed in mid-July, SRB thrived in the sulfate rich hypolimnion, which led to the depletion of the bottom water sulfate concentration in the Fall.

SRB activity in the hypolimnion in the fall appears to have led to the production of $MeHg_D$ through the process of water column methylation. The substantial depletion of sulfate in the hypolimnion during late September demonstrates water column sulfate reduction was a prominent process in the hypolimnion. The bottom water column was also enriched with $MeHg_T$, predominantly as $MeHg_D$, during that period (Figures 2.2 and 2.3). The presence of $MeHg_D$ in the bottom water coincides with the depletion of sulfate and the presence of high concentrations DOC at the same depths (Figure 2.3). The highly statistically significant negative correlation between $MeHg_D$ and sulfate in the water column in July through December, as well as the statistically significant multiple regression correlation between bottom water $MeHg_D$ with DOC (positive correlation) and sulfate (negative correlation) from mid-August to mid-October, suggests that sulfate reduction and high concentrations of DOC in the water column led to the production of $MeHg_D$ in Hodges Reservoir. Eckley and Hintelmann (2006) reported water column methylation in anoxic water columns that was positively correlated with DOC concentration and water column sulfate depletion. They hypothesized the MeHg production to be due to SRB active in the water column. Another study on water column methylation found that SRB methylated at high rates while residing in anaerobic microzones inside of settling particles in the water column (Díez et al., 2016). Our results suggest that the colonization of SRB in the hypolimnion led to high rates of sulfate reduction and water column methylation, resulting in the accumulation of $MeHg_D$.

5. Conclusions

Although research has identified genes and species of bacteria that have the capacity to produce MeHg, much less is known about conditions that favor this production and mechanisms that allow for the release of MeHg produced in sediment into the water column. This study presents evidence that sub-oxic conditions may facilitate the highest rates of MeHg production and that iron-reduction may lead to the release of MeHg-rich OM into the water column. This study found that the release of MeHg present in sediment at the onset of thermal stratification was a large summertime source of MeHg to the water column. Our study also showed that the depletion of Fe(III)a in the sediment and the presence of sulfate and DOC in the porewater led to profundal sediment SRB methylation in mid-summer. However, a high sediment binding capacity prevented the release of MeHg that was produced during the mid-summer. The high level of sulfate reduction that led to the production of the mid-summer MeHg in the sediment depleted resources such as porewater sulfate and DOC, leading to methanogenesis and high levels of demethylation of the sediment bound MeHg. This appears to have dramatically reduced the potential of the MeHg produced during mid-summer to make it into the food-web. However, SRB activity in water column increased after resources were depleted in the sediment, resulting in the production of $MeHg_D$ in the hypolimnion. Thus, there appears to be two hot moments of MeHg input to the aquatic ecosystem of hypereutrophic Hodges Reservoir: MeHg efflux from sediment during the onset of thermal stratification and water column production in the fall.

6. References

Adhikari, D., Yang, Y., 2015. Selective stabilization of aliphatic organic carbon by iron oxide. Scientific Reports, 5(1).

Baird, R.B., Eaton, A.D., Rice, E.W., Bridgewater, L.L., 2005. Standard methods for the examination of water and wastewater. New York, NY: American Public Health Association.

Beutel, M.W., Fuhrmann, B., Herbon, G., Chow, A., Brower, S., Pasek, J., 2020. Cycling of methylmercury and other redox-sensitive compounds in the profundal zone of a hypereutrophic water supply reservoir. Hydrobiologia.

Beutel, M.W., Duvil, R., Cubas, F.J., Grizzard, T.J., 2017. Effects of nitrate addition on water column methylmercury in Occoquan Reservoir, Virginia, USA. Water Research, 110, 288-296.

Beutel, M.W., Cox, S.E., Gebremariam, S., 2016. Effects of chironomid density and dissolved oxygen on mercury efflux from profundal lake sediment. Lake and Reservoir Management, 32(2), 158-167.

Beutel, M., Dent, S., Reed, B., Marshall, P., Gebremariam, S., Moore, B., Shallenberger, E., 2014. Effects of hypolimnetic oxygen addition on mercury bioaccumulation in Twin Lakes, Washington, USA. Science of The Total Environment, 496, 688-700.

Bigham, G.N., Murray, K.J., Masue-Slowey, Y., Henry, E. A., 2016. Biogeochemical controls on methylmercury in soils and sediments: implications for site management. Integrated Environmental Assessment and Management, 9999, 1-14.

Bose-O'Reilly, S., McCarty, K. M., Steckling, N., Lettmeier, B., 2010. Mercury exposure and children's health. Current Problems in Pediatric and Adolescent Health Care, 40, 186-215.

Bravo, A.G., Zopfi, J., Buck, M., Xu, J., Bertilsson, S., Schaefer, J.K., Poté, J., Cosio, C., 2018. Geobacteraceae are important members of mercury-methylating microbial communities of sediments impacted by waste water releases. The ISME Journal, 12(3), 802-812.

Colleran, E., Finnegan, S., Lens, P., 1995. Anaerobic treatment of sulphate-containing waste streams. Antonie Van Leeuwenhoek, 67(1), 29-46.

Dean, J.W., 1974. Determination of carbonate and organic matter in calcareous sediments and sedimentary rocks by loss on ignition: comparison with other methods. SEPM Journal of Sedimentary Research, Vol. 44.

Diao, M., Sinnige, R., Kalbitz, K., Huisman, J., Muyzer, G., 2017. Succession of bacterial communities in a seasonally stratified lake with an anoxic and sulfidic hypolimnion. Frontiers in Microbiology, 8.

Díez, E. G., Loizeau, J.-L., Cosio, C., Bouchet, S., Adatte, T., Amouroux, D., Bravo, A. G., 2016. Role of settling particles on mercury methylation in the oxic water column of freshwater systems. Environmental Science and Technology, 50(21), 11672–11679.

Duvil, R., Beutel, M.W., Fuhrmann, B., Seelos, M., 2018. Effect of oxygen, nitrate and aluminum addition on methylmercury efflux from mine-impacted reservoir sediment. Water Research, 144, 740-751.

Eckley, C.S., Hintelmann, H., 2006. Determination of mercury methylation potentials in the water column of lakes across Canada. Science of The Total Environment, 368(1), 111–125.

Feyte, S., Tessier, A., Gobeil, C., Cossa, D., 2010. In situ adsorption of mercury, methylmercury and other elements by iron oxyhydroxides and organic matter in lake sediments. Applied Geochemistry, 25(7), 984–995.

Fleming, E.J., Mack, E.E., Green, P.G. and Nelson, D.C., 2006. Mercury methylation from unexpected sources: molybdate-inhibited freshwater sediments and an iron-reducing bacterium. Applied Environmental Microbiology, 72(1), pp.457-464

Flores, R.M., 2014. Origin of coal as gas source and reservoir rocks. Coal and Coalbed Gas, 97–165.

Fuhrmann, B., Beutel, M., O'Day, P., Tran, C., Funk, A., Brower, S., Pasek, J., Seelos, M., 2020. Consequences of inorganic mercury, organic carbon, and microbial inhibitors on mercury methylation in profundal sediment of a hypereutrophic reservoir. Water Research (in review).

Futsaeter, G., and Wilson, S., 2013. The UNEP global mercury assessment: sources, emissions and transport. E3S Web of Conferences, 1, 1-44.

Gobeil, C., Cossa, D., 1993. Mercury in sediments and sediment pore water in the Laurentian Trough. Canadian Journal of Fisheries and Aquatic Sciences, 50(8), 1794–1800.

Gilmour, C.C., Gill, G.A., Stordal M.C., Spiker E., 1998. Mercury methylation and sulfur cycling in the Northern Everglades. Biogeochemistry 40, 326–346.

Hintelmann, H., Harris, R., 2004. Application of multiple stable mercury isotopes to determine the adsorption and desorption dynamics of Hg(II) and MeHg to sediments. Marine Chemistry, 90(1-4), 165–173.

Hollweg, T., Gilmour, C., Mason, R., 2009. Methylmercury production in sediments of Chesapeake Bay and the mid-Atlantic continental margin. Marine Chemistry, 114(3-4), 86–101.

Horne, A.J., Goldman, C.R., 1994. Limnology. New York, NY: McGraw-Hill.

Hylander, L.D., Meili, M., 2003. 500 years of mercury production: global annual inventory by region until 2000 and associated emissions. Science of The Total Environment, 304(1-3), 13–27.

Korthals, E.T., Winfrey, M.R., 1987. Seasonal and spatial variations in mercury methylation and demethylation in an oligotrophic lake. Applied and Environmental Microbiology, 53(10), 2397-2404.

Kronberg, R., Schaefer, J.K., Björn, E., Skyllberg, U., 2018. Mechanisms of methyl mercury net degradation in alder swamps: the role of methanogens and abiotic processes. Environmental Science and Technology Letters, 5(4), 220-225.

Lalonde, K., Mucci, A., Ouellet, A., Gélinas, Y., 2012. Preservation of organic matter in sediments promoted by iron. Nature, 483(7388), 198–200.

Marvin-Dipasquale, M.C., Lutz, M.A., Krabbenhoft, D.P., Aiken, G. R., Orem, W.H., Hall, B.D., Brigham, M.E., 2008. Total mercury, methylmercury, methylmercury production potential, and ancillary streambed-sediment and pore-water data for selected streams in Oregon, Wisconsin, and Florida, 2003-04. National Water-Quality Assessment, USGS.

Molongoski, J.J., Klug, M.J., 1980. Anaerobic metabolism of particulate organic matter in the sediments of a hypereutrophic lake. Freshwater Biology, 10(6), 507–518.

Pak, K.R., Bartha, R., 1998. Mercury methylation and demethylation in anoxic lake sediments and by strictly anaerobic bacteria. Applied and Environmental Microbiology, 64(3), 1013-1017.

Paranjape, A.R., Hall, B.D., 2017. Recent advances in the study of mercury methylation in aquatic systems. Facets, 2(1), 85-119.

Podar, M., Gilmour, C., Brandt, C., Soren, A., Brown, S, 2015. Global prevalence and distribution of genes and microorganisms involved in mercury methylation. Sci. Adv., 1-12.

Skyllberg, U., 2008. Competition among thiols and inorganic sulfides and polysulfides for Hg and MeHg in wetland soils and sediments under suboxic conditions: illumination of controversies and implications for MeHg net production. Journal of Geophysical Research: Biogeosciences, 113(G2).

Ullrich, S.M., Tanton, T.W., Abdrashitova, S.A., 2001. Mercury in the aquatic environment: a review of factors affecting methylation. Critical Reviews in Environmental Science and Technology, 31, 241-293.

United States Environmental Protection Agency (USEPA), 2001. Method 1630: methyl mercury in water by distillation, aqueous ethylation, purge and trap, and CVAFS. EPA-821-r-01-020 (Washington, D.C).

United States Environmental Protection Agency (USEPA), 1993. Method 300.0: determination of inorganic anions in water by ion chromatography (Cincinnati, OH).

Vlassopoulos, D., Kanematsu, M., Henry, E.A., Goin, J., Leven, A., Glaser, D., O'day, P.A., 2018. Manganese(iv) oxide amendments reduce methylmercury concentrations in sediment porewater. Environmental Science: Processes and Impacts, 20(12), 1746-1760.

Wahid, P.A., and Kamalam, N.V., 1993. Reductive dissolution of crystalline and amorphous Fe(III) oxides by microorganisms in submerged soil. Biology and Fertility of Soils, 15(2), 144–148.

Zhu, W., Song, Y., Adediran, G.A., Jiang, T., Reis, A.T., Pereira, E., Björn, E., 2018. Mercury transformations in resuspended contaminated sediment controlled by redox conditions, chemical speciation and sources of organic matter. Geochimica Et Cosmochimica Acta, 220, 158–179.

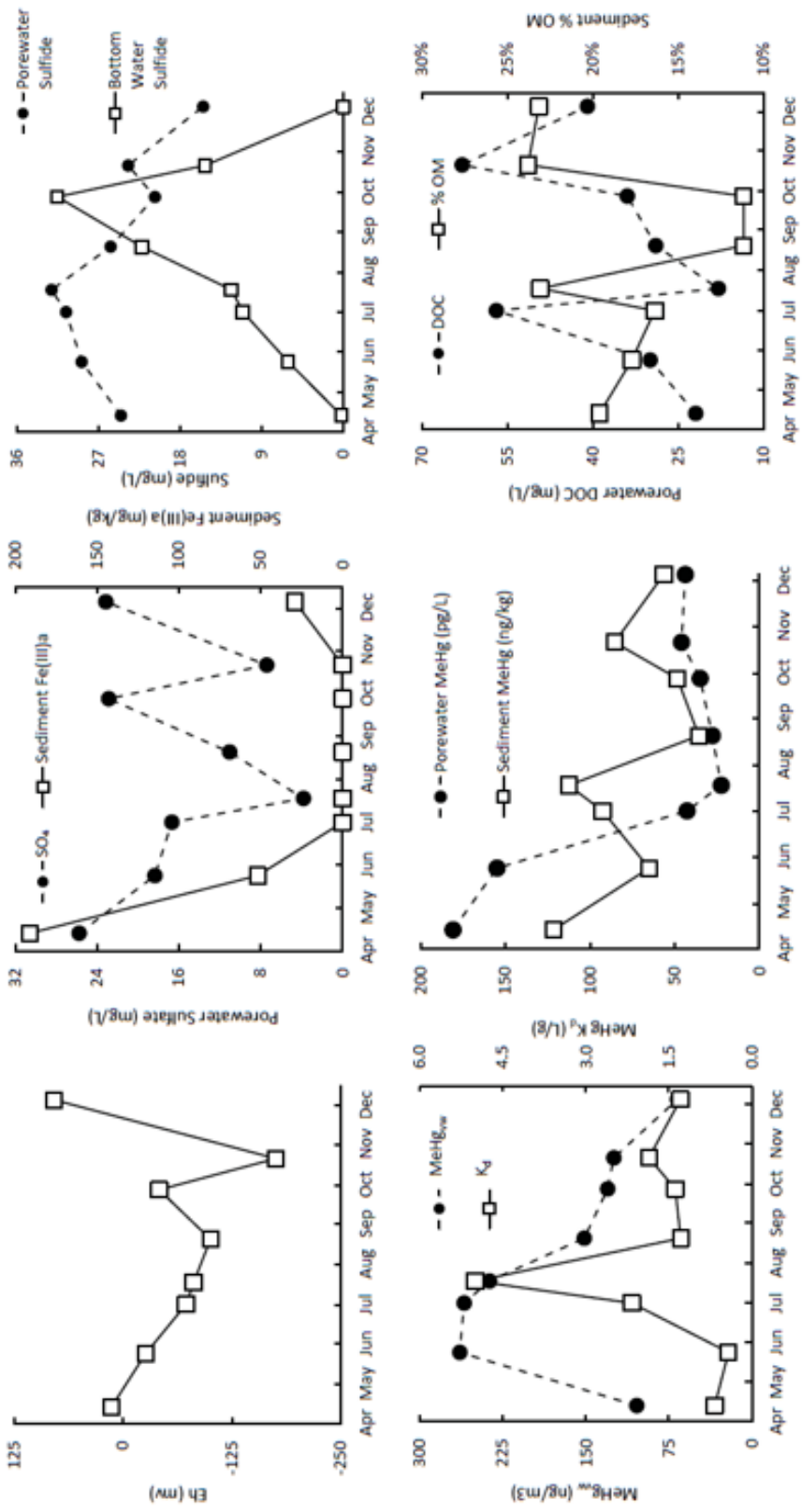

Figure 2.1 Temporal porewater, sediment, and water quality characteristics in 2018. Oxidation-reduction potential (Eh) (top left), porewater sulfate (SO_4) and sediment amorphous iron oxide [Fe(III)a] (top middle), porewater sulfide and bottom water (19m depth) sulfide (top right), water column MeHg volumetric weighted average ($MeHg_{vw}$) and MeHg sediment-partitioning coefficient (K_d) (bottom left), porewater MeHg ($MeHg_{pore}$) and sediment MeHg ($MeHg_{sed}$) (bottom middle), and porewater dissolved organic carbon (DOC) and sediment percent organic matter (% OM) (bottom right).

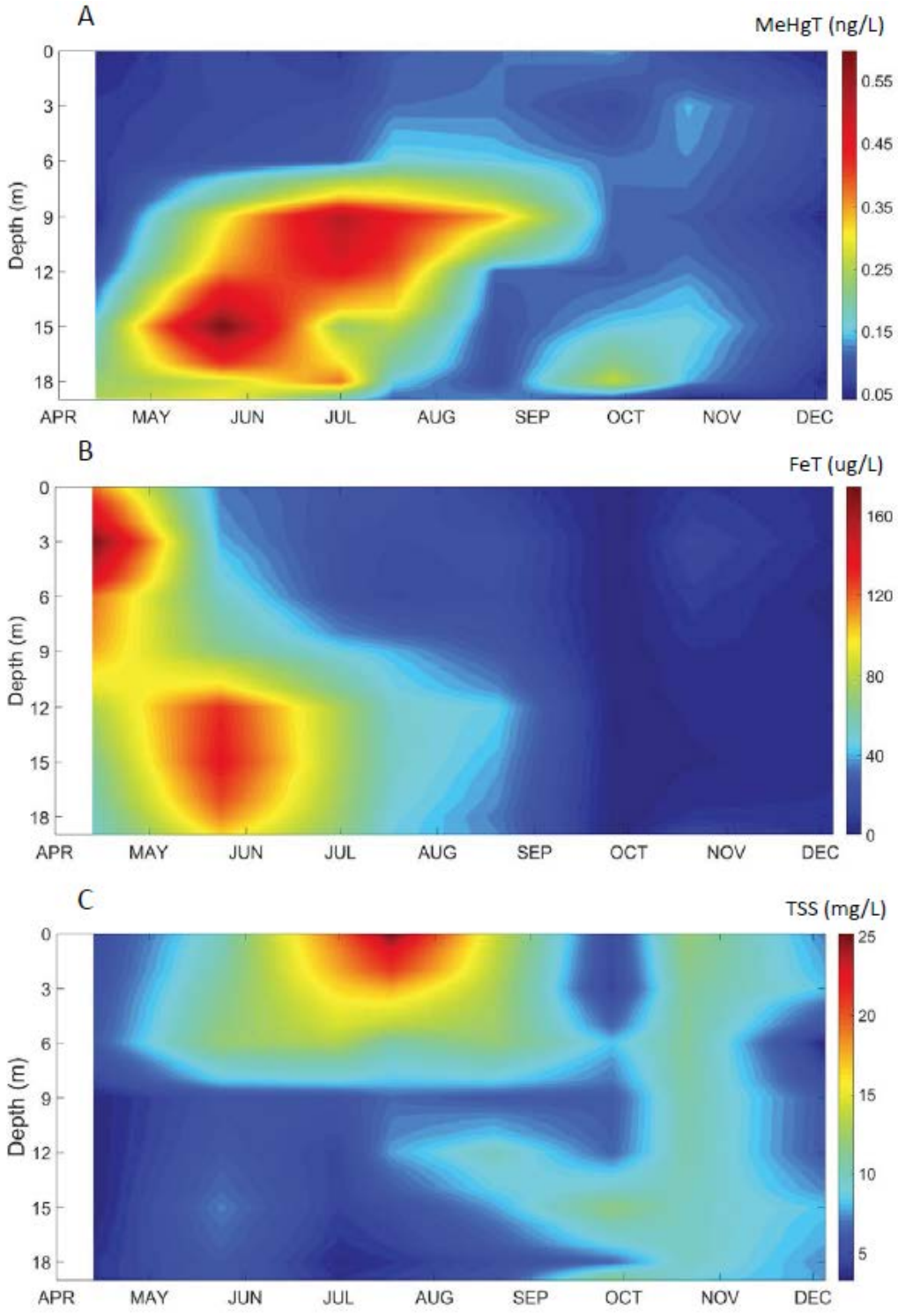

Figure 2.2 Spatio-temporal dynamics of water quality parameters in 2018. **(A)** total methylmercury ($MeHg_T$), **(B)** total dissolved iron (Fe_T)**, (C)** total suspended solids (TSS).

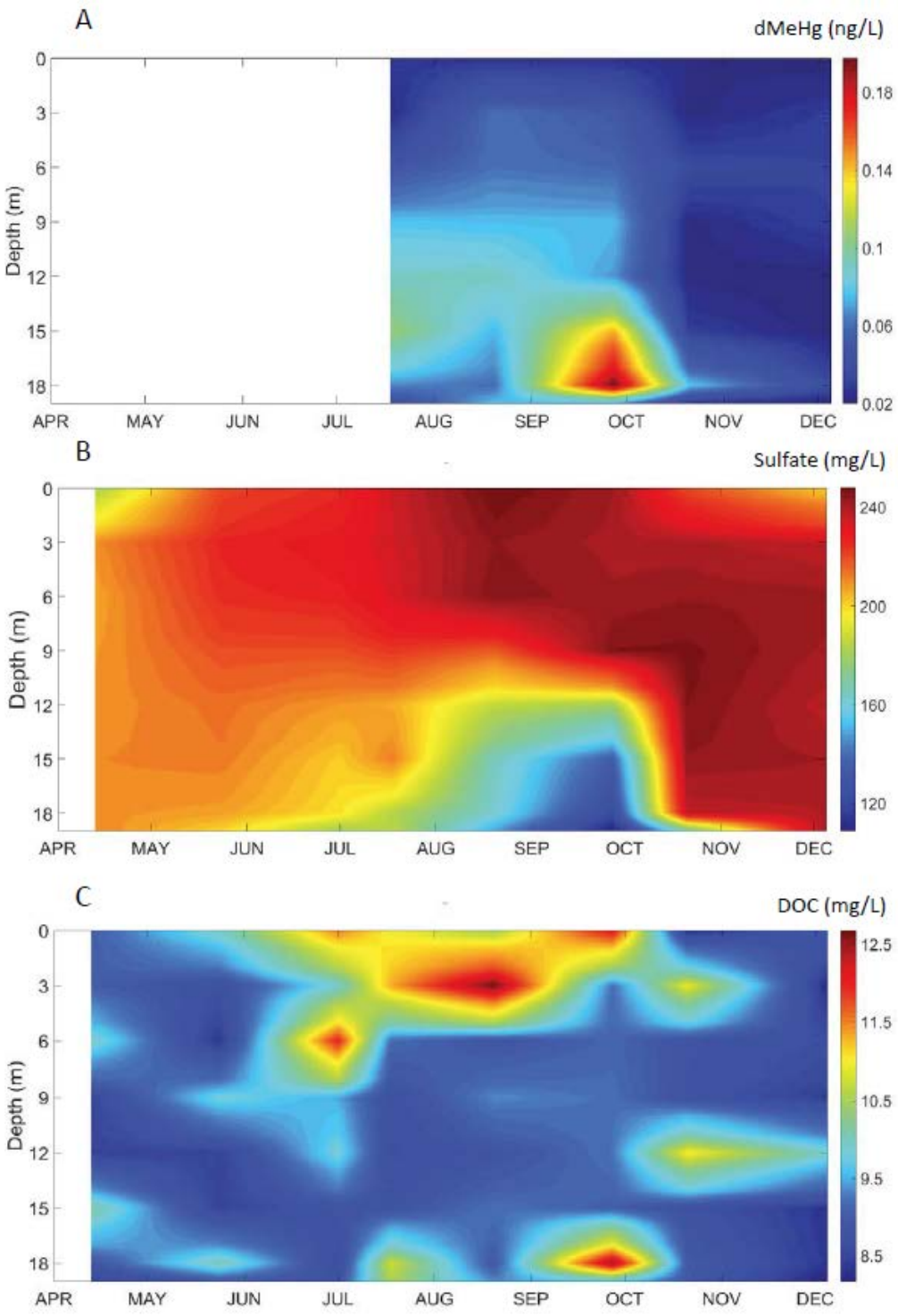

Figure 2.3 Spatio-temporal dynamics of water quality parameters in Hodges Reservoir in 2018. **(A)** dissolved methylmercury ($MeHg_D$), **(B)** sulfate, **(C)** dissolved organic carbon (DOC).

Table 2.1 Pearson's correlation matrix of porewater, sediment, water column, and partition parameters (n = 8)

		Porewater					Sediment			Water Column		Partitioning
		ORP (mv)	Sulfate (mg/L)	DOC (mg/L)	Sulfide (mg/L)	MeHg (pg/L)	Fe(III)a (mg/kg)	% Organic Matter	MeHg (ng/kg)	Bottom Water Sulfide (mg/L)	$MeHg_{vw}$ Avg (ng/m^3)	Kd (L/kg)
Porewater	ORP (mv)	1										
	Sulfate (mg/L)	0.782*	1									
	DOC (mg/L)	-0.389	-0.104	1								
	Sulfide (mg/L)	-0.488	-0.555	-0.176	1							
	MeHg (pg/L)	0.381	0.529	-0.315	0.077	1						
Sediment	Fe(III)a (mg/kg)	0.676	0.657	-0.386	-0.205	0.908**	1					
	% Organic Matter	0.072	-0.259	0.166	-0.037	0.095	0.238	1				
	MeHg (ng/kg)	-0.048	-0.131	-0.114	0.469	0.368	0.313	0.587	1			
Water Column	Bottom Water Sulfide (mg/L)	-0.547	-0.270	0.075	0.029	-0.576	-0.745*	-0.674	-0.505	1		
	$MeHg_{vw}$ Avg (ng/m^3)	-0.320	-0.402	-0.055	0.890**	0.029	-0.237	-0.120	0.204	0.047	1	
Partitioning	K_d (L/kg)	-0.419	-0.669	0.140	0.272	-0.795	-0.738*	0.255	0.258	0.295	0.145	1

* Correlation is significant at the 0.05 level (2 tailed).
** Correlation is significant at the 0.01 level (2 tailed).

Table 2.2 Sediment and porewater parameters

Parameter	12-Apr	24-May	2-Jul	19-Jul	22-Aug	28-Sep	22-Oct	6-Dec
Sediment Fe(III)a (mg/kg)	191	51.6	ND	ND	ND	ND	ND	28.6
Sediment Organic Matter (%)	19.6%	17.7%	16.4%	23.1%	11.2%	11.2%	23.8%	23.2%
Sediment MeHg (ng/kg)	122	65.1	92.6	113	35.8	48.4	85.6	56.5
Porewater MeHg (pg/L)	181	155	42.7	22.5	27.8	35.0	46.0	43.8
Porewater Sulfate (mg/L)	25.7	18.4	16.7	3.82	11.0	22.9	7.42	23.1
Porewater DOC (mg/L)	22.4	30.0	57.2	17.7	29.1	33.5	63.3	40.8
Porewater Eh (mV)	13.5	-25.7	-72.3	-81.1	-100	-41.4	-175	79.0
Porewater Sulfide (mg/L)	24.5	28.8	30.6	32.2	25.6	20.8	23.7	15.5
K_d (L/kg)	673	420	2170	5003	1288	1383	1861	1290

Table 2.3 Water column total MeHg ($MeHg_T$)

Depth (m)	12-Apr	24-May	2-Jul	19-Jul	22-Aug	28-Sep	22-Oct	6-Dec
0	0.04	0.08	0.06	0.11	0.12	0.13	0.09	0.05
3	0.06	0.08	0.09	0.12	0.12	0.08	0.14	0.08
6	0.06	0.09	0.11	0.16	0.15	0.12	0.13	0.08
9	0.05	0.30	0.52	0.45	0.34	0.12	0.11	0.05
12	0.09	0.36	0.45	0.39	0.12	0.11	0.13	0.08
15	0.17	0.60	0.23	0.26	0.09	0.15	0.16	0.08
18	0.23	0.27	0.38	0.15	0.09	0.27	0.14	0.05
18.5				0.11				
19		0.31	0.17		0.13	0.09	0.04	0.07
21	0.25							
$MeHg_{vw}$	104	264	260	237	152	130	125	67.2

Table 2.4 Water column total iron (Fe_T)

Depth (m)	12-Apr	24-May	2-Jul	19-Jul	22-Aug	28-Sep	22-Oct	6-Dec
0	120	34	26	24	13	ND	ND	ND
3	179	41	24	20	22	ND	16	ND
6	118	55	24	17	20	ND	11	ND
9	111	69	48	42	27	ND	6	ND
12	79	133	78	53	47	ND	5	ND
15	64	140	79	55	41	ND	4	ND
18	56	118	73	49	34	ND	8	ND
18.5				47				
19		101	69		37	ND	17	ND
21	54							

Table 2.5 Water column total suspended solids (TSS)

Depth (m)	12-Apr	24-May	2-Jul	19-Jul	22-Aug	28-Sep	22-Oct	6-Dec
0	4.9	9.9	19.5	25.2	14.4	4.9	12.2	7.1
3	5.5	11.0	16.5	17.7	13.1	4.4	11.0	8.3
6	6.1	12.1	13.2	10.5	12.1	8.2	11.0	3.3
9	3.3	5.5	5.6	6.7	6.0	6.1	10.5	6.1
12	3.3	6.1	4.5	7.7	9.9	6.6	10.4	6.0
15	3.3	7.2	4.4	5.0	7.6	11.8	9.8	8.3
18	3.9	6.0	3.5	3.9	4.9	6.6	9.8	7.3
18.5				4.4				
19		6.0	3.9		5.5	11.8	8.8	7.8
21	3.9							

Table 2.6 Water column filtered MeHg ($MeHg_D$)

Depth (m)	19-Jul	22-Aug	28-Sep	22-Oct	6-Dec
0	0.03	0.03	0.03	0.02	ND
3	0.02	0.06	0.05	0.02	0.03
6	0.05	0.06	0.06	0.04	0.03
9	0.08	0.08	0.07	0.02	0.03
12	0.09	0.09	0.07	0.02	ND
15	0.11	0.07	0.14	0.03	0.02
18	0.07	0.06	0.20	0.08	0.04
18.5	0.04				
19		0.08	0.07	0.02	0.02

Table 2.7 Water column sulfate

Depth (m)	12-Apr	24-May	2-Jul	19-Jul	22-Aug	28-Sep	22-Oct	6-Dec
3	182	221	225	235	248	242	220	201
6	210	227	230	235	244	241	240	237
	207	225	227	234	245	242	244	243
9	209	219	219	223	217	246	247	241
12	210	214	209	206	186	180	246	238
15	211	213	202	212	165	135	243	241
18	210	208	199	184	162	121	237	239
18.5				185				
19		200	180		148	109	167	242
21	211							

Table 2.8 Water column dissolved organic carbon (DOC)

Depth (m)	12-Apr	24-May	2-Jul	19-Jul	22-Aug	28-Sep	22-Oct	6-Dec
0	9.1	10.0	11.5	11.0	10.5	12.1	8.3	8.9
3	9.0	8.7	9.9	11.3	12.7	9.2	10.9	8.2
6	9.9	8.3	12.0	9.2	8.9	9.1	8.8	8.7
9	8.5	9.8	9.5	8.7	9.3	9.2	8.8	8.4
12	8.5	8.5	9.8	8.6	8.8	9.2	11.0	9.9
15	10.2	8.5	8.8	8.8	9.2	9.0	8.7	8.3
18	8.9	10.1	8.6	10.8	9.0	12.5	9.0	8.4
18.5				10.6				
19		8.9	8.8		9.4	9.7	8.9	8.2
21	8.5							

Table 2.9 Water column sulfide

Depth (m)	12-Apr	24-May	2-Jul	19-Jul	22-Aug	28-Sep	22-Oct	6-Dec
0	ND	ND	ND	ND	ND	ND	ND	ND
3	ND	ND	ND	ND	ND	ND	ND	ND
6	ND	ND	ND	ND	0.5	ND	ND	ND
9	ND	1.0	4.1	5.2	11.2	ND	ND	ND
12	ND	2.0	4.7	6.9	12.5	9.5	ND	ND
15	ND	2.2	6.6	9.4	14.4	26.6	0.8	ND
18	ND	4.4	9.5	11.5	20.9	28.0	2.2	ND
18.5				12.3				
19		6.1	11.1		22.2	31.5	15.2	ND
21	0.2							

Chapter 3

Effects of mercury, organic carbon, and microbial inhibitor addition on methylmercury cycling at the profundal sediment-water interface of a sulfate-rich hypereutrophic reservoir

Abstract

Methylmercury (MeHg) produced by anaerobic bacteria in lakes and reservoirs, poses a threat to ecosystem and human health due to its ability to bioaccumulate in aquatic food webs. This study used 48-hour microcosm incubations of profundal sediment and bottom water from a sulfate-rich, hypereutrophic reservoir to assess seasonal patterns of MeHg cycling under various treatments. Treatments included addition of air, inorganic mercury, organic carbon, and microbial inhibitors. Both aeration and sodium molybdate, a sulfate-reducing bacteria (SRB) inhibitor, generally decreased MeHg concentration in microcosm water, likely by inhibiting SRB activity. The methanogenic inhibitor bromoethanesulfonate increased MeHg concentration 2- to 4-fold, suggesting that methanogens were potent demethylators. Pyruvate increased MeHg concentration under moderately reduced conditions, likely by stimulating SRB, but decreased it under highly reduced conditions, likely by stimulating methanogens. Acetate increased MeHg concentration, likely due to the stimulation of acetogenic SRB. Results suggest that MeHg production at the sediment-water interface is elevated under moderately reduced conditions (-100 to -50 mV). In contrast, it is suppressed under oxic conditions due to low SRB activity, and under highly reduced conditions (> -100 mV) due to enhanced demethylation by methanogens.

1. Introduction

Many lakes and reservoirs are contaminated with mercury (Hg), predominantly from widespread atmospheric deposition, but also from point sources including mines and industrial sites (Bigham et al., 2016; Ullrich et al., 2001). In the process of methylation, Hg can be transformed by anaerobic bacteria into toxic methylmercury (MeHg). MeHg bioaccumulates in aquatic food webs, with large fish exhibiting MeHg concentrations thousands of times greater than in water and plankton (Ullrich et al., 2001). In eutrophic lakes and reservoirs that thermally stratify in the summer, oxic profundal waters can become anaerobic as bacteria biodegrade sinking algal organic matter. Anaerobic conditions are highly correlated with the production and release of MeHg from profundal sediment, leading to the buildup of MeHg in bottom waters (Beutel et al., 2014; Watras, 2009). MeHg then bioaccumulates in pelagic biota when it diffuses or mixes into surface waters (Herrin et al., 1998; Slotton et al., 1995; Stewart et al., 2008).

Seasonal production of MeHg, combined with the high potential for its bioaccumulation in the aquatic food web, has led to widespread instances of elevated Hg in fish tissue in California lakes and reservoirs (California Water Boards, 2013; CRWQCB-SFBR, 2008). Regulatory measures aimed at reducing MeHg in fish tissue are being developed in California where over a hundred reservoirs are currently identified as Hg impaired (California Water Boards, 2013). While there is regulatory pressure on reservoir managers to lower fish tissue MeHg concentrations, many potentially effective management strategies are either largely untested, site specific, and/or influenced by complex food web dynamics. Dredging and capping has been used for reservoirs with extensive Hg contamination (Davis et al., 2012). This approach requires removing the contaminated sediment and covering the remaining sediment with clean sand or uncontaminated sediment. This process is expensive and has shown mixed results, with many cases failing to show substantial improvements in fish tissue Hg concentration (Bigham et al., 2016). Another strategy involves the addition of oxygen, nitrate, or metal oxides of iron and manganese to raise the reduction-oxidation (redox) potential at the sediment water interface (Austin et al., 2016; Beutel et al., 2014; Bigham et al., 2016; Mehrotra and Sedlak, 2005; Vlassopoulos et al., 2018). This can potentially decrease MeHg concentrations by inhibiting the activity of anaerobic bacteria that methylate Hg and thus lowering efflux to the overlying water, and by lowering the bioavailability of Hg for methylation via sorption to native and added metal oxides. Although redox manipulation has shown promising results in repressing the production and release of MeHg from sediments in laboratory and field studies, long-term field trials that demonstrate decreases in fish tissue concentrations are lacking. Thus, these novel strategies to control redox potential require further investigation (McCord et al., 2016). An additional approach to managing MeHg production in aquatic sediment is the use of sorbents such as activated carbon or metal oxides to adsorb Hg and MeHg thereby limiting their mobility in the environment (Duvil et al., 2018; Ghosh et al., 2011).

The uncertainty regarding MeHg management strategies in aquatic sediments highlights the need for additional research into Hg cycling in lakes and reservoirs. In addition to uncertainties in management strategies, much remains unknown about

sediment microbiology and MeHg accumulation in water bodies. Previous research has generally regarded sulfate-reducing bacteria (SRB) as the dominant methylating organisms in sediments, and aerobic bacteria as the dominant demethylating, or MeHg degrading, organisms (Ullrich et al., 2001). However, more recent studies using genetic sequencing have revealed a much larger cohort of potential methylators (Gilmour et al., 2013; Podar et al., 2015). In addition, studies using stable isotopes have found that MeHg demethylation rates can often exceed Hg methylation rates in reducing environments (Korthals and Winfrey, 1987; Kronberg et al., 2018). There are also conflicting studies that have shown methanogens to be prominent Hg methylators in some systems but demethylators in others, and other studies that have shown SRB to be important demethylators in certain environments (Hamelin et al., 2011; Gilmour et al., 2018; Pak and Bartha, 1998). The variability in the impact of SRB and methanogens on MeHg production and degradation highlights the need for a better understanding of which biogeochemical conditions favor methylation and which favor demethylation.

This study used monthly sediment-water microcosm incubations throughout the period of thermal stratification from April to November to assess profundal-zone Hg cycling in a sulfate-rich, hypereutrophic reservoir. We added inorganic Hg and carbon sources to evaluate how potentially limiting substrates affected MeHg production relative to the changing biogeochemical conditions of the profundal sediment-water interface. We also used microbial inhibitors to assess how various microbial groups impact MeHg production as conditions at the sediment-water interface became more reduced over time. In situ sediment and porewater chemistry were used to detail temporal environmental characteristics related to Hg cycling in the profundal zone, as well as to characterize the sediment at the start of each incubation. This facilitated the assessment of how the changing biogeochemical parameters of lake sediment such as redox, electron acceptor availability, and sulfide affected MeHg production. A better understanding of environmental factors that stimulate or repress both Hg methylation and MeHg demethylation will help to inform the development of in situ management strategies aimed at reducing MeHg production in the profundal zone. A reduction in net MeHg should ultimately result in fish with lower MeHg concentrations and a lower health risk to humans and wildlife.

2. Methods

2.1 Study site

Hodges Reservoir is a hypereutrophic reservoir in San Diego, California with a maximum capacity of 37 million cubic meters, a maximum depth of 29.1 m, and a maximum mean depth of 8.5 m (Figure 3.1). Typically, the reservoir is operated at a maximum depth of 20-22 m. The reservoir is owned and operated by the City of San Diego and supplies water to the San Dieguito Water District and the Santa Fe Irrigation District, while also acting as a backup water supply for the region. Poor water quality in Hodges Reservoir makes it an unattractive potable water source from a treatability perspective. The reservoir is located within the 64,000-hectare San Dieguito watershed and receives agricultural and urban runoff. As a result, the reservoir experiences severely

degraded water quality and the accumulation of MeHg in bottom water associated summertime anoxia (Beutel et al., 2020; Lee and Biggs, 2015). Although no legacy Hg contamination from mining or industrial activity is suspected, some typically larger fish have exceeded the proposed California regulatory MeHg target of 0.2 mg/kg wet weight for sport fish (J. Pasek, personal correspondence).

Bottom water anoxia typically begins in April and lasts through November (Beutel et al., 2020). Redox potential in the profundal zone progressively drops through the late spring, summer, and fall until overturn around November. Over time, bottom waters exhibit a progressive increase in concentrations of redox-sensitive species including manganese, iron, and sulfide, as well as the key algal nutrients ammonia and phosphate. Biogeochemistry is especially influenced by the high sulfate levels in the reservoir (~180 mg/L), and sulfate reduction is a dominate microbial process in the profundal zone from around June through November. Bottom waters late in the season can have > 20 mg/L sulfide (Beutel et al., 2020). MeHg buildup in bottom waters typically begins in April, peaks around July, then diminish from August to October (Beutel et al., 2020). This observed seasonal pattern of MeHg concentration in bottom waters makes Hodges Reservoir a compelling study site due to it apparently high potential for MeHg production in the spring and summer, but low potential later in the fall.

2.2 Collection of sediment and hypolimnetic water

Profundal sediment and water from the hypolimnion were collected at two deep sampling stations at Hodges Reservoir monthly from April through November 2018 (Figure 3.1). Station A is near the dam and was around 20 m deep. Station B is 2.1 km upstream of the dam and was around 15 m deep. This station is impacted by a pumped storage system operated by the San Diego County Water Authority that appears to enhance vertical mixing in this area of the reservoir (J. Pasek, personal correspondence). Sediment samples were collected with an Ekman dredge. The upper 3 cm of sediment was then quickly subsampled into an acid washed glass container with no headspace. Hypolimnetic bottom water from each station was also collected using a 1.2-L Teflon Kemmerer water sampler in a 1-L PTFE bottle. Sediment and bottom water samples were kept in the dark and on ice after procurement, and during transport to the laboratory. Samples were stored overnight in a dark refrigerator at 4 ^{o}C and transferred to an anaerobic glovebox containing 95% nitrogen and 5% hydrogen gas the following day. In the anaerobic glovebox, sediment samples from each station were thoroughly homogenized. After homogenization, half of the collected sediment was used for sediment and porewater characterization, while the other half was used for microcosm incubations.

2.3 Porewater and sediment chemical analysis

Porewater was extracted from the sediment by centrifuging at 4,000 RPM for 20 minutes at 4 ^{o}C. In an anaerobic glovebox, porewater was analyzed for oxidation-reduction potential (ORP) using a calibrated Hatch HQ30D multiparameter portable

meter. ORP was standardized to the hydrogen electrode as described in APHA (2017). Porewater samples were preserved for sulfide analysis with zinc acetate, and for dissolved sulfate by filtration through a 0.45 µm nylon filter and frozen at -6 ° C for later analysis using standard methods (APHA, 2017). Sulfide (method detection limit [MDL] of 0.4 mg/L) was measured by iodometric titration. Sulfate (MDL 0.5 mg/L) was measured by ion chromatography. Sediment was also analyzed for amorphous ferric iron (Fe(III)a), a poorly crystalline form of iron hydroxide considered to be available for microbial reduction. Fe(III)a (MDL 10 mg/kg) was extracted from sediment with 0.5 M hydrochloric acid and hydroxylamine then determined spectrophotometrically using Ferrozine according to Marvin-DiPasquale et al. (2008).

2.4 Microcosm incubation experiments

From April through early December, triplicate microcosms were assembled approximately monthly (8 sampling events total) in an anaerobic glove box. Microcosms consisted of 1 g of sediment in 30 ml of bottom water added to 40 mL flat bottomed trace metal glass vials. Microcosms had a well-defined sediment-water interface and enough water to facilitate subsequent water quality analysis. Vials were spiked with a range of experimental treatments intended to manipulate the sediment-water environment and test the expected response related to MeHg buildup in water over the 48-hr experimental incubation (Table 3.1). In addition to time 0 vials and 48-hr controls (no amendment addition), 48-hr treatments included: inorganic Hg, acetate (started in May), pyruvate, ambient air, molybdate, pyruvate/molybdate (started in May), bromoethanesulfonate (BES), and BES/molybdate (started in early July). Vials were incubated in the dark at 15 ˚C (to mimic profundal conditions) on an orbital shaker at 100 rpm to allow for modest mixing without disrupting the sediment-water interface. The ambient air treatment was incubated with its cap off to facilitate air exchange with the atmosphere. Vials were decanted and water was filtered with a 0.45 µm nylon membrane, preserved with 0.5% HCl, and refrigerated in the dark for later MeHg analysis.

MeHg analysis was performed on a MERX automated modular Hg system (Brooks Rand Labs, Seattle, WA, USA) using cold vapor atomic fluorescence spectroscopy (CVAFS) based on USEPA method 1630 (USEPA 2001) (MDL 0.02 ng/L). Strict quality control procedures were followed including calibration blanks (< 50 pg per 25 ml sample), method blanks (< 1 pg per 25 ml sample), matrix spikes and matrix spike duplicates (acceptable recovery range 71-125%), and ongoing precision recovery samples (acceptable recovery range 77-123%).

For each microcosm treatment, a mean normalized MeHg concentration ($MeHg_n$, units of ng/L·kg) was calculated as the average of MeHg water concentration (ng/L) dividend by the dry mass (kg) of sediment for each set of triplicate incubations. For the control incubations (no treatment), control response (CR) was calculated as:

$$CR = \frac{[CMeHg_n]_{48}}{[CMeHg_n]_0}$$

where $[CMeHg_n]_0$ is the mean normalized MeHg concentration for 0-hr triplicate vials and $[CMeHg_n]_{48}$ is the mean normalized MeHg concentration for 48-hr triplicate controls. CR > 1 indicates that dissolved MeHg concentration increased during the incubation period, while CR < 1 indicates that dissolved MeHg concentration decreased. Significant differences between the 0-hr vials and 48-hr controls were assessed by comparing mean normalized MeHg concentrations using a Student's t-Test (n = 3).

For the treatment incubations, treatment response (TR) was calculated as:

$$TR = \frac{[TMeHg_n]_{48}}{[CMeHg_n]_{48}}$$

where $[TMeHg_n]_{48}$ is the mean normalized MeHg concentration for triplicate 48-hr treatments, and $[CMeHg_n]_{48}$ is the mean normalized MeHg concentrations for 48-hr triplicate controls. TR > 1 indicates that dissolved MeHg concentration increased in treatment incubations relative to control incubations over the incubation period. TR < 1 indicates that dissolved MeHg concentration decreased. Significant differences between the 48-hr controls and 48-hr treatments were assessed by comparing mean normalized MeHg concentrations using a Student's t-Test (n = 3). For both the CR and TR metrics, the conventional value of $p < 0.05$ was used to signify a statistically significant difference between a treatment and the control, while a value of $p < 0.10$ was designated as nearly statistically significant.

3. Results

3.1 Porewater and sediment

Profundal sediment was largely anaerobic during the course of this study (Figure 3.2, Table 3.3). Porewater ORP was similar between station A and B, but always slightly lower at station A. Generally, ORP decreased from April to October at both stations while the reservoir was stratified (14 to -175 mV at station A, 39 to -71 mV at station B) and rose substantially after mixing in November. However, there was an exception with an apparent increase in the porewater ORP at both stations in September. Sulfate in the porewater of both stations was elevated in April, declined to a minimum concentration in July (3.8 mg/L at station A, 6.5 mg/L at station B), and rose slightly afterwards. Sediment-extracted Fe(III)a was only present in April, May and November at both stations, as well as in September and October at station B. Fe(III)a concentration was generally low when it was present (29-191 mg/kg at station A, 30-169 mg/kg at station B). Sulfide concentrations in the pore water were moderate in April at both stations, rose to a maximum value in July at station A (32.2 mg/L) and June at station B (24.4 mg/L), and then generally declined with time until the end of the study.

3.2 Control response and treatment response

Incubations from both stations showed a general trend of CRs ~1 or < 1 in April and May and significantly high CRs (2-4) from July to August (Figure 3.3, Table 3.3). Station A had a significantly low CR in September (0.6) but a significantly high CR in October (1.4). In contrast, station B displayed a significantly high CR in September (1.8). MeHg buildup in microcosm experiments was particularly elevated in the summer months at both stations.

Treatment responses (TRs) were most affected by the addition of organic carbon and BES (Figure3.4, Table 3.4). Addition of inorganic Hg generally had a positive but statistically insignificant effect on TRs except in July at station B (1.8). Ambient air treatment showed a mixed pattern of TRs, with values < 1 on most dates and a significantly low value (0.4) in mid-July at station B. Sulfate concentration did not decrease substantially during the 48-hour incubation (data not shown), indicating that SRB were suppressed during the ambient air treatment. Pyruvate addition had a dramatic effect on TRs at both stations. TRs were significantly high (< 5) at the beginning and end of the season, in some cases exceeding 10. But TRs were < 1 in the middle of the season, especially in August at both stations (0.2). Acetate addition was always associated with TRs > 1 and on 2-3 dates at each station TRs (> 2-4) were statistically significant.

Molybdate addition generally had TRs < 1 but values were statistically insignificant except in mid-July with a significantly low TR (0.4) at station A and a nearly significant low TR (0.5) at station B (Figure 3.4). TRs for combined pyruvate/molybdate addition generally followed the same trend as molybdate only, but with more extreme and statistically significant values. At station A, TRs were low (< 0.4) for May through October. At station B there was a statistically significant pattern of low TRs (< 0.3) in July/August but significantly high TRs (< 2.6) in September and October. Sulfate concentration did not decrease substantially during the 48-hour incubation (data not shown), indicating that SRB were suppressed during the molybdate and pyruvate/molybdate treatments.

BES addition, as with pyruvate addition, had one of the clearest effects on TRs of all treatments (Figure 3.4). At both stations on all dates, TR was positive and over half of TRs were statistically significant with values generally > 2-3 and as high as 9.4. TRs for combined BES/molybdate addition were generally > 1 at both stations but not statistically significant except for a significantly high TR (2.0) at station A in August.

4. Discussion

4.1 Control responses and sediment quality

Seasonal patterns of CR, a metric that quantified whether the sediment-water interface experimental systems accumulated (CR > 1) or lost (CR < 1) dissolved MeHg in water over the 48-hour incubation period, appeared to correspond with some sediment and porewater characteristics. Of particular importance was porewater ORP, sediment-extracted Fe(III)a, and porewater sulfate. No trends were observed with porewater

sulfide. With regards to ORP, peak CRs (CR > 2) occurred in the summer at both stations and corresponded with a narrow ORP range of -100 to -50 mV (Figs. 2 and 3). Above and below this ORP, CRs tended to be ~1 or < 1 (Figure 3.5). Previous research has demonstrated that moderately reduced conditions, such as those at the oxic-anoxic interface, tend to lead to the MeHg buildup, with either elevated redox (e.g., aerobic conditions) or low redox (e.g., levels associated with methanogenesis) leading to lower MeHg concentrations comparatively (Duvil et al., 2018; Paranjape and Hall, 2017; Ullrich et al., 2001). Our study supports previous research and suggests that moderately reduced conditions are most favorable to MeHg production in profundal surficial sediment.

Periods of relatively low CR (~1) in the spring and fall corresponded with the presence of Fe(III)a (Figures 3.2 and 3.3). In contrast, elevated CRs (> 2) in the summer were associated with no Fe(III)a in profundal sediment (Figure 3.5). These observations indicate that the presence of Fe(III)a is an indicator of low potential for MeHg production in profundal sediment, likely since it is indicative of elevated redox conditions that do not favor SRB. IRB have been shown to outcompete SRB for resources in aquatic sediments, thereby reducing levels of sulfate reduction (Lovley, 1987). Although IRB have been shown to be prominent methylators in iron-rich sediments (Bravo et al., 2018; Fleming et al., 2006), they do not appear so in Hodges Reservoir, likely because high sulfate in porewater and low iron in sediment favor SRB.

At both stations, elevated CRs also corresponded with low sulfate concentrations in porewater (Figure 3.5). Sulfate in porewater was above 25 mg/L in April at both stations when the CR was ~1, but was typically below ~10 mg/L when CRs were at a peak from July through August (Figures 3.2 and 3.3). This paradoxical negative correlation between MeHg production and sulfate concentration was also observed in wetland sediment by Gilmour et al. (1998), who found that although methylation appeared to be mediated by SRB, elevated sulfate concentrations corresponded with decreased methylation rates and MeHg concentrations. Altered SRB microbial community structure and the associated impact on net methylation is a potential explanation for the negative correlation between sulfate concentration and MeHg concentration. Lower sulfate concentrations are known to favor “metabolically flexible” SRB that can use a range of electron acceptors (Colleran et al., 1995; Plugge et al., 2011). These metabolically flexible SRB are often acetogenic and generally grow syntrophicaly with other anaerobic bacteria (Plugge et al., 2011), conditions that correspond with enhanced MeHg production in aquatic sediment (Yu et al., 2018; Bae et al., 2014). In addition to the possibility that net methylation was greater at low sulfate concentration, higher sulfate concentrations could have led to enhanced rates of demethylation. Previous studies have shown that SRB are MeHg demethylators (Korthals and Winfrey, 1987; Pak and Bartha, 1998). In a seasonal study on methylation and demethylation rates in profundal lake sediment, Korthals and Winfrey, 1987 observed that temporal methylation rates were moderately steady and net methylation was generally driven by demethylation rates. These findings suggest that the negative correlation between CRs and porewater sulfate may be explained by higher rates of methylation stimulated by syntrophic bacterial communities during low sulfate availability and enhanced rates of demethylation in environments where sulfate was not limited.

4.2 Hg(II) and ambient air treatments

Two factors are required to support microbial MeHg production in aquatic sediment: bioavailable inorganic Hg and substrates that stimulate anaerobic microbial activity such as organic matter and sulfate (Bigham et al., 2016; Paranjape and Hall, 2017). We hypothesized that inorganic Hg addition would enhance MeHg buildup in microcosm incubations leading to TR > 1. In general, inorganic Hg TRs were > 1, but values were only significant in early July at station B (1.8). A lack of a clear enhancement of MeHg production after inorganic Hg addition was likely associated with high levels of sulfide in porewater which commonly exceeded 30 mg/L (Figure 3.2). Gilmour et al. (1998) found that methylation rates were highest in wetland sediment with the lowest sulfide levels and observed that the addition of sulfide significantly reduced methylation rates. Decreased methylation rates in sulfidic environments may be due to the formation of larger or more ordered β-HgS nanocolloids which have lower surface area reactivity and lower rates of dissolution (Poulin et al., 2017).

We also hypothesized that passively aerating microcosm would suppress the methylating activity of SRB, which are obligate anaerobes (Colleran et al., 1995), and result in TRs < 1. Several studies have documented lower rates of MeHg production in aquatic sediment under aerobic versus anaerobic conditions, including in Hodges Reservoir (Beutel et al., 2020). In addition, some lake managers and environmental regulators are exploring ways to minimize MeHg production and subsequent bioaccumulation by managing redox conditions in the profundal zone via aeration/mixing (Perron et al., 2014), oxygenation (Beutel et al., 2020, Beutel et al., 2014, McCord et al., 2016), and nitrate addition (Matthews et al., 2013). However, ambient air treatment yielded ambivalent results. Aerated TRs were generally < 1, suggesting suppression of MeHg production (Figure 3.4). Maintaining oxic conditions at the sediment-water interface may repress MeHg accumulation via several mechanisms including suppression of SRB (Ullrich et al., 2001), sorption of MeHg/DOC complexes to native iron oxides (Dent et al., 2014, Matthews et al., 2013), and enhanced aerobic microbial demethylation of MeHg via the MerA/B detoxification pathway (Boyd and Barkay, 2012). However, ambient air TRs in May suggested an enhancement effect (≤ 1.7) at both stations. Oxic sediment may be a source of MeHg via enhanced recycling of sulfide back to sulfate, which could both stimulate SRB and promote inorganic Hg bioavailability for methylation (Paranjape and Hall, 2017). Oxic conditions may also enhance oxidative dissolution of labile Hg-sulfide compounds (Duvil et al., 2018), and liberate Hg from organic matter during high rates of mineralization associated with transition from anoxic to oxic conditions (Hulthe et al., 1998).

4.3 Pyruvate and acetate treatments

Pyruvate is a near universally utilizable carbon source for bacteria that can be aerobic Pyruvate is a near universally viable carbon source for bacteria that can be aerobically metabolized or anaerobically fermented (Baltscheffsky, 1996). It is also a key metabolic intermediate that can be converted into a wide variety of biological compounds or oxidized to generate energy (Gray et al., 2013; Muller at al., 2012). This wide

metabolic application results in high microbial competition for pyruvate and associated enhanced use of favorable electron acceptors (Achtnich et al., 1995). In the context of our study, we hypothesized that pyruvate addition under moderately reduced conditions would enhance the depletion of intermediate electron acceptors (e.g., nitrate, manganese oxides, iron oxides) and open up a niche for SRB, resulting in enhanced MeHg production (TR > 1). But under highly reduced conditions, we hypothesized that pyruvate addition would lead to the depletion of favorable electron acceptors including sulfate, thereby opening a niche for methanogenic bacteria known to demethylate MeHg (Pak and Bartha, 1998) and leading to negative net methylation (TR < 1). This hypothesis was generally supported by experimental results. When ORP measured in the sediment was above around -50 mV, pyruvate TR at both stations was typically > 3 and statistically significant (Figure 3.4). In contrast, during the late summer at station A and in August at station B, porewater ORP was generally below this threshold and pyruvate TR levels were < 1. We also found a weak but statistically significant positive correlation between pyruvate TR and porewater ORP (Figure 3.6, $R^2 = 0.28$, n = 16, p = 0.034). This result illustrates the linkage between sediment redox conditions and the potential for pyruvate to either enhance (at high redox) or suppress (at low redox) MeHg production in profundal sediment from the study site through stimulation of different microbial populations. Our results are similar to Compeau and Bartha (1985), who showed that pyruvate addition to estuarine sediment slurries resulted in a three-fold increase in MeHg production. They attributed this observation to the stimulation of Desulfovibrio desulfuricans, a model SRB methylator (Gilmour et al., 2013; Hsu-Kim et al., 2013)

Unlike pyruvate, acetate metabolism is limited to specific cohorts of bacteria and high concentrations can inhibit certain microbial species (Pinhal et al., 2019). Acetate can be utilized by SRB when sulfate is present, and by acetogens or methanogens when sulfate is absent (Colleran et al., 1995; Oude Elferink et al., 1994). SRB capable of acetate degradation are generally metabolically flexible and can also grow as acetogens in the absence of sulfate (Oude Elferink et al., 1994; Plugge et al., 2011). Acetate-degrading SRB are known to methylate Hg at higher rates than SRB that do not degrade acetate (King et al., 2000; Ekstrom and Morel, 2008). In this study, acetate addition was hypothesized to enhance acetate-degrading SRB activity and yield a TR > 1, and this pattern was generally observed in the experimental results (Figure 3.4). Additionally, for summer months when Fe(III)a was not present in sediment and SRB were thought to be the dominate anaerobes, a correlation between the acetate TR and porewater sulfate concentration was observed (Figure 3.7; $R^2 = 0.56$, p = 0.033). This relationship suggests that the presence of sulfate and acetate enhanced the activity of acetate-degrading SRB, which in turn methylated Hg and yielded elevated acetate TRs.

4.4 Molybdate treatments

SRB are generally considered the dominant Hg methylators in aquatic sediments (Bigham et al., 2016; Paranjape and Hall, 2017; Ullrich et al., 2001). Molybdate addition, by repressing SRB activity and associated Hg methylation, was hypothesized to lower MeHg buildup in microcosm incubations and yield TR values < 1. This was generally observed, though TRs were significantly lower only in late July (Figure 3.4). In July and

August at both stations, the lowest molybdate TRs, which are indicative of repressed SRB methylation, corresponded with peak CRs (Figure 3.3), which are suggestive of high MeHg production potential at the sediment-water interface. This observation supports the contention that SRB were prominent Hg methylators during the summer of 2018 in Hodges sediment. The muted response of the molybdate treatment overall, which in some months appeared to stimulate MeHg buildup, though not significantly, may be related to the fact that molybdate has been shown to be bacteriostatic (prevents growth and metabolism), rather than bactericidal (directly kills the organism) (Isa and Anderson, 2005; Newport and Nedwell 1988). Thus, in our experimental incubations treated with molybdate, metabolically flexible SRB may have remained active and may have continued to methylate Hg.

The pyruvate/molybdate treatment, by suppressing SRB but providing a highly bioavailable organic carbon source for microbes, was hypothesized to open a niche for MeHg production by IRB. A variety of IRB species carry the genes required for Hg methylation and some IRB are efficient methylators in pure culture and in iron-rich sediment (Bravo et al., 2018; Kerin et al., 2006; Podar et al., 2015; Si et al., 2015). As was observed in the molybdate only treatment, TRs were generally < 1 suggesting SRB suppression with no concurrent enhancement of MeHg production by IRB. However, at station B there was a shift in pyruvate/molybdate TR from significantly < 1 in August to significantly > 1 in September and October (Figure 3.4). In addition, pyruvate/molybdate TRs were > 1, although not significantly, in May and December at both stations. These dates correspond with higher ORP and the presence of Fe(III)a in profundal sediment (Figure 3.2), conditions advantageous to IRB activity. But during these periods, CR values which were generally ~1, except for station B in October which was 1.8 (Figure 3.3), indicating that native sediment had little capacity for MeHg production. Collectively, results indicate that IRB were not especially significant methylators except perhaps for a brief window in the spring and likely in shallower profundal sediment.

4.5 BES treatments

The BES treatment had one of the clearest, positive MeHg production responses of all the treatments, supporting the hypothesis that inhibition of methanogens that demethylate will enhance MeHg buildup at the profundal sediment-water interface. BES TRs averaged > 2 at station A and > 4 at station B, and over half of the monthly incubations had a TR significantly higher than the control. This observation conflicts with studies that show decreases in MeHg production in BES-treated sediment and soil (Correia and Guimaraes, 2017; Kronberg et al., 2016). Studies have also identified methanogens as MeHg sources in pure culture and periphyton biofilm (Gilmour et al., 2018; Hamelin et al., 2011; Yu et al., 2013). However, other studies have found that BES addition to aquatic sediment enhances MeHg production and/or suppresses demethylation (Avramescu et al., 2011; Bae et al., 2014; Gilmour et al., 1998; Kronberg et al., 2018). In lake sediment, Pak and Batha (1998) found that methanogens were capable of demethylation but not methylation, while Korthals and Winfrey (1987) measured elevated rates of demethylation in deeper sediment where enhanced methanogenic metabolism occurs. In Hodges Reservoir, field studies showed a loss of MeHg from the

profundal water column under highly reduced conditions in the late summer, which has been attributed, in part, to enhanced demethylation by methanogens (Beutel et al., 2020). The conflicting impact of methanogens on MeHg cycling is not surprising considering the breadth of this microbial classification and its wide distribution in the environment (Mah and Smith, 1981).

BES/molybdate addition, having suppressed both SRB and methanogen activity, was intended to isolate the impact of fermentative, acetogenic, and/or cellulolytic organisms which have shown the ability to methylate Hg (Christensen et al., 2016; Gilmour et al., 2013; Podar et al., 2015). At both stations, TRs were generally < 1 in spring and > 1 in summer and fall, though only one value was significant (Figure 3.4). The fact that BES/molybdate TRs were positive as bottom waters became more reduced (Figure 3.2) suggests that this cohort of microbes were active in the experimental incubations and may be of modest environmental significance in Lake Hodges profundal sediment.

5. Conclusions

This study evaluated MeHg cycling at the profundal sediment-water interface of a sulfate-rich hypereutrophic reservoir. The study is unique in that it not only tracked effects of multiple sediment treatments on MeHg production, but also how these effects changed over time as environmental conditions in the profundal zone changed. Our study found that the inhibition of SRB, through aeration or molybdate addition, generally led to decreased MeHg accumulation in microcosm water. Carbon additions appeared to impact MeHg cycling by stimulating different microbial communities. The addition of pyruvate led to significant increases in MeHg concentration during moderately-reduced conditions, likely by stimulating SRB that methylate Hg. During highly reduced conditions, the pyruvate treatment led to significant decreases in MeHg concentration, likely due to stimulating the activity of methanogens that demethylate MeHg. Acetate led to increased MeHg accumulation in microcosm water, especially during periods of low sulfate in the sediment porewater, potentially by stimulating syntrophic and acetogenic SRB that methylate at high rates. Inhibition of methanogenesis led to a significant increase in MeHg concentration, indicating that methanogenesis suppressed MeHg accumulation in microcosm water, likely due to high rates of demethylation.

Overall, results suggest that net methylation at the sediment-water interface is enhanced under moderately reduced conditions associated with SRB activity and suppressed under oxic conditions where SRB are not favored or under highly reduced conditions where methanogens demethylate at high rates. From a management perspective, results suggest that strategies such as lake oxygenation or nitrate addition, which poise redox potential at the sediment-water interface above that which favors SRB, should suppress MeHg production and efflux from profundal sediment. One concern to acknowledge is that insufficient oxygenation of the sediment-water interface could shift the profundal zone from highly reduced conditions that favor demethylation to moderately reduced conditions that favor MeHg production, thereby accidently exacerbating the potential for MeHg bioaccumulation into aquatic biota. Another concern is that insufficient oxygen penetration into the profundal sediment, may allow for sulfate

reduction to continue just below the interface and MeHg to diffuse into the bottom water. Profundal sediment redox management may therefore be a valuable tool for reducing MeHg bioaccumulation in the food web if care is taken to ensure moderately reduced conditions at the sediment-water interface are fully averted.

6. References

Achtnich, C., Bak, F., Conrad, R., 1995. Competition for electron donors among nitrate reducers, ferric iron reducers, sulfate reducers, and methanogens in anoxic paddy soil. Biology and Fertility of Soils, 19(1), 65–72.

American Public Health Association (APHA), 2017. Standard methods for the examination of water and wastewater. 23rd ed. American Public Health Association Washington, D.C.

Austin, D., Scharf, R., Carroll, J., Enochs, M., 2016. Suppression of hypolimnetic methylmercury accumulation by liquid calcium nitrate amendment: redox dynamics and fate of nitrate. Lake and Reservoir Management, 32(1), 61–73.

Avramescu, M., Yumvihoze, E., Hintelmann, H., Ridal, J., Fortin, D., Lean, D. R., 2011. Biogeochemical factors influencing net mercury methylation in contaminated freshwater sediments from the St. Lawrence River in Cornwall, Ontario, Canada. Science of the Total Environment, 409(5), 968-978.

Bae, H., Dierberg, F.E., Ogram, A., 2014. Syntrophs dominate sequences associated with the mercury methylation-related gene hgcA in the water conservation areas of the Florida Everglades. Applied and Environmental Microbiology, 80(20), 6517-6526.

Baltscheffsky, H., 1996. Origin and evolution of biological energy conversion (pp. 16-18, 59-63). New York, NY: Wiley-VCH.

Beutel, M., Fuhrmann, B., Herbon, H., Chow, C., Brower, S., Pasek, J., 2020. Cycling of methylmercury and other redox-sensitive compounds in the profundal zone of a hypereutrophic water supply reservoir. Hydrobiologia.

Beutel, M., Dent, S., Reed, B., Marshall, P., Gebremariam, S., Moore, B., Shallenberger, E., 2014. Effects of hypolimnetic oxygen addition on mercury bioaccumulation in Twin Lakes, Washington, USA. Science of The Total Environment, 496, 688-700.

Bigham, G.N., Murray, K.J., Masue-Slowey, Y., Henry, E.A., 2016. Biogeochemical controls on methylmercury in soils and sediments: Implications for site management. Integrated Environmental Assessment and Management, 13(2), 249-263.

Boyd, E., Barkay, T., 2012. The mercury resistance operon: from an origin in a geothermal environment to an efficient detoxification machine. Frontiers in Microbiology, 3, 1-13.

Bravo, A.G., Zopfi, J., Buck, M., Xu, J., Bertilsson, S., Schaefer, J.K., Poté, J., Cosio, C., 2018. Geobacteraceae are important members of mercury-methylating microbial communities of sediments impacted by waste water releases. The ISME Journal, 12(3), 802-812.

California Water Boards, 2013. Statewide mercury control program for reservoirs. facts sheet for the statewide mercury program. September 2013. https://www.waterboards.ca.gov/water_issues/programs/mercury/reservoirs/docs/factsheet.pdf

Christensen, G.A., Wymore, A.M., King, A.J., Podar, M., Hurt, R.A., Santillan, E.U., Brandt, C.C., Brown, S.D., Palumbo, A.V., Wall, J.D., Gilmour, C.C., Elias, D.A., 2016. Development and validation of broad-range qualitative and clade-specific quantitative molecular probes for assessing mercury methylation in the environment. Applied and Environmental Microbiology, 82(19), 6068-6078.

Colleran, E., Finnegan, S., Lens, P., 1995. Anaerobic treatment of sulphate-containing waste streams. Antonie Van Leeuwenhoek, 67(1), 29-46.

Compeau, G.C., Bartha, R., 1985. Sulfate-reducing bacteria: principal methylators of mercury in anoxic estuarine sediment. Applied and Environmental Microbiology, 50(2), 498-502.

Correia, R.R., Guimarães, J.R., 2017. Mercury methylation and sulfate reduction rates in mangrove sediments, Rio de Janeiro, Brazil: The role of different microorganism consortia. Chemosphere, 167, 438-443.

CRWQCB-SFBR, 2008. Guadalupe river watershed mercury total maximum daily load (TMDL) project, basin plan amendment. Adopted October 8, 2008. https://www.waterboards.ca.gov/sanfranciscobay/water_issues/programs/TMDLs/guadalupe_river_mercury/C1_Guad_SR_Sep08.pdf. Accessed July 17, 2018.

Davis, J.A., Looker, R.E., Yee, D., Marvin-DiPasquale, M., Grenier, J.L., Austin, C.M., McKee, L.J, Greenfield, B.K., Brodberg, R., Blum, J., 2012. Reducing methylmercury accumulation in the food webs of San Francisco Bay and its local watersheds. Environmental Research, 119, 3-26.

Dent, S.R., M.W. Beutel, P.A. Gantzer, B.C. Moore, 2014, Response of iron, manganese and mercury in an anoxic water column to short-term hypolimnetic oxygenation, Lake and Reservoir Management, 30, 119 – 130.

Duvil, R., Beutel, M.W., Fuhrmann, B., Seelos, M., 2018. Effect of oxygen, nitrate and aluminum addition on methylmercury efflux from mine-impacted reservoir sediment. Water Research, 144, 740-751.

Ekstrom, E.B., Morel, F.M., 2008. Cobalt limitation of growth and mercury methylation in sulfate-reducing bacteria. Environmental Science and Technology, 42(1), 93–99.

Fleming, E.J., Mack, E.E., Green, P.G. and Nelson, D.C., 2006. Mercury methylation from unexpected sources: molybdate-inhibited freshwater sediments and an iron-reducing bacterium. Applied Environmental Microbiology, 72(1), 457-464.

Ghosh, U., Luthy, R.G., Cornelissen, G., Werner, D., Menzie, C.A., 2011. In-situ sorbent amendments: a new direction in contaminated sediment management. Environmental Science and Technology, 45, 1163–1168.

Gilmour, C.C., Bullock, A.L., Mcburney, A., Podar, M., Elias, D.A., 2018. Robust mercury methylation across diverse methanogenic archaea. MBio, 9(2).

Gilmour, C.C., Podar, M., Bullock, A.L., Graham, A.M., Brown, S.D., Somenahally, A.C., Johs, A., Hurt Jr., R.A., Bailey, K.L., Elias, D.A., 2013. Mercury methylation by novel microorganisms from new environments. Environmental Science and Technology, 47(20), 11810-11820.

Gilmour, C.C., Riedel, G.S., Ederington, M.C., Bell, J.T., Benoit, J.M., Gill, G.A., Stordal, M.C., 1998. Methylmercury concentrations and production rates across a trophic gradient in the northern everglades. Biogeochemistry, 40, 327-345.

Gray, L.R., Tompkins, S.C., Taylor, E.B., 2013. Regulation of pyruvate metabolism and human disease. Cellular and Molecular Life Sciences, 71(14), 2577-2604.

Hamelin, S., Amyot, M., Barkay, T., Wang, Y., Planas, D., 2011. Methanogens: principal methylators of mercury in lake periphyton. Environmental Science and Technology, 45(18), 7693-7700.

Herrin, R.T., Lathrop, R.C., Gorski, P.R., Andren, A.W., 1998. Hypolimnetic methylmercury and its uptake by plankton during fall destratification: A key entry point of mercury into lake food chains? Limnology and Oceanography, 43(7).

Hsu-Kim, H., Kucharzyk, K.H., Zhang, T., Deshusses, M.A., 2013. Mechanisms regulating mercury bioavailability for methylating microorganisms in the aquatic environment: a critical review. Environmental Science and Technology, 47(6), 2441-2456.

Hulthe, G., Hulth, S., Hall, P.O., 1998. Effect of oxygen on degradation rate of refractory and labile organic matter in continental margin sediments. Geochimica Et Cosmochimica Acta, 62(8), 1319–1328.

Isa, M.H., Anderson, G., 2005. Molybdate inhibition of sulphate reduction in two-phase anaerobic digestion. Process Biochemistry, 40(6), 2079–2089.

Kerin, E.J., Gilmour, C.C., Roden, E., Suzuki, M.T., Coates, J.D., Mason, R.P., 2006. Mercury methylation by dissimilatory iron-reducing bacteria. Applied and Environmental Microbiology, 72(12), 7919-7921.

King, J.K., Kostka, J.E., Frischer, M.E., Saunders, F.M., 2000. Sulfate-reducing bacteria methylate mercury at variable rates in pure culture and in marine sediments. Applied and Environmental Microbiology, 66(6), 2430-2437.

Korthals, E.T., Winfrey, M.R., 1987. Seasonal and spatial variations in mercury methylation and demethylation in an oligotrophic lake. Applied and Environmental Microbiology, 53(10), 2397-2404.

Kronberg, R., Schaefer, J.K., Björn, E., Skyllberg, U., 2018. Mechanisms of methyl mercury net degradation in alder swamps: the role of methanogens and abiotic processes. Environmental Science and Technology Letters, 5(4), 220-225.

Kronberg, R., Jiskra, M., Wiederhold, J.G., Björn, E., Skyllberg, U., 2016. Methyl mercury formation in hillslope soils of boreal forests: the role of forest harvest and anaerobic microbes. Environmental Science and Technology, 50(17), 9177-9186.

Lee, R.M., Biggs, T.W., 2015. Impacts of land use, climate variability, and management on thermal structure, anoxia, and transparency in hypereutrophic urban water supply reservoirs. Hydrobiologia, 745(1): 263–284.

Lovley, D.R., Phillips, E.J., 1987. Competitive mechanisms for inhibition of sulfate reduction and methane production in the zone of ferric iron reduction in sediments. Applied and Environmental Microbiology, 53(11), 2636–2641.

Mah, R. A., Smith, M. R., 1981. The methanogenic bacteria. In: Starr M.P., Stolp H., Trüper H.G., Balows A., Schlegel H.G. (eds) The prokaryotes. (pp. 948-977). Berlin, Germany: Springer.

Marvin-DiPasquale, M.C., Lutz, M.A., Krabbenhoft, D.P., Aiken, G.R., Orem, W.H., Hall, B.D., DeWild, J.F., Brigham, M.E., 2008. Total mercury, methylmercury, methylmercury production potential, and ancillary streambed-sediment and pore-water data for selected streams in Oregon, Wisconsin, and Florida, 2003-04. National Water-Quality Assessment, USGS.

Matthews, D., Babcock, D., Nolan, J., Prestigiacomo, A., Effler, S., Driscoll, C., Todorova, S., Kuhr, K., 2013. Whole-lake nitrate addition for control of methylmercury in mercury-contaminated Onondaga Lake, NY. Environmental Research, 125: 52–60.

McCord, S.A., Beutel, M.W., Dent, S.R., Schladow, S.G., 2016. Evaluation of mercury cycling and hypolimnetic oxygenation in mercury-impacted seasonally stratified reservoirs in the Guadalupe River watershed, California. Water Resources Research, 52(10), 7726-7743.

Mehrotra, A.S., Sedlak, D.L., 2005. Decrease in net mercury methylation rates following iron amendment to anoxic wetland sediment slurries. Environmental Science and Technology, 39(8), 2564-2570.

Muller, M., Mentel, M., Hellemond, J.J. V., Henze, K., Woehle, C., Gould, S.B., Yu, R.Y., van der Giezen, M., Tielens, A.G., Martin, W.F., Martin, W.F., 2012. Biochemistry and evolution of anaerobic energy metabolism in eukaryotes. Microbiology and Molecular Biology Reviews, 76(2), 444–495.

Newport, P., Nedwell, D.B., 1988. The mechanisms of inhibition of Desulfovibrio and Desulfotomaculum species by selenate and molybdate. Journal of Applied Bacteriology, 65(5), 419–423.

Oude Elferink, S., Visser, A., Pol, L., Stams, A., 1994. Sulfate reduction in methanogenic bioreactors. FEMS Microbiology Reviews, 15(2-3), 119-136.

Pak, K.R., Bartha, R., 1998. Mercury methylation and demethylation in anoxic lake sediments and by strictly anaerobic bacteria. Applied and Environmental Microbiology, 64(3), 1013-1017.

Paranjape, A.R., Hall, B.D., 2017. Recent advances in the study of mercury methylation in aquatic systems. Facets, 2(1), 85-119.

Perron, T., Chételat, J., Gunn, J., Beisner, B.E., Amyot, M., 2014. Effects of experimental thermocline and oxycline deepening on methylmercury bioaccumulation in a Canadian shield lake. Environmental Science and Technology 48(5), 2626–2634.

Pinhal, S., Ropers, D., Geiselmann, J., Jong, H. D., 2019. Acetate metabolism and the inhibition of bacterial growth by acetate. Journal of Bacteriology, 201(13).

Plugge, C.M., Zhang, W., Scholten, J. C., Stams, A. J., 2011. Metabolic flexibility of sulfate-reducing bacteria. Frontiers in Microbiology, 2.

Podar, M., Gilmour, C., Brandt, C., Soren, A., Brown, S, 2015. Global prevalence and distribution of genes and microorganisms involved in mercury methylation. Scientific Advances, 1-12.

Poulin, B.A., Gerbig, C.A., Kim, C. S., Stegemeier, J.P., Ryan, J.N., Aiken, G.R., 2017. Effects of sulfide concentration and dissolved organic matter characteristics on the structure of nanocolloidal metacinnabar. Environmental Science and Technology, 51(22), 13133-13142.

Si, Y., Zou, Y., Liu, X., Si, X., Mao, J., 2015. Mercury methylation coupled to iron reduction by dissimilatory iron-reducing bacteria. Chemosphere, 122, 206-212.

Slotton, D.G., Reuter, J.E., Goldman, C.R., 1995. Mercury uptake patterns of biota in a seasonally anoxic northern California reservoir. Water Air and Soil Pollution 80: 841–850.

Stewart, A.R., Saiki, M.K., Kuwabara, J.S., Alpers, C.N., Marvin-DiPasquale, M. and Krabbenhoft, D.P., 2008. Influence of plankton mercury dynamics and trophic pathways on mercury concentrations of top predator fish of a mining-impacted reservoir. Canadian Journal of Fisheries and Aquatic Sciences, 65(11), pp.2351-2366.

Ullrich, S.M., Tanton, T.W., Abdrashitova, S.A., 2001. Mercury in the aquatic environment: a review of factors affecting methylation. Critical Reviews in Environmental Science and Technology, 31, 241-293.

USEPA, 2001. Method 1630: methyl mercury in water by distillation, aqueous ethylation, purge and trap, and CVAFS. EPA-821-R-01-020. Washington, D.C.

Vlassopoulos, D., Kanematsu, M., Henry, E.A., Goin, J., Leven, A., Glaser, D., Brown, S.S., O'Day, P.A., 2018. Manganese(iv) oxide amendments reduce methylmercury concentrations in sediment porewater. Environmental Science: Processes and Impacts, 20(12), 1746-1760.

Watras, C.J., 2009, Mercury pollution in remote freshwater lakes. In Likens, G. (Eds), Encyclopedia of Inland Waters (pp. 100–109) New York, NY: Elsevier.

Yu, R., Reinfelder, J.R., Hines, M.E., Barkay, T., 2018. Syntrophic pathways for microbial mercury methylation. The ISME Journal, 12(7), 1826-1835.

Yu, R., Reinfelder, J.R., Hines, M.E., Barkay, T., 2013. Mercury methylation by the methanogen Methanospirillum hungatei. Applied and Environmental Microbiology, 79(20), 6325-6330.

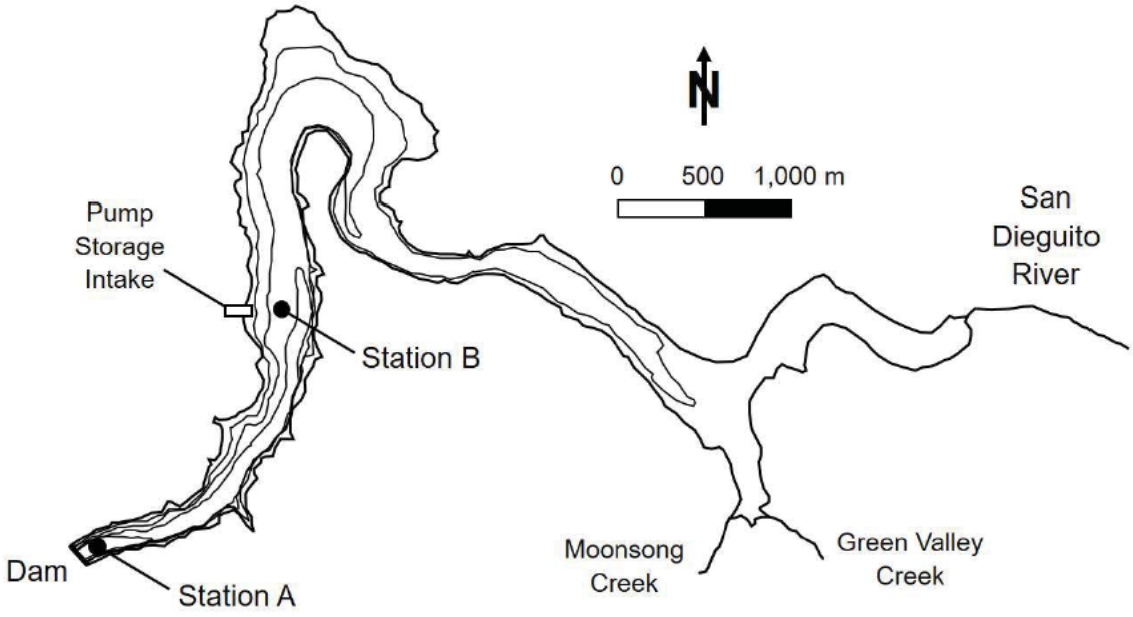

Figure 3.1 Map of Hodges Reservoir including sampling stations A and B. Contours are every 5 m and mapped water surface elevation is 5 m below spill elevation, which is a typical scenario for the reservoir.

Table 3.1 Chemical treatments and hypothetical impact

Sample	Treatment	Purpose of Treatment	Expected Result
Time 0	No treatment	Provides initial reference	
Control	No treatment	Provides 48-hour reference	
Inorganic Hg	3 ng/L $HgCl_2$	Increase concentration of bioavailable inorganic Hg	An increased pool of bioavailable Hg will enhance MeHg accumulation (TR > 1)
Ambient Air	Vial open to ambient air	Inhibit anaerobic bacteria	Inhibition of anaerobic bacteria that methylate Hg will suppress MeHg accumulation (TR < 1)
Pyruvate	100 mM pyruvic acid	Reduce redox of sediment-water interface and provide labile carbon source for all anaerobic bacteria	Under modestly reduced redox will cause a drop in redox that favors SRB that methylate Hg and enhance MeHg accumulation (TR > 1) Under highly reduced redox will cause a drop in redox that favors methanogens that demethylate MeHg and suppress MeHg accumulation (TR < 1)
Acetate	100 mM acetic acid	Provide labile carbon source for SRB	Stimulation of SRB that methylate Hg will enhance MeHg accumulation (TR > 1)
Molybdate	20 mM sodium molybdate	Inhibit SRB	Inhibition of SRB that methylate Hg will suppress MeHg accumulation (TR < 1)
Pyruvate/ molybdate	100 mM pyruvic acid and 20 mM sodium molybdate	Provide a labile carbon source while inhibiting SRB	Stimulation of IRB activity will enhance MeHg accumulation (TR > 1)
BES	30 mM 2-bromoethane sulfonate	Inhibit methanogens	Inhibition of methanogens that demethylate MeHg will suppress MeHg accumulation (TR > 1)
BES/ molybdate	30 mM 2-bromoethane sulfonate and 20mM sodium molybdate	Inhibit SRB and methanogens	Stimulation of fermentative, acetogenic and/or cellulolytic organisms will enhance MeHg accumulation (TR > 1)

Note: SRB = sulfate-reducing bacteria; IRB = iron-reducing bacteria; Hg = mercury; MeHg = methylmercury; BES = bromoethanesulfonate

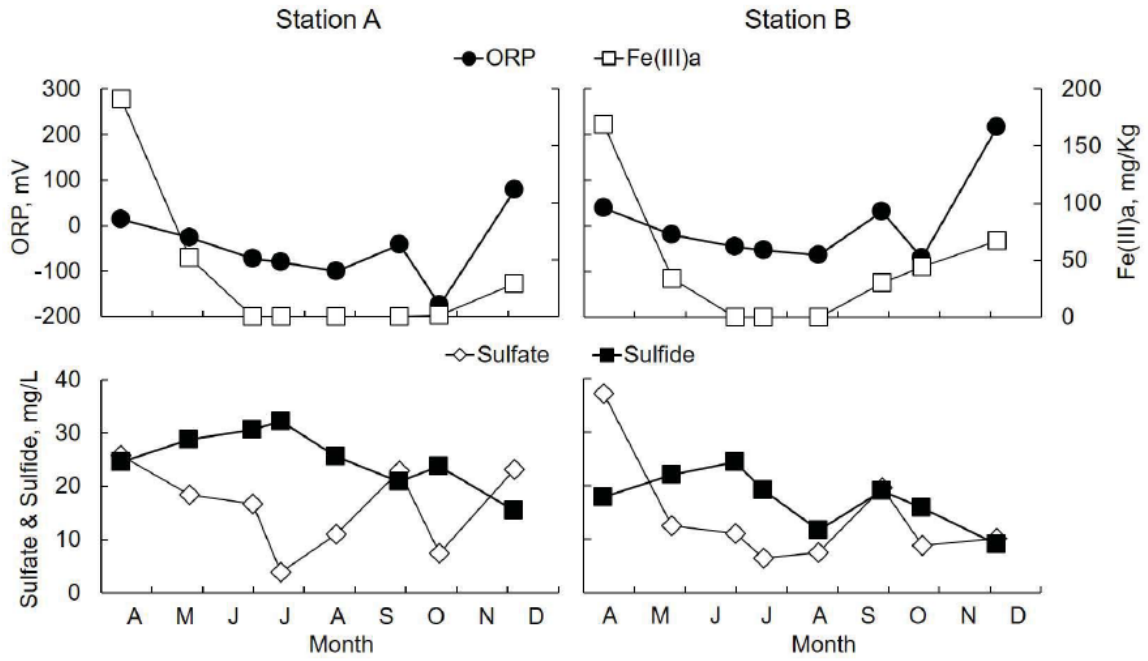

Figure 3.2 Temporal patterns of porewater oxidation-reduction potential (ORP), sulfate and sulfide, and sediment amorphous ferric iron (Fe(III)a) at Stations A and B.

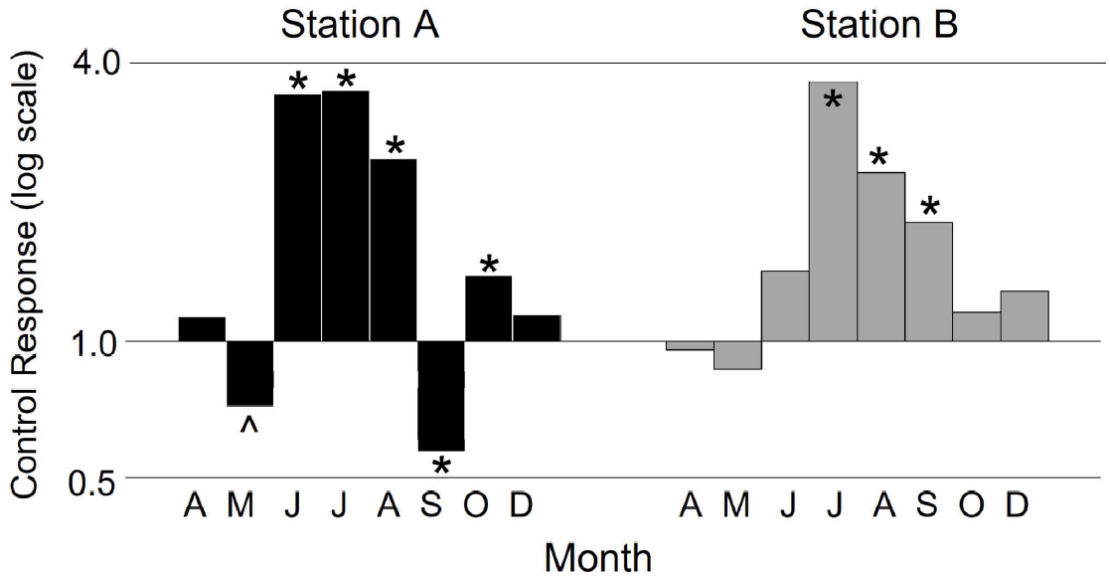

Figure 3.3 Temporal patterns of control responses (CR) for microcosm incubation at Stations A and B. Values are mean of triplicate incubations collected approximately monthly from April through early December. *p < 0.05, ^p < 0.10.

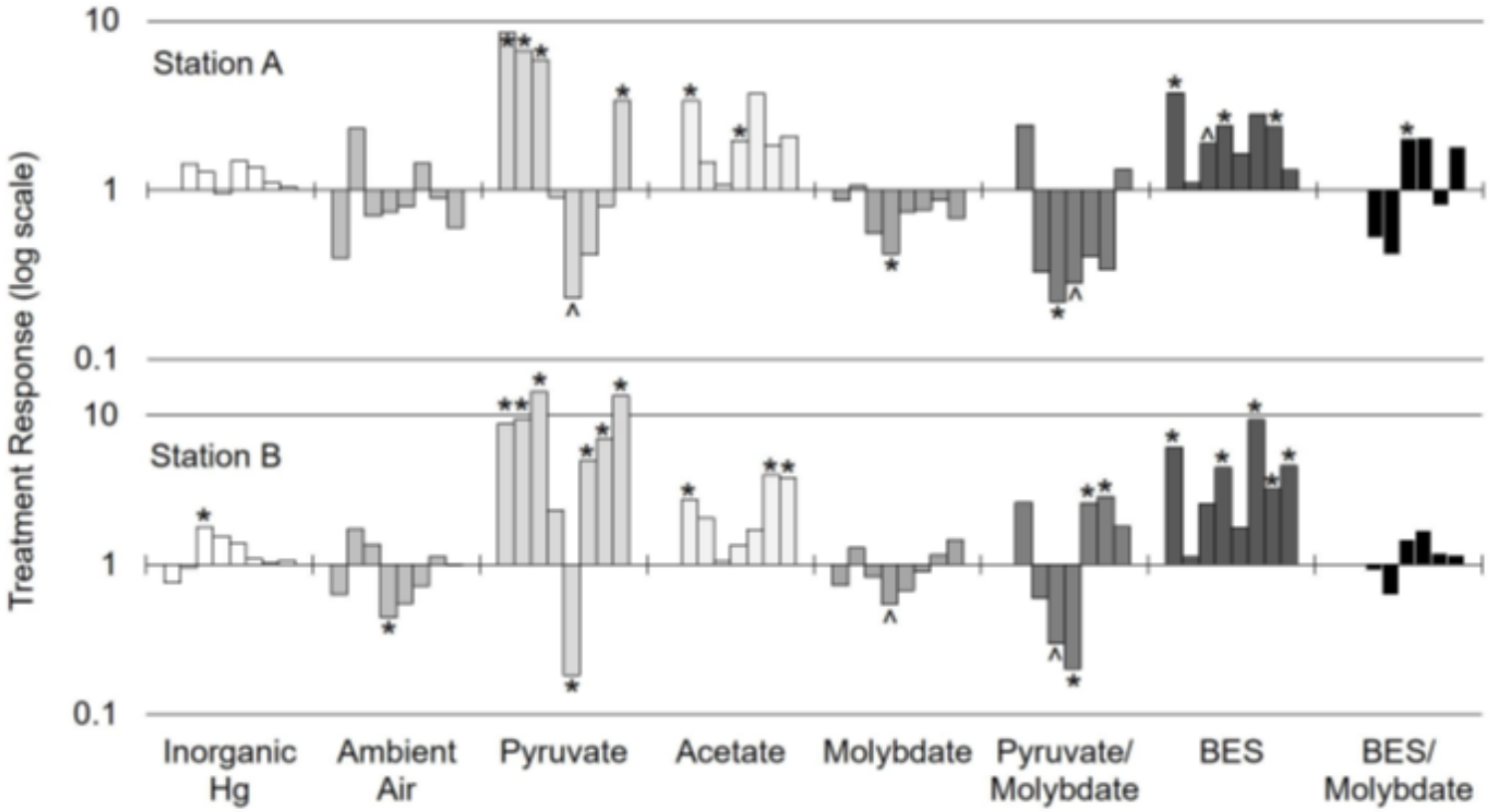

Figure 3.4 Temporal patterns of treatment responses (TR) for microcosm incubation at Stations A and B. Treatments included: Hg(II) addition, acetate addition, pyruvate addition, open to ambient air, molybdate addition, pyruvate/molybdate addition, bromoethanesulfonate (BES) addition, and BES/molybdate addition. Values are mean of triplicate incubations collected approximately monthly from April through early December. *$p < 0.05$, ^$p < 0.10$.

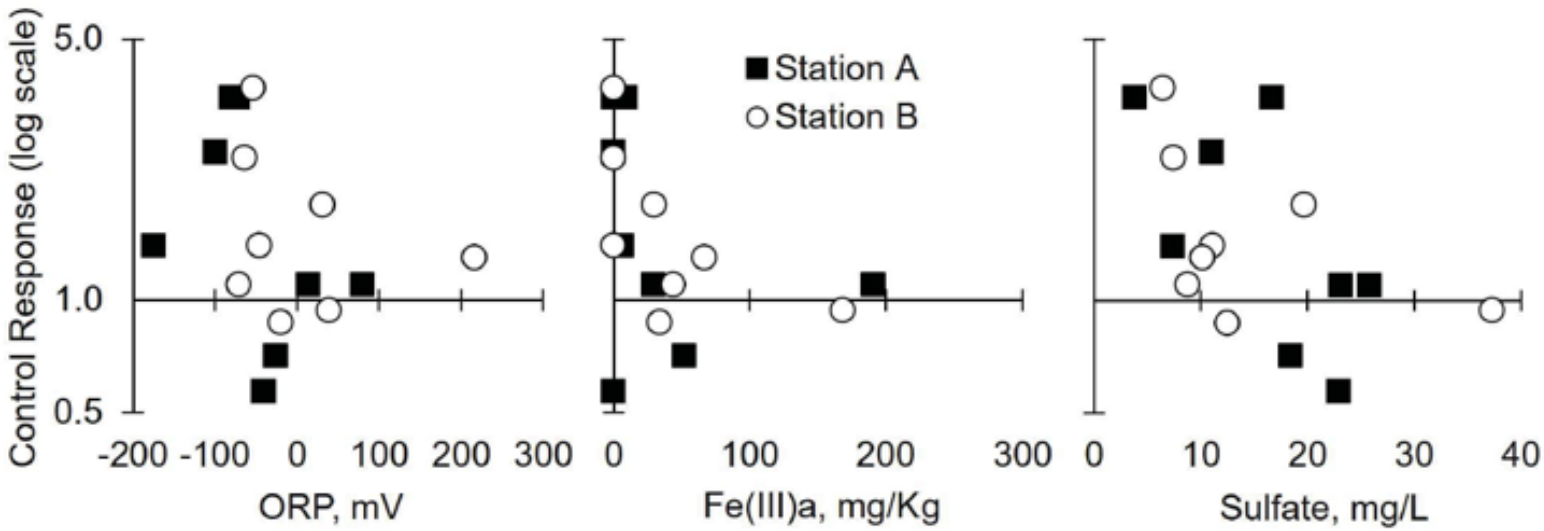

Figure 3.5 Control response (CR) versus key sediment quality metrics including: porewater oxidation-reduction potential (ORP) (left); sediment amorphous ferric iron (Fe(III)a) (middle); and porewater sulfate (right).

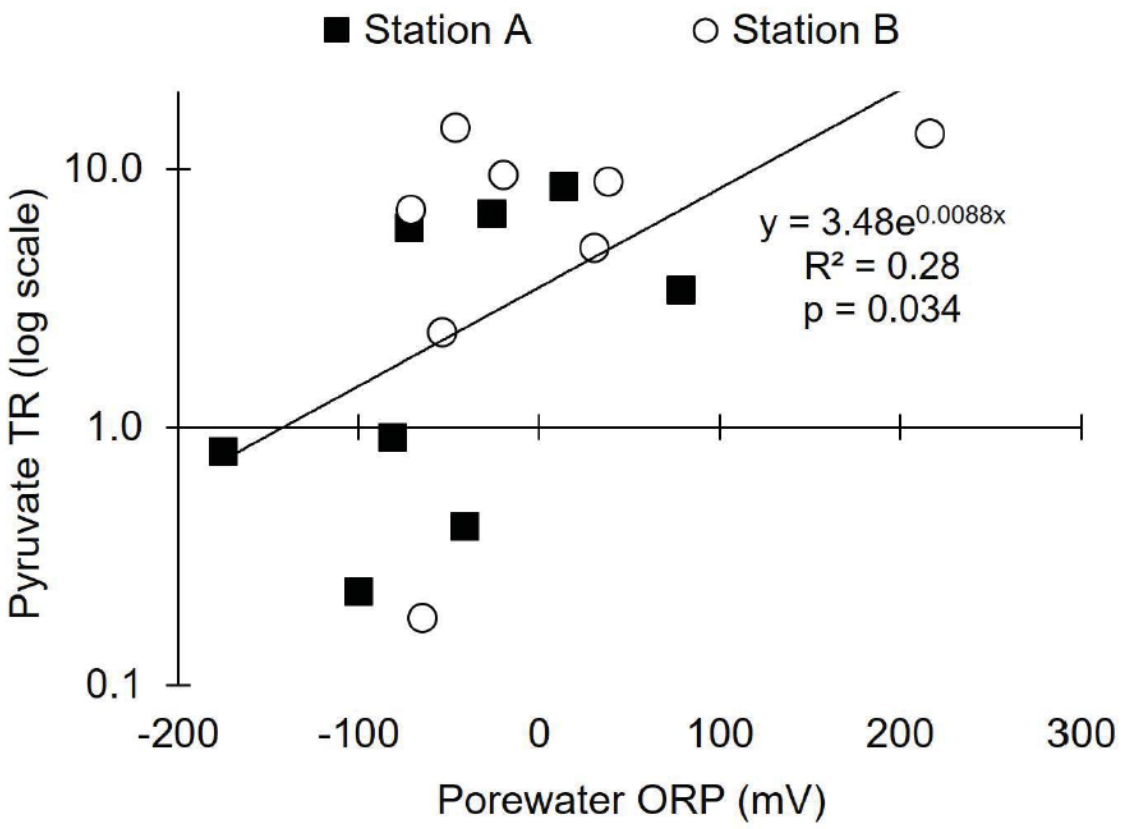

Figure 3.6 Pyruvate treatment response (TR) versus porewater oxidation-reduction potential (ORP) at Stations A and B. Line is linear regression of log of pyruvate TR and porewater ORP.

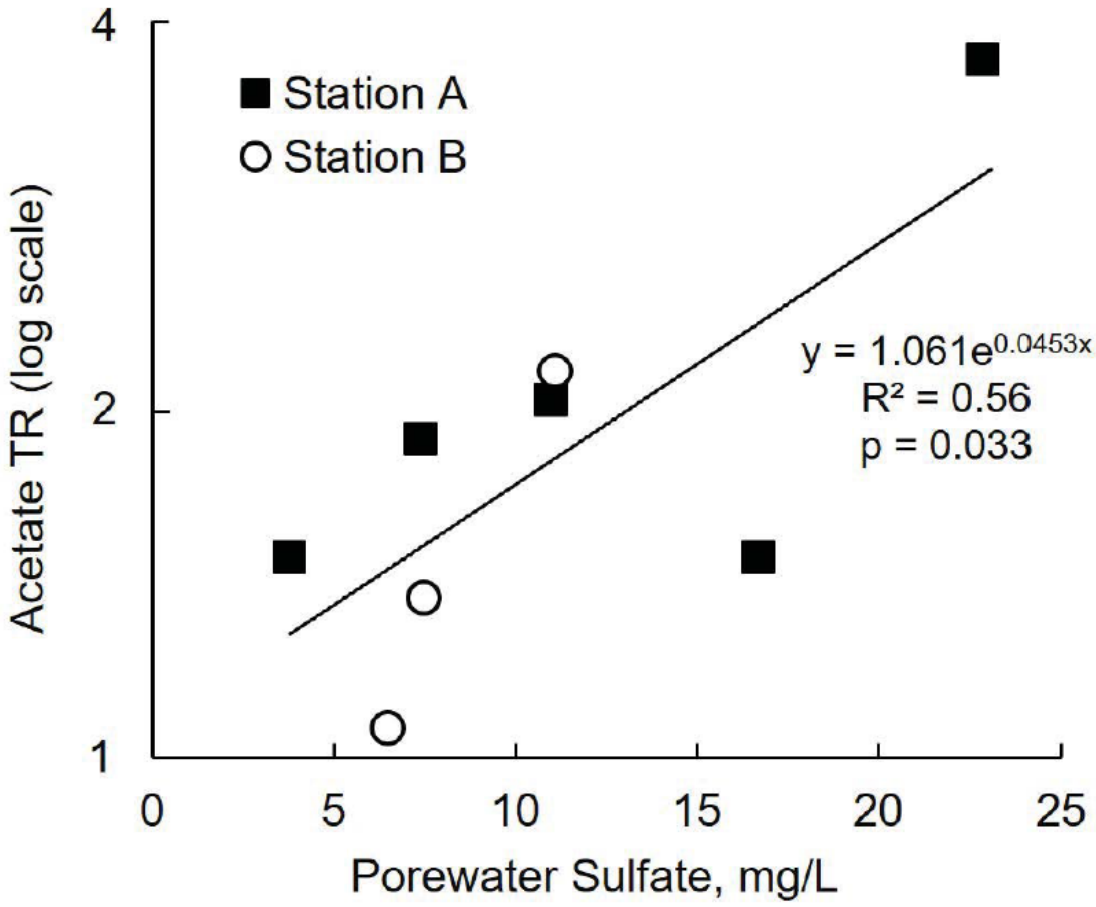

Figure 3.7 Acetate treatment response (TR) versus porewater sulfate at Stations A and B. Line is linear regression of log of acetate TR and porewater sulfate. Data includes period when SRB were dominant methylators as indicated by the absence of extractable amorphous ferric iron in surficial sediment.

Table 3.2 Hodges reservoir 2018 porewater and sediment quality

Date	ORP (mV)	pH	Sulfide (mg/L)	Sulfate (mg/L)	Fe(III)a (mg/kg)
Station A					
13-Apr	14	7.2	24.5	25.8	191
24-May	-26	7.1	28.8	18.4	52
1-Jul	-72	7.0	30.6	16.7	9
18-Jul	-81	7.0	32.2	3.8	0
20-Aug	-100	7.0	25.6	11.0	0
27-Sep	-41	6.9	20.8	22.9	0
21-Oct	-175	6.8	23.7	7.4	6
5-Dec	79	6.9	15.4	23.1	29
Station B					
13-Apr	39	7.9	17.9	37.3	169
24-May	-20	7.8	22.1	12.5	34
1-Jul	-46	7.1	24.4	11.1	0
18-Jul	-53	6.9	19.2	6.5	0
20-Aug	-64	7.1	11.7	7.5	0
27-Sep	31	6.9	19.0	19.7	30
21-Oct	-71	7.1	15.9	8.8	44
5-Dec	217	7.4	9.0	10.2	67

Table 3.3 Control microcosm incubation results

Sample Date	Time Zero MeHg (ng/L·kg)	48-Hr Control MeHg (ng/L·kg)	Control Response
	Station A		
13-Apr	65 ± 2.7	74 ± 3.1	1.1
24-May	34 ± 4.3	24 ± 2.9	0.71^
1-Jul	14 ± 1.0	49 ± 7.0	3.5*
18-Jul	31 ± 4.0	110 ± 5.5	3.5*
20-Aug	34 ± 5.4	86 ± 14	2.5*
27-Sep	84 ± 2.7	48 ± 3.5	0.57*
21-Oct	49 ± 6.5	68 ± 6.0	1.4*
5-Dec	47 ± 1.4	54 ± 2.8	1.1
	Station B		
13-Apr	71 ± 3.70	67 ± 6.9	0.94
24-May	24 ± 3.7	21 ± 1.8	0.87
1-Jul	25 ± 2.6	35 ± 4.6	1.4
18-Jul	20 ± 1.9	75 ± 1.3	3.7*
20-Aug	45 ± 8.4	110 ± 10	2.4*
27-Sep	26 ± 2.2	47 ± 2.6	1.8*
21-Oct	21 ± 3.2	24 ± 3.6	1.1
5-Dec	28 ± 5.2	37 ± 3.4	1.3

MeHg values are average plus/minus standard error of triplicate incubations
*Control MeHg significantly different from time zero MeHg at $p < 0.05$
^Control MeHg nearly significantly different from time zero MeHg at $p < 0.10$

Table 3.4 Treatment microcosm incubation results

Date	Inorganic Hg		Ambient Air		Pyruvate		Acetate		Molybdate		Pyruvate/ Molybdate		BES		BES/ Molybdate	
	MeHg	TR	MeHg	TR	MeHg	TR	MeHg	TR	MeHg	TR	MeHg	TR	MeHg	TR	MeHg	TR
								Station A								
13-Apr	75 ± 4.8	1.0	29 ± 12	0.4	630 ± 120	8.5*			64 ± 15	0.9			280 ± 37	3.8*		
24-May	34 ± 4.0	1.4	56 ± 8.9	2.3	160 ± 23	6.7*	81 ± 5.7	3.4*	26 ± 3.0	1.1	58 ± 6.7	2.4	27 ± 1.8	1.1		
1-Jul	63 ± 5.5	1.3	35 ± 5.3	0.7	290 ± 37	5.9*	72 ± 4.7	1.5	27 ± 1.2	0.6	16 ± 1.0	0.3	93 ± 3.4	1.9^	26 ± 6.8	0.5
18-Jul	100 ± 4.4	0.9	81 ± 15	0.7	99 ± 12	0.9	120 ± 14	1.1	45 ± 14	0.4*	24 ± 5.2	0.2*	260 ± 28	2.4*	45 ± 0.82	0.4
20-Aug	130 ± 17	1.5	69 ± 18	0.8	20 ± 0.67	0.2^	170 ± 15	2.0*	64 ± 8.4	0.7	24 ± 3.5	0.3^	140 ± 3.4	1.6	180 ± 6.4	2.0*
27-Sep	65 ± 5.6	1.4	69 ± 21	1.4	20 ± 0.28	0.4	180 ± 15	3.8	36 ± 8.7	0.8	19 ± 0.2	0.4	130 ± 21	2.7	98 ± 24	2.0
21-Oct	76 ± 10	1.1	61 ± 0.61	0.9	55 ± 13	0.8	120 ± 12	1.8	60 ± 4.0	0.9	23 ± 2.2	0.3	160 ± 19	2.4*	55 ± 6.5	0.8
5-Dec	56 ± 8.0	1.0	33 ± 4.5	0.6	180 ± 16	3.3*	110 ± 7.7	2.0	37 ± 9.5	0.7	72 ± 11	1.3	71 ± 7.1	1.3	98 ± 34	1.8
								Station B								
13-Apr	52 ± 17	0.8	43 ± 7.8	0.6	600 ± 49	8.9*			49 ± 3.2	0.7			415 ± 74	6.1*		
24-May	20 ± 0.28	1.0	36 ± 2.9	1.7	190 ± 13	9.1*	56 ± 2.1	2.7*	27 ± 5.7	1.3	54 ± 11	2.6	23 ± 0.40	1.1		
1-Jul	63 ± 3.6	1.8*	48 ± 9.7	1.4	507 ± 32	14.4*	73 ± 15	2.1	29 ± 3.0	0.8	21 ± 2.5	0.6	90 ± 11	2.6	33 ± 2.6	0.9
18-Jul	120 ± 6.7	1.6	33 ± 5.8	0.4*	173 ± 8.7	2.3*	79 ± 7.6	1.1	41 ± 16	0.6^	22 ± 4.6	0.3^	340 ± 17	4.5*	47 ± 15	0.6
20-Aug	150 ± 9.2	1.4	58 ± 5.0	0.5	19 ± 0.25	0.2*	140 ± 10	1.3	72 ± 7.0	0.7	21 ± 2.1	0.2*	190 ± 30	1.8*	160 ± 12	1.5
27-Sep	51 ± 1.0	1.1	34 ± 2.3	0.7	230 ± 13	4.9*	81 ± 8.2	1.7	42 ± 0.76	0.9	120 ± 10	2.6*	440 ± 78	9.4*	80 ± 10	1.7
21-Oct	25 ± 3.7	1.0	28 ± 6.4	1.1	170 ± 6.4	7.0*	98 ± 5.0	4.1*	28 ± 3.7	1.2	69 ± 8.0	2.8*	78 ± 9.9	3.2*	29 ± 1.6	1.2
5-Dec	39 ± 7.1	1.1	36 ± 4.4	1.0	500 ± 60	13.5*	140 ± 46	3.8*	54 ± 1.3	1.5	66 ± 5.5	1.8	170 ± 64	4.6*	42 ± 5.3	1.2

MeHg values are average plus/minus standard error of triplicate incubations
MeHg in units of ng/L·kg
BES = bromoethanesulfonate
*Treatment MeHg significantly different from 48-hr control MeHg at $p < 0.05$
^Treatment MeHg nearly significantly different from 48-hr control MeHg at $p < 0.10$

Appendix 1

Supporting Information for the Economic analysis and life cycle assessment of hypolimnetic oxygenation of Upper San Leandro Reservoir

Table A1 List of variables used in the life cycle assessment

Input variables	Units	Description
Mass_Stainless_Steel	kg	Mass of stainless steel used to produce LOX storage system
Distance_Stainless_China	km	Distance from the stainless-steel source to the port of Shanghai
Distance_Stainless_Ocean	km	Distance from the port of Shanghai to port of San Francisco
Distance_Stainless_US	km	Distance from port of San Francisco to LOX manufacturer
Distance_LOX_US	km	Distance from LOX manufacturer to USL reservoir
Electricity_LOX_manufact	kWh	Electricity to weld steel for LOX
HOS_Oxygen_Requirement	kg/d	Daily HOS oxygen use
Distance_Oxygen_USL	km	Distance from oxygen supplier to USL reservoir
LOX_install_time	hr	Time required to install LOX with crane
Mass_Galvanized_Steel	kg	Mass of galvanized steel used to create security fence
Distance_Galvanized_China	km	Distance from the galvanized steel source to the port of Shanghai
Distance_Galvanized_Ocean	km	Distance from the port of Shanghai to port of San Francisco
Distance_Galvanized_US	km	Distance from port of San Francisco to chain link fence manufacturer
Steel_Cable_Mass	kg	Mass of steel cables used in HOS
Steel_Cable_US	km	Distance from steel cable producer to USL reservoir
Mass_HDPE	kg	Mass of HDPE used in HOS
Recycled_HDPE_used	-	Fraction of recycled HDPE used in HOS
Distance_HDPE_US	km	Distance from HDPE producer to USL reservoir
Mass_Porous_Hose	kg	Mass of porous hose used in HOS

Distance_Porous_Hose_US	km	Distance from Porous Hose producer to USL reservoir
Replacement_Schedule	yr	Frequency of porous hose replacement
Mass_Concrete	kg	Mass of concrete used in HOS
Fraction_Steel_Recycled	-	Fraction of all steel recycled at end of HOS lifetime
Fraction_HDPE_Recycled	-	Fraction of HDPE recycled at end of HOS lifetime
Distance_Recycle	km	Distance from USL reservoir to recycling center
Distance_Landfill	km	Distance from USL reservoir to landfill
Mass_Barge	kg	Mass of the barge used to install the HOS
Distance_Barge_Transport	km	Distance from barge owner to USL reservoir
Distance_Barge_Operation	km	Distance covered by barge at USL reservoir
Diver_Time_Required	hr	Time required for divers to install HOS
Distance_Oxygen_USLWTP	km	Distance from oxygen supplier to USLWTP
Ozone_Requirement	kg/MG	Requirement of ozone for water treatment
Electricity_Produce_Ozone	kWh/kg	Electricity required to produce ozone from oxygen
H2O2_Requirement	gal/MG	Requirement of hydrogen peroxide for water treatment
Distance_H2O2_US	km	Distance from hydrogen peroxide producer to USLWTP
Distance_NaCl_USLWTP	km	Distance from NaCl supplier to USLWTP
Chlorine_Requirement	kg/MG	Requirement of chlorine for water treatment
Electricity_Produce_Cl2	kWh/kg	Electricity required to produce chlorine gas from NaCl
Treatment_Volume	MG/d	Daily potable water production at USLWTP
Annual_Operation	d/yr	Annual operation of the HOS
Reservoir_Area	km^2	Surface area of USL reservoir

1. LCA construction, installation, and maintenance parameters and assumptions

The masses of raw materials used in the HOS initial construction and 2012 expansion as well as the oxygen required for the HOS were often provided in units of pounds (lbs) or tons (2,000 lbs) which were converted into kilograms (kg) for use in the LCA model. It was assumed that bulk quantities of HDPE, steel cable, chain link fencing, and porous hose were obtained from the largest regional suppliers. All transportation distances used in the LCA were calculated in km using google maps, with the shortest distance used as the minimum value parameter, the longest suggested distance used as the maximum value parameter, and the recommended route used as the baseline value parameter. Emissions attributed to transportation by medium or heavy truck were obtained from the U.S. EPA's "Inventory of U.S. greenhouse gas emissions and sinks: 1990 – 2010" report (Hockstad and Cook, 2012), emissions related to electricity were obtained from the U.S. EPA Office of Atmospheric Programs "2018 Emissions & Generation Resource Integrated Database". All other material or process attributed emissions were obtained through the National Renewable Energy Laboratory U.S. Life cycle inventory database (2008).

1.1 Steel use

The stainless steel required for the HOS was based on the requirement of stainless steel to produce the liquid oxygen storage tank (LOX). The stainless steel used in the production of the LOX system was assumed to have been obtained from the Chinese company Anshan Iron and Steel, one of the largest steel manufacturers in the world (Byrd, 1992). This long-range transportation assumption was made in order to prevent a potentially significant underestimation of the total impact of stainless-steel use for the HOS. It was assumed that the stainless steel was transported by freight train to the port of Shanghai and then transport by cargo ship to the port of San Francisco. Air Liquide was the producer and supplier of the LOX which has a 6,000-gallon capacity (Mobley, 2003). The closest Air Liquide corporate location is in Pittsburg, CA and it was assumed that the stainless-steel was transported from the Port of San Francisco to Pittsburg, CA by a heavy truck. It was assumed that the LOX was manufactured at the Air Liquide location in Pittsburg by gas welding, which is more energy intensive than arc welding, but results in a higher quality final product which would be required for the LOX storage system. The baseline parameter value assumption is that it required 10 hours of gas welding to produce the final LOX storage tank, while 5 hours was used as the minimum parameter value and 40 hours was used as the maximum parameter value. After being manufactured, the LOX system was assumed to have been transported by a heavy truck to USL where it was installed with a crane. The baseline parameter value assumption is that it required 2 hours of total crane use to position the LOX, while 0.5 hours of crane use was used as the minimum parameter value and 4 hours was used as the maximum parameter value. It appears as if the LOX was a custom ordered horizontal tank for bulk storage, of which specifications were not available. Therefore, the weight was assumed to be the same as the closest commercially available model, the Chart VS-DSS series 6,010-gallon tank which weighs 21,900 lbs (Chart Inc., 2019). This value was used for the

baseline parameter value for the stainless-steel requirement, while 50% of that value was used for the minimum parameter value and 200% of that value was used for the maximum parameter value. Galvanized steel was required for production of the security chain link fence that surrounds the LOX system (Mobley, 2003). It was also assumed that the galvanized steel was obtained from the Anshan Iron and Steel company and transported along the same route as stainless steel until reaching the port of San Francisco. After reaching the San Francisco port, it was assumed that the galvanized steel was transported to Steel & Fence Supply in San Jose to produce chain link fencing material and then transported to USL after production. The amount of galvanized steel required for the chain link fence was estimated based on a photograph of the system and the known 16 ft long, 8 ft diameter size of the LOX. The baseline assumption was that 100 ft^2 of 6 ft tall, 10 gauge, 2" diamond mesh fencing was required, with a minimum assumption of 75 ft^2 of 6 ft tall, 11 gauge, 2" diamond mesh fencing and a maximum assumption of 150 ft^2 of 6 ft tall 9 gauge, 2" diamond mesh fencing. The density of the fencing in the calculation of galvanized fencing used was 3.5 lbs/ft^2 for 6 ft tall, 10 gauge fencing; 4.2 lbs/ft^2 for 6 ft tall, 9 gauge fencing; and 2.75 lbs/sq ft for 6 ft tall, 11 gauge fencing (Galvanized Chain Link Fence Fabric (GBW), 2020). Including the initial installation and the 2012 expansion, 940 approximately one ft long, 3/4" steel cables were required to secure the HOS delivery system to concrete anchors stationed in the hypolimnion of USL (Mobley, M., personal communication, September 10, 2019). The total mass of cable required assumed 1,000 ft of cable at a density of 1.04 lbs/ft (Wire Co World Group, 2012). The steel cable emissions source used in the LCA was cradle to gate for US production and the cable was assumed to have been produced, obtained, and transport from Western Steel & Wire located in San Francisco.

1.2 HDPE use

The total mass of HDPE required for the initial HOS installation and the expansion was determined based the length of pipe required and the standard dimension ratio (SDR) of the pipe used. This information was provided by the lead project engineer for the project (Mobley, M., personal communication, September 10, 2019). The amount of HDPE pipe required was 14,000 ft of 2" SDR 11 HDPE pipe at 0.64 lbs/ft; 21,500 feet of 3" SDR 11 HDPE pipe at 1.39 lbs/ft; 2,000 ft of 3" SDR 17 HDPE pipe at 0.94 lbs/ft; and 9,500 ft of 4" SDR 21 at 1.27 lbs/ft. The fraction of recycled HDPE used was unknown and the baseline parameter assumption was set to 0.5, with the minimum value parameter set as 0 and the maximum value parameter set to 1.0. It was assumed that HDPE was produced at and transported from P & F Distributors in Brisbane, CA.

1.3 Concrete use

The mass of concrete used was 48,000 lbs in the initial installation and 86,400 lbs in the 2012 expansion, making the total concrete requirement to 134,400 lbs. This information was provided by the lead project engineer for the project (Mobley, M., personal communication, September 10, 2019). It was assumed that concrete was obtained and transported from Central Concrete Supply in Oakland, CA.

1.4 Porous hose use and replacement

Approximately 23,200 ft of 1" diameter porous hose was required in total for the initial HOS installation and the expansion. The porous hose has an expected lifetime of 10-15 years. This information was provided by the lead project engineer for the project (Mobley, M., personal communication, September 10, 2019). A baseline expectation is that the porous hose will be replaced every 12 years, with the minimum maintenance schedule parameter set to 10 years and the maximum maintenance schedule parameter set to 15 years. The porous hose was assumed to have a standard weight of 0.2 lbs/ft, resulting in a total weight of 4,640 lbs required for the initial installation and each subsequent replacement. It was assumed that the porous hose had been and will be obtained and transported from Ewing Irrigation & Landscape Supply in Pacheco, CA.

1.5 Installation Requirements

The entire HOS spans a distance of 4.4 miles and is comprises of 10 ft sections of HDPE pipe and porous hose with cables that attach to a concrete achor. It was assumed that a barge was used to transport the concrete blocks and 10 ft sections of the HOS to each section of the reservoir during installation and divers were used to position the HOS and deliver the 10 ft sections. The emissions related to the use of the barge for the HOS installation were determined by the distance traveled and assumed for an average fuel mix. The distance traveled by the barge was assumed to be a minimum of 8.8 miles per trip, the distance from the dock to the end of the HOS and back to the dock. The baseline and maximum scenarios assumed that the pathlength was not perfectly straight, that additional navigation was required during the installation. Under this assumption, the baseline parameter distance per trip was set as equal to three times the length of the HOS (13.2 miles) and the maximum scenario set this distance to four times the length of the HOS (17.6 miles). There was an initial installation and an expansion in 2012, so the total distance covered by the barge was doubled for the total distance each scenario. The barge used was assumed to have been a Trig Lind or similar sized barge, with a gross weight of 122 tons and provided by Lind Marine in Vallejo, CA. The Trig Lind has a gross mass of 122 tons which was used as the baseline parameter value for the mass of the barge, while 50% of that mass was used for the minimum parameter value and 200% of the mass was used for the maximum parameter value. The transportation distance required to deliver the barge to USL for use was set to four times the distance from Lind Marine to USL to account for the return after use and a second use for the 2012 expansion. Emissions due to the use of scuba divers was assumed based on the amount of energy required to produce the compressed air needed for the total diving time. Divers typically require 1.5 L of air per minute while diving (Wilmshurst, 1998). Approximately 352 ft^3 of compressed air can be produced per kWh (Marshall, 2013). The total dive time required for installation and expansion was estimated to be 100 hours for the baseline, with 25 hours serving as the minimum scenario and 200 hours serving as the maximum scenario. Under these assumptions and using a conversion factor of 28.32 L per ft^3, the minimum parameter value for the electricity required to produce the compressed air was set to 0.22

kWh, the baseline parameter was set to 0.90 kWh, and the maximum parameter value was set to 1.80 kWh.

1.6 Landfilling and Recycling

The HOS is still currently in use so the fraction of material that will be recycled is unknown. It was assumed that the porous hose will not be recycled because it has a certain usable lifetime. For HDPE, 0 was assumed to be the minimum parameter value, 0.5 was assumed for the baseline parameter value and 1.0 was assumed for the maximum parameter value. Steel is more likely to be recycled so 0.25 was assumed to be the minimum parameter value, 0.75 was assumed for the baseline parameter value and 1.0 was assumed for the maximum parameter value. Landfilling and recycling values for HDPE material could not be obtained from the source used for HDPE production related emissions. The landfilling and recycling values for HDPE were calculated based on a similar material, PVC. The ratio of the emissions per kg of PVC produced to the decrease in emissions per kg of PVC recycled and the ratio of emissions per kg of PVC produced to kg of PVC landfilled was calculated. These ratios were used to back calculate the assumed values of emissions per kg of HDPE landfilled or emission decreases per kg of HDPE recycled based on the emissions per kg of HDPE produced. All material not recycled was assumed to be landfilled at the end of the HOS lifetime.

2. Operational parameters and assumptions

2.1 Operation lifetime

The HOS and LOX system has an expected lifetime of between 50-100 years with an average expectation of 60 years (Mobley, M., personal communication, September 10, 2019). In order to produce comparable results, the normal scenario and the HOS scenario were assigned the same model timeframe. For each scenario, the baseline parameter value was set to 60 years, the minimum parameter value was set to 50 years and the maximum parameter value was set to 100 years.

2.2 Annual operation period

Hypolimnetic oxygenation in reservoirs typically only provides a substantial benefit during the period of thermal stratification. Therefore, HOS are not generally operated after fall turnover or before the onset of spring thermal stratification (Beutel and Horne, 1999). During the first year of use, the HOS was operated for a period of 173 days (Jung, 2003). This period was assumed to be representative of an average annual use and 173 days per year was used as the baseline parameter value for the annual HOS operational period. The annual length of thermal stratification could be moderately variable based on temperature regime, but over a longer period of time the average yearly operation should remain moderately close to this baseline value. Due to the lack of yearly HOS operational data, the range was assumed to be 20 days above and below the baseline, with the

minimum parameter value set to 153 days of operation and the maximum parameter value set to 193 days of operation.

3. Treatment Operations

3.1 Daily potable water production

The average production of potable water by the USLWTP was 19.9 million gallons per day (MGD) for the three years prior to the HOS installation and this was generally in line with the historical production capacity (Jung, 2003). The treatment capacity was previously restricted to 30 MGD before the HOS installation in order to increase the residence time and allow for enhanced disinfection. The average daily potable water production was approximately 23 MGD for the year following the installation of the HOS. Based on this information, it was assumed that 23 MGD would be the baseline parameter value for the potable water production rate, 19.9 MGD would be the minimum parameter value for the potable production rate, and 30 MGD would be the maximum parameter value for the potable production rate for the HOS scenario. For the normal scenario, it was assumed that the baseline potable production rate would be 19.9 MGD. The maximum and minimum production rates were assumed to be proportional to the difference between the baseline value and the minimum and maximum parameter values for the HOS scenario (86.5% of the baseline for the minimum value and 130% of the baseline value for the maximum value). Therefore, the minimum parameter value for the normal scenario potable water production rate was assumed to be 17.2 MGD and the maximum parameter value for the potable production rate was assumed to be 25.9 MGD. These daily potable water production parameter values were used in conjunction with the chemical and electrical requirements for reservoir water treatment operations in order to determine the overall chemical and electrical demands for potable water production in each scenario.

3.2 Ozone treatment

Ozone is produced on-site at USLWTP using pure liquid oxygen and an electrical current (Luong, 2017). A 10% weight for weight conversion of liquid oxygen to ozone and an energy requirement of 11.3 kWh per kg ozone produced was found at another San Francisco bay area water treatment plant using a pure oxygen feed ozone generation system with a similar treatment capacity to that of USLWTP (Goel and Salveson, 2012). Therefore, this LCA assumed that 1 kg of on-site ozone generation required 10 kg of liquid oxygen and 11.3 kWh in each scenario. USLWTP operational data showed a pre-HOS ozone requirement of 5 mg/L for treatment and that this demand was reduced by 45% to 2.75 mg/L after HOS implementation (Jung, 2003). The 5 mg/L pre-HOS ozone requirement was used as the baseline parameter value in the normal scenario and the 2.75 mg/L post-HOS ozone requirement was used as the baseline parameter value in the HOS scenario. Due to the lack of historical ozone use data, an assumption was made that the minimum parameter value would be equal to 75% of the baseline parameter value and the maximum parameter value would be equal to 125% of the baseline parameter value in

each respective scenario (3.57-6.25 mg/L for the normal scenario, 2.06-3.43 mg/L for the HOS scenario). It was assumed that pure oxygen for ozone production was obtained and transported from Air Gas in Hayward, CA.

3.3 Hydrogen peroxide treatment

The elimination of the hydrogen peroxide feed system due to the HOS operation resulted in a cost savings of $12 per MG (Jung, 2003; Mobley, 2003). This amounts to a reduction of 1.55 gallons per MG assuming a standard rate of $425 per 55-gallon drum and this volumetric reduction in hydrogen peroxide use will be used as the baseline value parameter in the normal scenario. Is it unlikely that hydrogen peroxide treatment will be reimplemented while the HOS is operated, but it is possible that the future demand of hydrogen peroxide would have been different, based on future reservoir water quality under anaerobic conditions. Due to the lack of historical data, the minimum value parameter for hydrogen peroxide use under the normal scenario was assumed to be 75% of the baseline parameter value (1.16 gallons per MG) and the maximum value parameter was assumed to be 125% of the baseline parameter value (1.88 gallons per MG). It was assumed that hydrogen peroxide was obtained and transported from Ravago Chemicals in Walnut Creek, CA in the normal scenario.

3.4 Chlorine treatment

Electrochlorination is a popular method for producing on-site at water treatment plants because it is cost effective, operational equipment is moderately simple, and it only requires sodium chloride (NaCl) and electricity, reducing the need for transportation of hazardous chemicals (Pulido, 2005). It was assumed that the USLWTP utilizes on-site electrochlorination for chlorine production and this process generally requires a NaCl consumption to chlorine equivalent production rate of 3:1 (Hanley et al., 2011; Novak et al., 2011). In each LCA scenario, the assumption was made that 3 kg of NaCl was required for every 1 kg chlorine equivalent required by each scenario's chlorination treatment process. Electrochlorination power consumption can vary depending on the system efficiency, the concentration of the salt solution, the current density, and the flow rate. Hanley et al., 2011 found electrochlorination to be in the range of 4.8-5.5 kWh per kg chlorine equivalent while Novak et al., 2011 found it to be approximately 4.4 kWh per kg chlorine equivalent. Taking this data into account, 4.8 kWh/kg chlorine was chosen as the baseline parameter value electricity requirement for chlorine generation, 4.4 kWh/kg chlorine was set to the minimum parameter value and 5.5 kWh/kg chlorine was set as the maximum parameter value. USLWTP data showed that the demand for chlorine was reduced from 13.9 mg/L before the HOS implementation to 11.4 mg/L after the HOS implementation and these will be used as baseline parameter values in the respective normal and HOS scenarios. There is also a lack of historical chlorine use data so the maximum parameter value of chlorine use for the HOS scenario will be set to the baseline parameter value for the normal scenario (13.9 mg/L) and the minimum parameter value of chlorine use will be set to 75% of the baseline parameter value (8.55 mg/L). A similar, 75% baseline minimum and 125% maximum parameter value range

was assumed for the normal scenario (10.4 – 17.4 mg/L). It was assumed that the salt required for chlorine production was obtained and transported from Leslie Salt, one of the largest salt producers in California, located in Newark, CA.

4. Reservoir Management Activities

4.1 Methane Reservoir Emissions

Methane emissions for the normal scenario were assumed based a diffusive flux equation derived from the study of 53 seasonally anoxic lakes and reservoirs (Bastviken et al., 2004) according to the following formula:

$$Log(Methane\ Diffusive\ Flux) = 0.234 + 0.927log(Reservoir\ Surface\ Area)$$

where the methane diffusive flux is g C/yr and reservoir surface area is in km^2

The global warming potential of methane was modeled to be 23 times that of carbon dioxide based on the findings from the IPCC third assessment report (Houghton et al., 2001). The surface area of USL was stated to be approximately 620 acres (2.51 km^2) in a recent article on the HOS in USL (Moore et al., 2015) and the surface area was stated as 3.19 km^2 in a USGS report from 1974 (Britton et al., 1974). A baseline parameter value of the more recent surface area (2.51 km^2) will be assumed for a more conservative and realistic approach to modern reservoir methane emissions. A minimum parameter value of 10% smaller than the baseline value (2.26 km^2) and a maximum reservoir surface area of 10% larger than that stated in the 1974 USGS report (3.51 km^2) was assumed for the range of surface areas used to estimate the reservoir methane emissions in the normal scenario. Methane emissions were assumed to be negligible under oxygenated conditions in the reservoir modeled in the HOS scenario.

4.2 HOS oxygen use

The HOS initially required a constant supply of 8 tons per day of oxygen due to the large amount of organic matter that had built up through years of eutrophic conditions and the slow initial spread of oxygen through the reservoir. Operations were optimized to “pulse feed” where the HOS was only periodically operated and after 3-4 months, the HOS demand had greatly reduced and stabilized at approximately 1.6 tons of oxygen per day while still maintaining an oxic hypolimnion (Jung, 2003). Including the large initial requirement of oxygen, the total first year oxygen use was 550 tons. Therefore, 550 tons of oxygen was used as a fixed parameter for initial oxygen use for the first year of operations in the HOS scenario. Afterwards, 1.6 tons of oxygen per day was assumed as the baseline parameter value for HOS operations as this appears to be the most likely long-term rate of HOS oxygen use. There is the possibility that enhanced mixing due to the delivery of oxygen near the sediment-water interface could lead to an increased sediment oxygen demand over time. Beutel, 2003 demonstrated that USL sediment oxygen demand was enhanced by approximately 25% under moderately mixed conditions

compared with unmixed conditions in a laboratory chamber mesocosm study. However, Ganzter et al., 2009 observed an approximately 50% decrease in the average overall oxygen demand over a 5 year period following hypolimnetic oxygenation in two reservoirs and concluded the decrease was likely due to the enhanced mineralization of organic matter from previous years which lowered the total mass of organic matter available for microbial respiration. Based on the findings from the Beutel, 2003 study, a 2 ton per day HOS oxygen requirement (25% increase from the baseline value) was used for the maximum parameter value and the a 0.8 ton per day HOS oxygen requirement was used as the minimum parameter value taking into account the 50% decrease in oxygen demand observed by Gantzer et al., 2009.

4.3 Potential benefits that were not quantified

The treatment benefits associated with the HOS system likely extend beyond that of the reduction in chlorine, ozone, and hydrogen peroxide use. After the implementation of the HOS, there was an observed reduction in cyanobacteria derived taste and odor (T&O) compounds such as geosmin and the production of disinfection biproducts (DBPs) like trihalomethanes. USLWTP uses activated carbon filtration to manage T&O and DBP levels, so a reduction likely enhanced the lifetime of the activated carbon media, leading to additional cost savings and GHG reductions associated with the production of the carbon media. The reduction in manganese in the reservoir source water may have lead to lower filter fouling frequency. This would likely increase the overall lifetime of the filters and led to reduced backflushing. Although the HOS implementation appeared to result in a slightly increased need for alum coagulant, it also resulted in a significant reduction in polymer requirement for coagulation. Overall, there appear to be additional benefits of the HOS that could potentially enhance the economic feasibility and sustainability of the system implementation in USL. However, the lack of numerical data regarding activated carbon use, filter maintenance, or coagulant/polymer use makes the quantification impossible and this change was not included in the LCA or economic analysis.

5. Economic Variable and Assumptions

For the economic analysis of the HOS at USL, a total of three scenarios were considered: a baseline scenario, a minimum benefit scenario, and a maximum benefit scenario. Construction costs for the initial installation and the expansion were known and therefore they remained fixed in all three economic scenarios. The baseline economic analysis scenario utilized the same baseline HOS lifetime, HOS annual operational period, treatment parameters, HOS oxygen use, and maintenance schedule as the baseline LCA scenarios. The normal operations were held constant for the maximum and minimum benefit economic scenarios while the HOS operations were altered, except for hydrogen peroxide use which is detailed below. The minimum benefit economic analysis scenario utilized the minimum lifetime of the HOS, the minimum HOS annual operational period, the minimum reduction in chemical use for treatability that could be expected, the maximum use of oxygen for HOS operations, and the most frequent and most expensive maintenance assumption. The maximum benefit economic analysis scenario utilized the

maximum lifetime of the HOS, the maximum HOS annual operational period, the maximum reduction in chemical use for treatability that could be expected, the minimum use of oxygen for HOS operations, and the least frequent and least expensive maintenance assumption.

5.1 Construction and maintenance costs

The construction cost for the 2002 initial HOS installation was $512,000 and the cost for the 2012 expansion was $520,000. The costs included materials and labor so no additional calculations were required. Maintenance costs were only expected to be attributed to the replacement of porous hose every 10-15 years. This information was provided by the lead project engineer for the project (Mobley, M., personal communication, September 10, 2019). The porous hose was assumed to cost $0.68/ft and the cost of labor to replace the porous hose was assumed to be $1/ft for the baseline scenario, $0.50 for the maximum benefit scenario, and $2/ft for the minimum benefit scenario.

5.2 Treatment operational savings

For the baseline economic analysis scenario, it was known that the first year of HOS operations resulted in a total cost savings (including electricity) of $15/MG in the reduction in ozone use, $12/MG due to the elimination of hydrogen peroxide use, and $3/MG in the reduction in chlorine use, based on the chemical usage for the three years prior to the HOS operation in USL (Jung, 2003; Mobley, 2003). Using this data, the savings per mg/L reduction for ozone and chlorine and gallon/MG reduction for hydrogen peroxide was calculated for use in the minimum and maximum benefit scenarios. The volumetric savings for ozone use reduction was found to be $15/(5 mg/L – 2.75 mg/L) or $6.67 per mg/L. For the minimum benefit scenario, this amounted to a total savings of $10.47/MG for ozone use reduction using the maximum value parameter in the LCA HOS scenario (3.43 mg/L) and the normal scenario baseline value parameter (5 mg/L). For the maximum benefit scenario, this amounted to a total savings of $19.60/MG for ozone use reduction using the minimum value parameter in the LCA HOS scenario (2.06 mg/L) and the normal scenario baseline value parameter (5 mg/L). The volumetric savings for hydrogen peroxide use reduction was found to be $12/MG for a 1.55 gal/MG reduction or $7.74 per gal/MG. The benefit from reducing hydrogen peroxide use was calculated using a different method because the same assumption was made as in LCA model, that hydrogen peroxide will not be reimplemented in the HOS scenario, but the usage will be varied under the normal operational scenario. Therefore, the HOS usage remained fixed at 0 gal/MG and the minimum benefit scenario used the minimum value parameter for the normal scenario while the maximum benefit scenario used the maximum value parameter for the normal scenario. For the minimum benefit scenario, this amounted to a total savings of $8.98/MG for hydrogen peroxide elimination using the minimum value parameter for the normal scenario (1.16 gal/MG). For the maximum benefit scenario, this amount to a total saving of $14.55/MG for hydrogen

peroxide elimination using the maximum value parameter for the normal scenario (1.88 gal/MG). The volumetric savings for chlorine use reduction was found to be $3/(13.9 mg/L – 11.4 mg/L) or $1.20 per mg/L. For the minimum benefit scenario, this amounted to no net benefit for chlorine treatment using the maximum value parameter in the LCA HOS scenario (13.9 mg/L) and the normal scenario baseline value parameter (13.9 mg/L). For the maximum benefit scenario, this amounted to a total savings of $6.42/MG for chlorine use reduction using to the minimum value parameter in the LCA HOS scenario (8.55 mg/L) and the normal scenario baseline value parameter (13.9 mg/L).

5.3 HOS oxygen costs

The cost of oxygen used in the economic analysis was based on the cost of oxygen from the first year of operations which was $101 (Jung, 2003). The use of oxygen followed the same assumptions as the LCA HOS scenario. The LCA HOS scenario baseline parameter value was of 1.6 tons per day was used for the baseline economic analysis scenario. The LCA HOS scenario minimum parameter value of 0.8 tons per day was used for the maximum benefit scenario in the economic analysis and the LCA HOS scenario maximum parameter value of 2.0 tons per day was used as the minimum benefit scenario for the economic analysis. This amounted to a cost of $162/day for the baseline scenario, $202/day for the minimum benefit scenario, and $80.80/day for the maximum benefit scenario.

6. Citations

Bare, J.C., 2012. TRACI 2.1 - The Tool for the Reduction and Assessment of Chemical and Other Environmental Impacts. Environmental Protection Agency, Office of Research and Development, Cincinnati, OH.

Bastviken, D., Cole., J., Pace, M., Tranvik, L., 2004. Methane emissions from lakes: Dependence of lake characteristics, two regional assessments, and a global estimate, Global Biogeochm. Cycles, 18, GB4009.

Beutel, M.W., 2003. Hypolimnetic Anoxia and Sediment Oxygen Demand in California Drinking Water Reservoirs. Lake and Reservoir Management, 19(3), 208–221.

Beutel, M.W., Horne, A.J., 1999. A Review of the Effects of Hypolimnetic Oxygenation on Lake and Reservoir Water Quality. Lake and Reservoir Management, 15(4), 285–297.

Britton, L.J., Ferreira, R.F., Averett, R.C., 1974. Limnological Data from Selected Lakes in the San Francisco Bay Region (pp. 24–25). Menlo Park, CA: United States Geological Survey, Water Resources Division.

Byrd, W., 1992. Chinese industrial firms under reform. Oxford: Published for the World Bank Oxford University Press.

Chart Inc., 2019. Bulk Storage Systems Equipment for Cryogenic Service, Bulk Storage Product Catelog. New Prague, MN. Retrieved from https://www.yourfencestore.com/cl/clgal.htm

Galvanized Chain Link Fence Fabric (GBW), 2020. Retrieved from https://www.yourfencestore.com/cl/clgal.htm

Gantzer, P.A., Bryant, L.D., Little, J.C., 2009. Effect of hypolimnetic oxygenation on oxygen depletion rates in two water-supply reservoirs. Water Research, 43(6), 1700–1710.

Goel, N., Salveson, A., 2012. City of Palo Alto Long Range Facilities Plan for the Rwqcp, Appendix P - Ozone Sizing and Cost Estimate for TOrC Removal (pp. 2–11). Palo Alto, CA: City of Palo Alto.

Hanley, R., Joyce, M., Hall, T., Monaghan, S., Wall, B., Page, D., 2011. Water Treatment Manual: Disinfection. Wexford, Ireland: Office of Environmental Enforcement.

Hockstad, L., Cook, B., 2012. Inventory of U.S. greenhouse gas emissions and sinks: 1990 – 2010. Washington D.C.: U.S. Environmental Protection Agency.

Horne, A. J., Rowan, R., Toms, C., 2003. The 2002 Oxygen Bubble Plume Hypolimnetic Oxygenation System in Upper San Leandro Reservoir: Effectiveness for Internal Nutrient Load Reduction, Effect on Benthic Blue-Green Algae and Potential to Reduce Taste and Odor Causing Blue Green Algae. Report to East Bay Municipal District. University of California, Berkeley.

Jung, R., 2003. Upper San Leandro Hypolimnetic Oxygenation System Preliminary Evaluation Report. Process Engineering Section, East Bay Municipal Utility District.

Luong, L., 2017. Upper San Leandro Water Treatment Plant Upgrade. Retrieved from https://www.ebmud.com/about-us/construction-and-maintenance/construction-my-neighborhood/upper-san-leandro-water-treatment-plant-upgrade/

Marshall, R., 2013. Is compressed air perfection an attainable goal or a myth? Winnipeg, Canada: Manitoba Hydro.

Mobley, M., Vice President and Principal Engineer, Mobley Engineering, personal communication, September 10, 2019.

Mobley, M., 2012. Upper San Leandro CA, 2012. Retrieved from http://www.mobleyengineering.com/usl2.html#

Mobley, M., Jung, R., Lai, H., 2003. Upper San Leandro Hypolimnetic Oxygenation System. North American Lake Management Society. Foxwoods Resort, Connecticut.

Moore, B., Mobley, M., Little, J., Kortmann, B., Gantzer, P., 2015. Aeration and Oxygenation Methods for Stratified Lakes and Reservoirs (pp. 21-28). NALMS: Lakeline.

Nath, H., Wang, X., Torrens, R., Langdon, A., 2010. A novel perforated electrode flow through cell design for chlorine generation. Journal of Applied Electrochemistry, 41(4), 389–395.

Novak, K., Loughlin, A., Mann, M., 2011. Bulk or on-site generation: what's your hypochlorite solution. Paper presented at the Ohio Water Environment Association, Sandusky, OH.

Pulido, M.E., 2005. Evaluation of an Electro-Disinfection Technology as an Alternative to Chlorination of Municipal Wastewater Effluents (dissertation).

Wilmshurst, P., 1998. ABC of oxygen: Diving and oxygen. Bmj, 317(7164), 996–999.

Wire Co World Group., 2012. Wire Rope User's Handbook (pp. 13–14). Kansas City, MO.

U.S. Life Cycle Inventory Database, 2012. National Renewable Energy Laboratory, 2008. https://www.lcacommons.gov/nrel/search